INK-JET PRINTING FOR ADDITIVE MANUFACTURING OF OPTICAL WAVEGUIDES ON POLYMER FOIL SUBSTRATES

Zur Erlangung des akademischen Grades eines

Doktors der Ingenieurwissenschaften (Dr.-Ing.)

von der KIT-Fakultät für Maschinenbau des
Karlsruher Institut für Technologie (KIT)
angenommene

Dissertation

von

M.Sc. PATRICK BOLLGRÜN

Autor   Patrick Bollgrün

Adresse   Karlsruher Institut für Technologie
                     Institut für Mikrostrukturtechnik
                     Hermann-von-Helmholtzplatz 1
                     76344 Eggenstein-Leopoldshafen

Hauptreferent   Prof. Dr. Jan G. Korvink
                     Institut für Mikrostrukturtechnik
                     Karlsruher Institut für Technologie

Korreferent   Prof. Dr. Thomas Hanemann
                     Institut für Mikrosystemtechnik
                     Universität Freiburg

Prüfungsvorsitzender

                     Karlsruher Institut für Technologie

Bearbeitungszeitraum   2/2013 – 6/2017

Datum der Disputation   26. 6. 2019

πάντα ῥεῖ.

ABSTRACT

Electronic circuits are facing limitations in terms of bandwidth, and, in some cases, application compatibility. A possible alternative technology to overcome these limitations are optical waveguides – but they are still only used in the form of discrete cables, and lack the level of integration in fabrication and application which is common for electronics. What is needed is a technology that is able to create integrated optical waveguides on planar substrates in a way that is technologically and industrially feasible. In this thesis, several promising technologies that are able to fulfil these requirements are evaluated, among which ink-jet printing is selected as the most promising method.

Several optically transparent ink materials were evaluated - two commercially available, solvent based inks, and an in-house developed, solvent-free formulation that employs a reactive diluent to reach the viscosity required for ink-jet printing. Two inks were used to print tracks, which were evaluated in their ability to guide light. The solvent-free material was chosen for further experiments, because it was more compatible with the selected PMMA substrate.

After demonstrating the ability to create uncladded waveguides, several different concepts to create a printed lower and upper cladding were evaluated. A design with an ink-jet printed core, an ink-jet printed upper cladding, and the substrate as lower cladding was selected. Samples of different length were fabricated, and the transmission properties were measured. The results show a relatively high attenuation value of $1.4\,\mathrm{dB/cm}$, with the main contribution to this value from the bulk attenuation of the selected material.

Unlike electrical tracks, optical waveguide structures require a certain aspect ratio in order to carry light and enable light coupling. This requirement can be difficult to achieve with ink-jet printing, because stacked, uncured layers of a printed track tend to spread out across the substrate. Two methods to control the ink behaviour on the substrate were developed and investigated: Thermally induced pinning, and a so-called *Lightplate*.

The first method uses heat and time to induce pinning at the edge of the printed track. By waiting a certain time interval between depositing the individual layers, the edge of the printed track spreads out less on the substrate. As a result, consecutively deposited layers show a higher aspect ratio.

The second method, the *Lightplate*, is a device that uses a transparent substrate plate which confines UV-light by total internal reflection at the surface and metallic reflection at the edges. A droplet of a UV-

polymerisable liquid that is deposited on the *Lightplate* breaks the confinement, causing light to couple into the droplet and cause polymerisation. A prototype was built to evaluate if the Lightplate is able to affect the morphology of printed structures. Polymerisation could be demonstrated, but no effect on the morphology was found.

To achieve the first step towards a network of optical waveguides with integrated functional components, a suitable light source was developed. After dismissing the concept of waveguide-integrated, chip-based LEDs due to the high complexity in fabrication and the required supply of electrical power on the polymer substrate, a much simpler solution was found. By printing fluorescent materials op top of the printed waveguides, a light source that requires neither electrical tracks nor precise optical alignment could be realised. Inks with red and blue fluorophores were characterised, and the red material chosen used to create a robust prototype of an optical waveguide with integrated light source fabricated entirely by ink-jet printing.

ZUSAMMENFASSUNG

Elektronik stößt immer öfter an die Grenzen der möglichen Bandbreite und Anwendungskompatibilität. Um diese Grenzen zu überwinden, sind Lichtwellenleiter eine mögliche Alternative – aber diese werden nach wie vor als individuelle Kabel verwendet, und erreichen noch nicht den Integrationsgrad, welcher in Herstellung und Anwendung bei Elektronik üblich ist. Hier ist eine Technologie nötig, welche die Herstellung integrierter Lichtwellenleiter auf planaren Substraten in einer technologisch und industriell sinnvollen Weise ermöglicht. In dieser Dissertation werden mehrere vielversprechende Technologien, welche diese Anforderungen erfüllen können, verglichen, und Tintenstrahldruck als vielversprechendste ausgewählt.

Mehrere optisch transparente Tinten wurden untersucht – zwei kommerziell verfügbare, lösungsmittelbasierte Tinten, und eine lösungsmittelfreie Formulierung, welche am Institut entwickelt wurde. Hier wird die für Tintenstrahldruck nötige Viskosität mittels einem Reaktivverdünner erreicht. Zwei der Tinten wurden zum Drucken von Linien verwendet, welche dann auf ihre lichtleitenden Fähigkeiten hin untersucht wurden. Das lösungsmittelfreie Material wurde für weitere Experimente ausgesucht, da es sich als geeigneter für das gewählte PMMA-Substrat herausstellte.

Nachdem ungeschirmte Lichtleiter erfolgreich hergestellt werden konnten, wurden mehrere Konzepte für eine gedruckte untere und obere Mantellage evaluiert. Eine Ausführung mit tintenstrahlgedrucktem Kern, tintenstrahlgedruckter oberer Mantellage, aber der Substratfolie als untere Mantellage zeigte sich hier am geeignetsten. Testmuster unterschiedlicher Längen wurden hergestellt, und die Lichtleitungseigenschaften gemessen. Die Ergebnisse zeigen eine relativ hohe Dämpfung von 1.4 dB/cm, mit der Volumendämpfung der gewählten Tinte als Hauptursache.

Anders als elektrische Leiterbahnen benötigen Lichtwellenleiter eine gewisse Höhe, um Licht zu führen und das Ein- und Auskoppeln zu ermöglichen. Mit Tintenstrahldruck ist diese Anforderung nicht leicht zu erfüllen, da mehrere übereinandergedruckte, flüssige Schichten die Tendenz haben, zu zerfließen, und sich auf dem Substrat auszubreiten. Zwei Methoden, um das Verhalten der Tinten auf der Substratfolie zu steuern, wurden erarbeitet und untersucht: Thermisch induziertes Pinning, und die sogenannte *Lightplate*.

Die erste Methode nutzt Wärme und Zeit, um Pinning an der Kante einer gedruckten Linie zu erzeugen. Indem eine gewisse Zeit zwischen dem Drucken einzelner Schichten abgewartet wird, breitet sich die Kante einer gedruckten, mehrlagigen Linie weniger weit auf dem

Substrat aus. Im Ergebnis zeigen nacheinander gedruckte Schichten ein höheres Aspektverhältnis.

Die Zweite Methode, die *Lightplate*, ist ein Gerät, bei der eine transparente Substratplatte verwendet wird, um UV-Licht durch Totalreflexion an der Oberfläche und metallischer Reflexion an den Kanten zu sammeln. Wenn ein Tropfen einer UV-polymerisierbaren Flüssigkeit auf der Oberfläche der *Lightplate* landet, wird die Totalreflexion gebrochen, und das Licht koppelt in den Tropfen ein, wo es eine Polymerisationsreaktion auslöst. Ein Prototyp wurde gebaut, um zu evaluieren, ob das Konzept fähig ist, die Form von gedruckten Strukturen zu beeinflussen. Polymerisation konnte gezeigt werden, ein Einfluss auf die Form allerdings nicht.

Um den ersten Schritt zu einem Netzwerk von Lichtwellenleitern mit integrierten funktionalen Elementen zu machen, wurde eine Lichtquelle entwickelt. Nachdem das Konzept einer chipbasierten, wellenleiterintegrierten Diode wegen zu hoher Komplexität in Herstellung und der nötigen Versorgung mit elektrischem Strom auf dem Polymersubstrat verworfen wurde, trat eine viel einfachere Lösung hervor. Indem ein fluoreszentes Material auf gedruckte Lichtwellenleiter aufgebracht wurde, konnte eine Lichtquelle realisiert werden, die weder elektrische Energie noch präzise Ausrichtung benötigt. Tinten mit roten und blauen Fluorophoren wurden charakterisiert, und das rote Material wurde verwendet, um einen robusten Prototypen eines Lichtwellenleiters mit integrierter Lichtquelle vollständig mittels Tintenstrahldruck herzustellen.

CONTENTS

LIST OF ACRONYMS

CVD   Chemical vapor deposition

EGDMA   Ethylen glycol dimethacrylate

GBL   Gamma-Butyrolactone

LED   Light-emitting diode

PCB   Printed circuit board

PMMA   Poly(methyl methacrylate)

SMD   Surface-mounted device

TIR   Total internal reflection

UV   Ultra-violet

INTRODUCTION

1.1 MINIATURISATION OF ELECTRONICS

Our everyday life is ruled by an incessant presence of computers and smartphones. This is only possible because the individual electronic components can be connected in a compact fashion, which is achieved with patterns of electrically conductive tracks, called printed circuit boards (PCBs). Before the availability of this technology, which was patented in 1943 [1, 2], the elements of electronic devices had to be connected by individual wires, which prohibited compact design and hampered an effective fabrication with low error rate. Only after the availability of preprepared PCBs that could easily be fitted with the correct electrical parts was it possible to manufacture electronic devices in an efficient manner. Eventually, lithography techniques replaced printing for the creation of the conductive tracks and enabled track widths significantly below 0.1 mm. This development, in combination with integrated circuits, enabled electronic technology to reach the level of development we see today.

Figure 1.1 shows an audio amplifier which employs both technologies, PCBs and open wires, visualising the benefits of printed circuit boards. Through adoption of PCB technology, and miniaturisation of electrical elements and their integration into electronic chips, the functionality of the device shown in 1.1 can today be integrated in a much smaller volume - the audio electronics of a smart phone typically have footprints below 1 cm^2, including the necessary wiring.
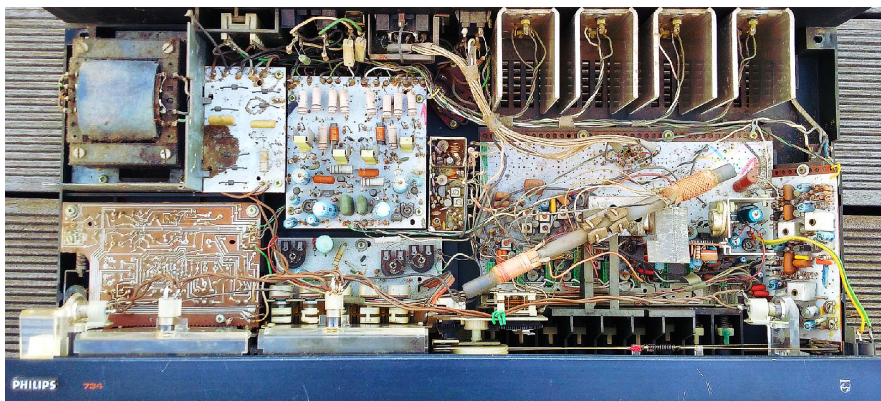
Figure 1.1: Photograph of a 1975 audio amplifier (RH 734, Philips, Eindhoven, Netherlands), with a footprint of approximately 60 cm × 30 cm. While most electrical elements are on PCB's, the design still relies on open wire connections, which had to be soldered individually by hand.

Although electronic technology is used in all aspects of modern life and suitable for numerous applications, there are certain limitations. Electromagnetic fields, coming either from adjacent electrical tracks or the environment, cause interference and hereby reduce signal quality, effectively limiting data rate. Especially at high frequencies in the GHz range, signal cross-talk between the electrical tracks [3] and a high ohmic resistance due to the skin-effect [4] pose a barrier for the further development of the technology.

To overcome this limitation, an alternative to electrically conductive tracks that carry electric pulses is required. A suitable technology are optical waveguides that carry light pulses. Neither is the optical pulse density limited by the optical attenuation, nor does an optical signal interfere with adjacent waveguides, except at distances below 1 µm.

Additionally, there are many sensor concepts that are based on optics, like spectroscopy and optical resonance. For such sensors, a high integration can be reached if the light is not created for each sensor individually from electrical power, but supplied directly by an entire network of of optical waveguides.

1.2   OPTICAL WAVEGUIDES IN A NUTSHELL

An optical waveguide is a device that uses an optically transparent material to carry a light beam by the phenomenon of total internal reflection (TIR). This effect occurs when light from an optically transparent material with a given refractive index encounters an interface to another transparent material with a lower refractive index at a relatively flat angle. Here, the light is reflected at the interface back to the original medium, and continues to travel within the material with the higher refractive index without significant attenuation from this reflection. By this phenomenon, the optical waveguide in a fibre optic cable can carry a light pulse over many kilometres [5].

The first experimental demonstration of an optical waveguide was performed by D. Colladon in the 19th century [6]. He used a jet of water running from a water tank into a bowl to demonstrate that a beam of light which enters the jet horizontally follows the curvature of the water jet, hereby illuminating the bowl. The experiment is shown in Figure 1.2, with the illuminated bowl at the bottom. However, as this phenomenon lacked a useful application, and sufficiently bright light emitters were still fragile sources of fire-hazard, the setup was merely considered a scientific toy. Only after the development of data transmission technology by light pulses through fiberoptic cables and the availability of compact light sources and detectors did the concept of optical waveguides find wide application [7].

While the experimental demonstration of the effect could be done with a liquid, it is an engineering challenge to fabricate solid optical waveguides that are sufficiently robust for everyday use. Electri-
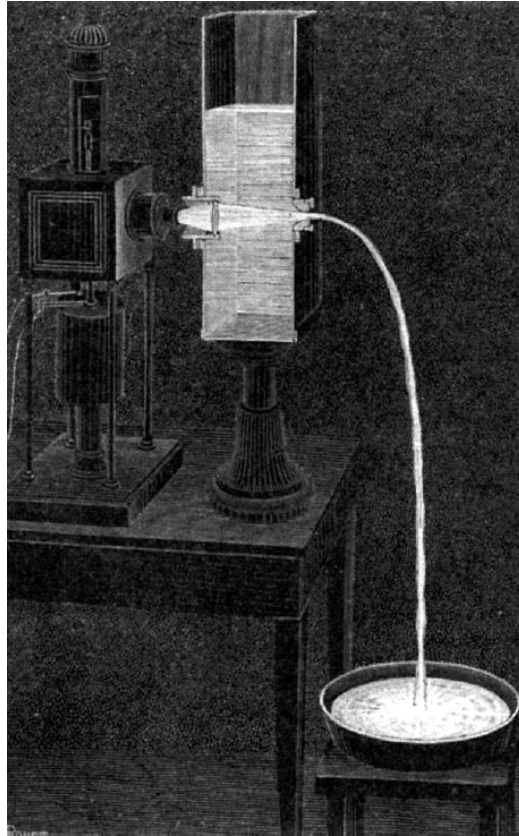
Figure 1.2: Colladon's "light pipe", demonstrating how a jet of water is able to curve the path of a beam of light. Reprinted from public domain [8].

cal cables only require an uninterrupted track of electrically conductive material and a sufficient protection against mechanical and electromagnetic influences from the environment for functionality. Optical waveguides are more complex, and require a highly transparent waveguide core material to minimise bulk scattering, an enclosing cladding layer made from a second highly transparent medium with a defined refractive index step to create TIR with an optically smooth interface to minimise reflection scattering, a third layer for mechanical protection, and a cross-section geometry that does not cause refraction of light out of the waveguide core.

Because of the requirement of smooth surfaces, the first experimental demonstration of an optical waveguide was achieved with a liquid material, where the surface tension creates such an surface. And still, fibre optic cables are typically fabricated by drawing fibres from materials in the liquid state [9], either polymers or glasses.

Today, optical waveguides have almost entirely replaced electrical long-distance data transmission infrastructure, because they show lower attenuation, and are able to support a higher data bandwidth. The technology continues to replace electrical data transmission in shorter distances in many applications [5, 10].

While glasses are the material category that is most commonly related to optics, there is an alternative material category that is continually replacing glass: polymers. The reason for this is that polymers are simpler to handle in industrial processes and and can typically be processed at room temperature, while glasses have to be handled at high temperatures and are typically less suitable for rapid mass production. Additionally, the lower processing temperature enables a much wider range of potential additives, especially from the typically temperature sensitive field of organic chemistry, to tune the properties and add functionalities like fluorescence at certain wavelengths.

An important characteristic of optical waveguides are the number of modes that can propagate within that waveguide due to the behaviour of light as a wave, which is explained in detail in Chapter 3. If the diameter of the waveguide is in the range of a few µm, only one mode can propagate straight through. This design is called *single-mode*. Larger waveguides allow the propagation of many modes at different reflection angles and are therefore called *multi-mode*. Both designs have advantages and disadvantages, but this thesis deals with manufacturing techniques which are only suitable for multi-mode waveguides.

1.3 OPTICAL WAVEGUIDE NETWORKS

With fibre optic cables typically being the best choice for long distance data transmission, and integrated optical circuits slowly appearing, optical waveguide technology is roughly where electrical technology was 75 years ago. In order to create an optical device with a high level of integration, many individual system elements have to be connected into a network. If the only available means to connect optical elements are fiber optic cables, a situation similar to the wires shown in Figure 1.1 occurs. Similarly to microelectronics, the integration of many individual devices to an integrated microsystem by a planar network of signal-guiding tracks as an optical analogue to printed circuit boards is the next logical step for advancing the application of optical technologies.

However, the tracks to guide the light are not the only system element that is required to advance the technology of optical networks. Equally important are beam splitters, light sources, light detectors, and optical sensors and transducers. An entire network based only on optical devices would allow a high integration density, with all benefits known from electronics, like superior efficiency, lower weight, lower manufacturing cost, etc. One concept that aims to make use of these benefits are large area optical sensor arrays on polymer foils [11]. By means of a network of light sources, sensors, and detectors, it would be possible to measure certain physical quantities over an area, similar to the human skin. Practical applications of suitable
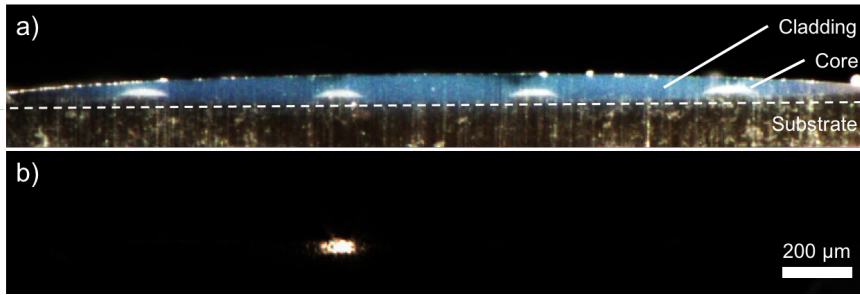
Figure 1.3: Side view of an array of four ink-jet printed optical waveguides embedded in a printed cladding. In the upper part a), the printed tracks are shown under ambient light. In the lower part b), one waveguide is shown to carry light. Reproduced with permission from [15].

sensor concepts for humidity [12, 13] and elongation [14] are under research. An important aspect of these sensors is their use of the light spectrum to show a change of the measurand. This way, the sensors are insusceptible to the optical attenuation of the optical waveguide that connects them to the network. Instead, the signal attenuation could be used to derive the distance between sensor and detector to identify the position of the sensor in the optical network.

Possible applications for such sensor networks are environments where a light and flexible array of sensors is desired, like the aerospace and automotive sector. Alternatively, special environments, where the use of metals and electrical devices is either not feasible or even prohibited, like environments with high electromagnetic fields, or contamination-critical single-use microfluidic devices, appear as useful applications for this concept.

1.4 INTERMEDIATE CONCLUSION - WHAT'S MISSING?

To fabricate an optical analogue to printed circuit boards, a fabrication technology that is able to create entire networks of optical waveguides, light sources, detectors, and other devices in an industrially effective way is required. After finding such a method, optical waveguide networks would be able to compete with PCBs for electronics, with potentially beneficial outcomes for all fields where PCBs are employed. In this thesis, the suitability of ink-jet printing to fulfil that role is investigated. In the next chapter, several manufacturing technologies with demonstrated ability to fabricate optical waveguides and related key publications will be presented and compared.

1.5 THESIS CONTRIBUTIONS

Within the research that led to this thesis, the first scientific publication on cladded optical waveguides fabricated entirely by ink-jet
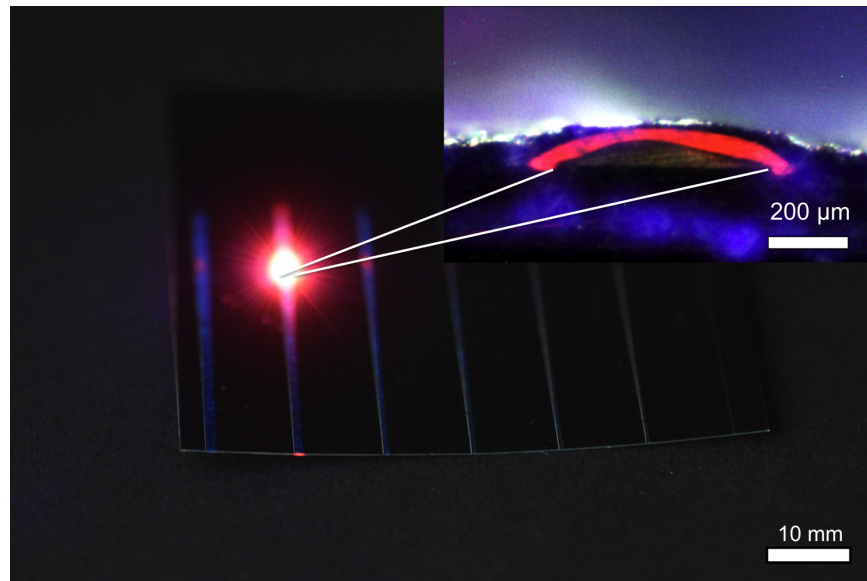
Figure 1.4: Printed optical waveguides with ink-jet printed fluorescent light sources. One element is illuminated by a blue laser, causing red fluorescence. The light travels along the waveguide and can be seen at the bottom. The inset shows the cross-section of the waveguide with the light source on top. Reproduced with permission from [16].

printing on flexible polymer foils was published[15]. Transmission over a distance of up to 50 mm could be demonstrated, as is shown in Figure 1.3. Because a solvent-free ink with relatively high bulk attenuation was chosen, the waveguide showed a relatively high attenuation of 1.4 dB/cm. Since the publication of this paper, several other groups have published in the field with improved attenuation values.

While working on ink-jet printed optical waveguides, it was observed that the line pinning of an oligomer on a heated substrate does not only depend on the temperature, but also on the deposition rate of individual layers. This phenomenon, which was not reported in scientific literature before, was characterised and published.

Additionally, an ink-jet printed, waveguide-integrated light source based on a fluorescent material that does not require any electrical elements was developed from concept to prototype[16]. With this design, a printed optical waveguide could be supplied with light externally without the need of precise optical alignment of other coupling structures. The demonstrator that was developed with this method is shown in Figure 1.4.

STATE OF THE ART

With optical networks being such a promising field, many researchers have investigated the manufacturing of such structures. In the following chapter, a number of manufacturing techniques with demonstrated ability to manufacture optical waveguide networks will be presented, and the achieved optical attenuation will be compared. Special focus will be given to ink-jet printed optical waveguides, as this is the topic of the thesis.

2.1 MANUFACTURING OF INTEGRATED MULTI-MODE WAVEGUIDES

Researchers have used both established and novel manufacturing techniques to fabricate multi-mode optical waveguides from transparent polymers. Many research projects investigated additive manufacturing techniques, which are methods that add material at the exact location where it is required, instead of removing unwanted material from a raw block. This enables a high degree of geometrical freedom, and is typically more material-efficient. Although already present in the 1980s, it only gained significant public interest after 2010 due to the availability of consumer-level machines.

All methods have in common that optical structures with two different refractive indices for core and cladding have to be created. Typically, the structures are not circular, but flat, and the lower cladding, the core, and the upper cladding layer are created subsequently. Often, the substrate forms the lower cladding layer.

In order to connect optical elements like sensors, detectors, and light sources via networks of optical fibres on a footprint of a few square centimetres for a small-scale technological application, the optical attenuation of the waveguides should not exceed 1 dB/cm in order to be feasible [17].

Ten techniques with a demonstrated ability to fabricate optical waveguides, shown in Figure 2.1, will be presented. The diameter of the structures typically is between 10 μm and 100 μm, which puts them into the domain of multi-modal waveguides.

2.1.1 *Lithography*

Lithography is an established method for micro-structuring [18]. In the simplest variant of this process, a layer of photopolymerisable material is deposited on a flat substrate, and selectively exposed to ultra-violet (UV) light by means of a shadow mask. Depending on
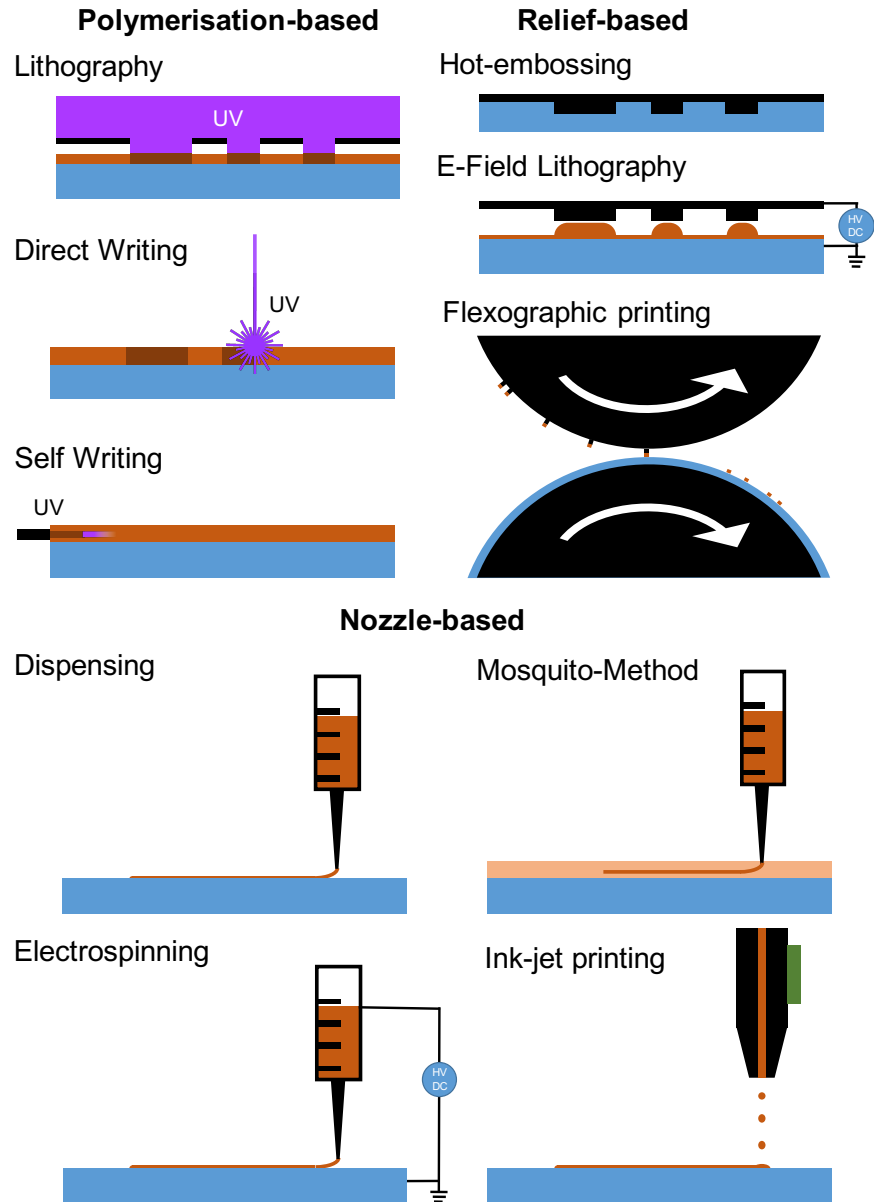
Figure 2.1: Working principles of ten methods suitable for the fabrication of optical waveguides. The substrate is coloured blue, tools are shown in black, the transparent polymer is light brown when unpolymerised, and darker when polymerised. The methods are grouped into three categories: Polymerisation-based techniques, relief-based techniques, and nozzle-based techniques.

the applied material, either the exposed or the unexposed material is chemically removed in a subsequent wet-etching step.

A. Borreman et al. [19] used this method to create optical waveguide cores from an epoxy-based photoresist (NANO SU-8-25, Microchem, Newton, MA, USA). The cladding was created by an acrylate (PMMA, *generic*) dissolved in chlorobenzene (C_6H_5Cl) with a ratio of 1:10. The width and length of the quadratic waveguides was

40 µm, and the attenuation was in the range of 0.5 dB/cm between 800 nm and 1100 nm.

J. S. Kim et al. [20] used the same material for the core, but created the cladding from thermally more stable Cyclotene ($C_6H_8O_2$). With this method, the waveguides could resist temperatures of up to 200 °C for several hours. The measured attenuation was 0.36 dB/cm at 830 nm.

2.1.2 *Direct Writing*

To perform lithography, a shadow mask is required, which has to be designed and fabricated in advance, typically by an external supplier. This means that the realisation of a design change takes weeks. To enable a more flexible fabrication process, linear tracks can be created by photopolymerisation directly by a focused laser beam that moves across the substrate, hereby creating polymerised tracks. This method is called *Direct Writing*. Similarly to lithography, the excess material is subsequently removed by wet-chemical development.

R. Dangel et al. [21] demonstrated that multilayer arrays of optical waveguides are possible by direct-writing in polyurethanes, acrylates, or siloxanes. By subsequent deposition of core and cladding layers, a 4×12 array of rectangular optical waveguides on a standard PCB substrate was created. The side length of the waveguides was 35 µm, the propagation losses were in the range of 0.05 dB/cm at wavelength of 850 nm.

Later, the group demonstrated this technique with a flexible polyimide foil substrate [22]. Here, a silicone material (WG1017, Dow Corning, Midland, MI, USA) was applied as cladding layer to achieve elasticity. The waveguide had an optical attenuation of 0.031 dB/cm, also at a wavelength of 850 nm.

However, these results were achieved with a single laser beam, which makes the technique relatively slow. This disadvantage can be removed by using a digitally controlled micromirror device (DMD, Texas Instruments, Dallas, TX, USA) which allows to selectively illuminate an entire area. This was demonstrated for single-mode fibres by M. Rahlves et al. [23].

2.1.3 *Self-Writing*

An intriguing variant of using a single beam of light to create polymerised tracks of material is the *self-written* waveguide. Here, a ray of light is created at a point within a volume of unpolymerised material, either by a collimated laser beam from outside, or an optical fibre with open facet pointing into the volume. With a suitable wavelength and material properties, the light causes the material within the beam to polymerise, thus creating a cylinder of polymerised material.

As, typically, polymerisation increases the refractive index of a material, this cylinder acts as a short optical waveguide, which confines the light from the fibre facet to the edge of the newly-created waveguide. Here, the polymerisation process continues, hereby gradually prolonging the cylinder. This way, an optical fibre can be written within a volume of polymerisable material.

S. J. Frisken [24] first demonstrated this technique in 1993 by placing an optical fibre from a 532 nm laser inside a volume of unpolymerised, liquid epoxy (*undisclosed*). On the opposite side of the beam, a glass microscope slide was positioned, which was observed by means of a digital camera. After a certain time frame, ranging from seconds to hours, depending on the process parameters, the microscope slide would show a distinct light point, indicating the formation of a waveguide. The attenuation was estimated to be less than 5 dB/cm at 1550 nm.

Recently, A. Günther et al. [25] published an application of this technique. A commercially available acrylate varnish (Syntholux, Synthopol, Buxdehude, Germany), mixed with 3 wt.-% photoinitiator (Ciba Irgacure 184, BASF, Basel, Switzerland) was deposited on the interface between two open-ended, butt-coupled fibres. On initiation of 406-nm laser light (MCLS1-406, Thorlabs, Newton, USA), the fibres were moved away from each other. By constant monitoring of the transmitted power of this gap, a continuous waveguide was ensured. This resulted in optical fibres with a diameter in the range of 100 μm and an attenuation of 0.76 dB/cm at 638 nm, and 0.69 dB/cm at 850 nm, respectively [26].

Typically, UV-light is required to polymerise the material, but this is not always the case. The group by H. Terasawa [27] published an elaborate material composition consisting of an acrylate monomer, a radical generator, a hardening accelerator, and a chromophore that is suitable for two-photon-polymerisation with pulsed infrared light at 1550 nm. With this method, they were able to bridge a 400 μm gap between two fibres, reducing the attenuation of this gap from 10.65 dB to below 0.5 dB. However, no value for the attenuation per length unit was given.

2.1.4 *Hot Embossing*

Hot embossing is an established method for the microstructuring of thermoplastic materials. Here, a microstructured stamp is pushed into a heated material, typically under vacuum to ensure a completely filled stamp. This way, the microstructures from the stamp are copied into the material. To create optical waveguides, these grooves serve as a mould for the optical waveguide cores. Aspect ratios up to 500 % [28] and surface roughness values below 5 nm [29] were demonstrated. Typically, the polymer substrates have to be in contact with

the stamp for several minutes [29, 30], which makes the fabrication technique relatively slow at such aspect ratios. The method can be made roll-to-roll compatible [31], however with lower aspect ratios. After creation of the grooves, a core material is deposited by a suitable deposition technique, and an upper cladding layer is deposited on top.

Several research groups have demonstrated the suitability of this method to fabricate optical waveguides. H. Mizuno et al. [32] showed that tracks of an UV-curable epoxy resin (*undisclosed*) filled into hot embossed tracks in an acrylate substrate (PMMA, *generic*) allowed optical waveguides with an attenuation of 0.19 dB/cm at 650 nm.

K. B. Yoon achieved 0.2 dB/cm at 850 nm with the technique [33], also by using an acrylate (PMMA, Ashahi Glass, Osaka, Japan) as a substrate, and an epoxy resin (*undisclosed*, Zen photonics, Daejeon, South Korea) as core material.

M. Rezem et al. [29] published attenuation values of 0.74 dB/cm (633 nm) and 0.09 dB/cm (850 nm) by using a commercially available optical adhesive (NOA63, Norland Products, Cranbury, NJ, USA) and a commercially available acrylate varnish (390119 UV Supraflex, Jaenecke + Schneemann Druckfarben, Sehnde, Germany) as core materials in an acrylate substrate (Plexiglas Film 99524, Röhm (Schweiz) AG, Brüttisellen, Switzerland). The material was deposited by doctor-blading, the fabricated grooves had a rectangular cross-section of 25 μm × 25 μm.

2.1.5 *E-Field Lithography*

An unusual method to create micro-structures is *e-field lithography*. The method is related to hot-embossing as it uses a prefabricated master tool. However, this tool is not imprinted into the substrate by heat and pressure, but used as patterned capacitor plate that creates an electric field between the master tool and the transparent polymer. The resulting electrostatic attractive force causes the liquid to lift and form elevated structures, which are polymerised by UV light while the structures continue to grow under the electric field. The suitability of this method to create optical waveguides was demonstrated by T. Hin et al. [34]. By using a polysiloxane material (Lightlink, MicroChem, Westborough, MA, USA), optical waveguides with height and width of 50 μm, and an attenuation of 1.97 dB/cm at 850 nm could be created. Similar to hot-embossing, the method is relatively slow, because the process takes several minutes to result in sufficiently large structures.

2.1.6 *Flexographic Printing*

Another method related to hot embossing is *flexographic printing*. This method also uses a stamp (called printing plate), but not to create grooves in a substrate, but to collect and deposit material (called ink, because it is a printing method) selectively on an untreated substrate foil. It is therefore an additive manufacturing method. The method is commonly used in a roll-to-roll setup for graphic printing because of its exceptionally high throughput of up to 35 m^2/s at a minimum feature size of 50 μm [35].

With this method, T. Wolfer et al. were able to create optical waveguides [35]. By printing an acrylate varnish (UV Glanzlack praegefaehig, Jaenecke + Schneemann Druckfarben, Sehnde, Germany) in several layers on an acrylate foil (Plexiglas Film 99524, Röhm (Schweiz) AG, Brüttisellen, Switzerland), an attenuation below 0.5 dB/cm at 635 nm [16] could be achieved. The substrate sheets were 40 cm long and 30 cm wide and carried arbitrarily shaped optical network patterns.

Additionally, the method of flexographic printing was used to deposit wetting conditioning lines on a polymer foil [36–39]. Then, aerosol-printing was used to deposit material between the conditioning lines, where it self-assembled to continuous tracks. This allowed the fabrication of 300 μm wide and 50 μm high lines. However, no attenuation data on this technique is available yet.

2.1.7 *Direct Dispensing*

Direct dispensing is a relatively simple fabrication method which dispenses a prepolymer on the substrate through a fine needle. Leng et al. [40] demonstrated that this method allows for the fabrication of optical waveguides with an attenuation below 0.1 dB/cm at 633 nm by dispensing an optical adhesive (NOA63, Norland Products, Cranbury, NJ, USA). However, laser-ablated trenches in the substrate were required to maintain the shape of the deposited material. Therefore, this work can also be seen as a complementary element of hot embossing, or similar techniques that create such grooves.

The problem of maintaining the cross-section shape on flat substrates was solved by Dingeldein et al. [41]. By careful tuning of the dispensing pressure, needle gauge, and deposition speed, continuous waveguides with an attenuation of 0.1 dB/cm could be demonstrated on untreated substrates. By application of pressures up to 500 kPa, photo-patternable polysiloxanes (OE 4140, OE 4141, Dow Corning, Midland, MI, USA) developed for photolithography as cladding and core were dispensed through needles with gauges between 21 and 33 onto FR4-substrates.

Optical waveguides with a width between 25 µm and 200 µm and an aspect ratio in the range of 1/10 could be fabricated. By increasing the non-volatile content of the dispensed material from 70 % to 85 %, thus increasing the viscosity and the necessary pressure, a higher aspect ratio was possible, which resulted in waveguides with an optical attenuation as low as 0.06 dB/cm at 850 nm. A dissertation [42] gives detailed overview of the work.

2.1.8 *Mosquito Method*

A variant of direct dispensing is the so-called *Mosquito-Method*. Here, the dispensing needle is not moved over a substrate, but pushed into another liquid prepolymer, which forms the cladding. By moving the needle through the liquid cladding layer, the needle creates a furrow with the waveguide core at the bottom, which closes after the needle has passed. An important benefit of this method is that core and cladding materials are in liquid state after deposition, which allows for a diffusion of the interface before polymerisation. The result of this is a graded index waveguide, which reduces the modal dispersion commonly seen in multi-modal optical waveguides.

S. Morikawa and T. Ishigure [43] demonstrated that by depositon of a mixture of P3FMA and PMMA into another with a different mixing ratio through an air-pulse dispenser (ML808FXcom, Musashi Engineering, Tokyo, Japan), it is possible to create optical waveguides with a circular cross-section. By using high viscosities ranging from 10 Pa·s up to 25 Pa·s, core diameters below 50 µm were possible.

K. Soma and T. Ishigure showed suitable process parameters to create circular, graded index fibers with a core diameter of 40 µm [44]. Both core and cladding materials were silicone resins (Core: FXW712, Cladding: FXW713, ADEKA, Tokyo, Japan). By having a graded index, an attenuation of 0.033 dB/cm at 850 nm could be demonstrated. Additionally, curved waveguide patterns with bending radii down to 1 mm [45] and multi-core array structures [46] were demonstrated. Further refinement of the process was achieved with a curved dispensing needle [47].

2.1.9 *Electrospinning*

Electrospinning is related to direct dispensing, but uses the electromotive force caused by a strong electric field in addition to the mechanical forces to dispense the material from a charged dispensing needle to a grounded substrate. For this process, the substrate has to be electrically conductive. A review paper by D. Wang et al. [48] explains the technique and provides a set of basic equations. E. Sutanto et al. [49] showed that this technique is suitable for the fabrication of optical microstructures, but the demonstrated structures are single-

mode, and no attenuation data is given. The technique was applied by V. Bhatia at the university of Freiburg to create 90 μm wide and 17 μm high structures of a methacrylate-poly(methyl methacrylate) (MMA-PMMA) polymer resin (Plexit 55, Evonik, Essen, Germany). Functionality could be demonstrated with a 785 nm laser, but no attenuation value was measured[50].

2.1.10 *Ink-Jet Printing*

Instead of dispensing the prepolymer in a continuous thread, the material can also be jetted onto the substrate as individual droplets. This method is called *ink-jet printing* [51, 52]. While the common application of this technology is graphic printing, the deposition of dyes on paper or polymer foil, it is also possible to deposit functional materials with this technique. Conductive tracks can be created by printing a dispersion of metal nanoparticles, which can, for example, be used to create coils for magnetic resonance imaging [53].

The method also allows to print prepolymers [54] suitable for optical and photonic applications [55], such as organic light-emitting displays [56], solar cells [57], or micro-lenses [58–60]. For the fabrication of optical waveguides, six groups have published research that investigates the suitability of ink-jet printing. These projects are presented in the following.

MicroFab

The first scientific paper on ink-jet printed optical waveguides was published in 1995 by researchers from MicroFab Technologies [61] (MicroFab Technologies, Plano, USA). Here, hot-melt printing of a thermoplast (*undisclosed*) with a refractive index of 1.704 at 145 °C on a glass substrate heated to 45 °C was reported. A drop spacing of 75 μm and droplet volume of 65 pl led to continuous, hemicylindrical lines with a width of 134 μm. However, while continuous lines and even homogeneous beam splitters were demonstrated, no data on the attenuation of the optical waveguides is provided. A second publication [62] shows an ink-jet printed 1×16 waveguide splitter, which is created from 100 μm wide tracks. Again, no information is given on the optical attenuation. The image is shown in Figure 2.2.

Drexel University

In 2010, a single conference paper was published by a research group from Drexel University [63] (Drexel University, Philadelphia, USA). Here, a Dimatix DMP 2831 printer was used to print a photoresist (SU-8 2002, MicroChem, Westborough, MA, USA) on a spin-coated layer of an optical adhesive (NOA 65, Norland Products, Cranbury,
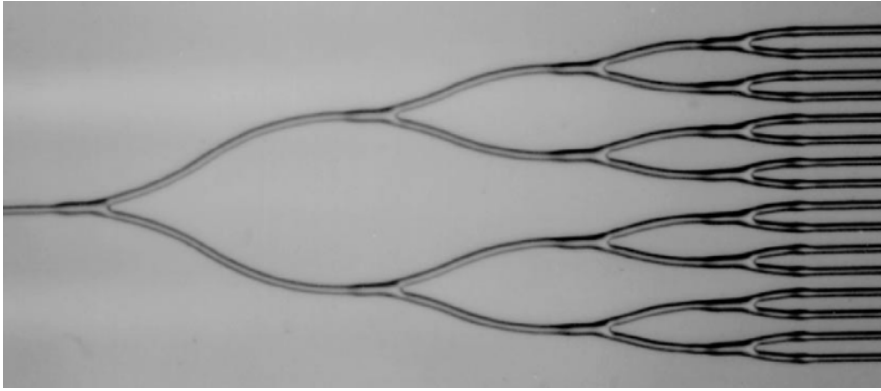
Figure 2.2: Ink-jet printed 1×16 optical waveguide splitter by Microfab technologies. Reprinted with permission from [62]

NJ, USA) carried by a glass substrate. The refractive index of the core material is given as 1.52, the cladding material is stated to be within the range of 1.5 and 1.6. By printing at a drop spacing of 15 μm, lines with a width of 34 ± 1 μm and a height of 1.6 μm were created. After printing, the waveguide was cladded with a second layer of spin-coated NOA 65. When measuring the attenuation of a 1 cm sample, an attenuation of of 23.2 dB/cm was derived. However, it should be noted that this value is the sum of the waveguide attenuation and the coupling losses at the two waveguide facets. No further results were published by the group. The researchers stated that it was very difficult to couple light into the structures because they were quite flat, and the round cross-section of the fibres to couple light into the samples was incompatible to the flat cross-section of the printed structures, so a portion of the light was carried by the cladding. Also, it is possible that the refractive indices of the materials were unsuitable, as the reported values are very vague, and it was not made clear if the given values describe the refractive index before or after polymerisation.

OPCB

Several papers on the topic were published by researchers from the *English Innovative electronics Manufacturing Research Centre (IeMRC)* flagship project *Integrated optical and electronic interconnect PCB manufacturing*, also known as *OPCB* [64]. The experiments were performed on modified printheads (760 GS8, Xaar, Cambridge, UK; Jetlab 4, Microfab, Plano, Texas, USA) with an acrylate material (Truemode, Exxelis, Edinburgh, UK), of which core and cladding formuations were available, and an optical silicone (OE4140, Dow Corning, Midland, MI, USA) [65–67] that was viscosity-modified for ink-jet printing by the manufacturer. Having identified the height of printed structures as a critical issue, a paper [68] was dedicated on the study of

the line stability of printed polymer. Several methods to change the behaviour of the ink on the substrate were shown, including a reduced temperature to increase the ink viscosity, the application of a hydrophobic intermediate layer, and an *in situ* curing device to polymerise each printed layer immediately, instead of deposition of several layers and subsequent polymerisation.

As described in a summary publication [69], waveguides with a width of 155 μm and an attenuation of 0.47 dB/cm at 850 nm were fabricated. Special attention should be given to the fact that this result was achieved with a polysiloxane material, which is commonly considered unsuitable for ink-jet printing.

Montanuniversität Leoben

A recent result was published by A. Samusjew et al. [70]. Here, a formulation of an aliphatic urethane acrylate resin (Genomer 4267, Rahn AG, Zürich, Switzerland), combined with ethylene glycol vinyl ether (EGVE) and 2-phenoxyethyl acrylate (PhEA) was deposited in a laboratory inkjet printer (DMP 2831, Fujifilm Dimatix, Santa Clara, CA, USA) on elastic polydimethylsiloxane (Sylgard 184, Dow Corning, Midland, MI, USA), resulting in an aspect ratio of up to 0.4. The benefit of this formulation is its mechanical elasticity. The optical characterisation was not included in the paper, but reported to be underway.

Instituto de Ciencia de Materiales de Aragón

By printing a monomer with both epoxy and silane functionalities, J. Alamán et al. [71] were also able to print optical waveguides on glass slides. At 633 nm an optical attenuation between 0.5 and 0.6 dB/cm was reported.

Centre Suisse d'Electronique et de Microtechnique

Another recent result was published by researchers from Centre Suisse d'Electronique et de Microtechnique (CSEM) [72]. The group created structures with an aspect ratio of 1:4 by printing tracks in two subsequent tracks: First, a track of individual droplets was printed. Then, these droplets were connected by a second row of individual droplets printed into the gaps between the first layer of droplets, forming capillary bridges. This way, circular droplet pinning could be exploited, with linear tracks as result. The core material was an acrylic polymer, printed on PET foil or glass slide as substrate. The upper cladding was formed by MgF_2. The optical attenuation at 650 nm was 0.61±0.26 dB/cm, with the best sample showing 0.19 dB/cm, which is to date the best published result on the topic.

2.2 COMPARISON OF THE MANUFACTURING TECHNIQUES

Having presented a selection of methods with demonstrated ability to fabricate optical waveguides from transparent prepolymers, the next section will discuss their suitability for mass-production and ability to be industrially effective. Additionally, the achieved attenuation values will be compared and discussed.

2.2.1 *Suitability for Industrial Use*

Several aspects of a manufacturing technique have to be considered for its suitability for industry. First, the technique should be relatively fast to allow for cost-effective manufacturing. In most cases, this correlates with the process being *planar*, which means that an entire area is structured by the method, and not only one *linear* track of material. The second important aspect is the ability for *machine flexibility*, which means that the pattern created by the method can be altered without much effort. This allows for rapid and cost-effective change of process parameters and geometries, or even smart and adaptive fabrication. The third aspect is the ability for *contact-free* deposition, which enables the process to be flexibly placed within the process chain. The fourth aspect is if the method is *additive*, which reduces raw material consumption and waste. The classification of the methods into these four categories is listed in Table 2.1. Cases where the classification is unclear are represented with brackets and discussed in the text. The classification is visualised by means of a Venn-diagram [73] in Figure 2.3. Here, an unclear classification is indicated by only half the item touching a circle.

Planar

The ability to create structures over an entire area is a critical requirement for rapid and cost-efficient mass-production. For example, an array of dots can be created on a sheet of paper by hand and a pen very slowly, quicker with a stamp roller, and in a single moment by a stamp or spray technique. For mass production, such planar methods are typically integrated into assembly lines and roll-to-roll systems, which enables to manufacture with a very high through-put. However, a clear classification is sometimes difficult, as many manufacturing methods can be scaled up by parallelisation, for example ink-jet printing.

From the discussed manufacturing techniques, lithography, hot-embossing, e-field-lithography and flexographic printing and are manufacturing techniques that structure an entire area. Direct Dispensing, the Mosquito Method, and electrospinning require a moving needle.

Table 2.1: Classification of different aspects of the manufacturing techniques suitable for manufacturing optical waveguides. Brackets indicate a limitation, which is explained in the text.

Manufacturing Method	Planar/ Linear?	Machine Flexibility	Contact-Free?	Subtractive / Additive?
Lithography	Planar	No	(Yes)	Subtractive
Direct Writing	Planar	Yes	(Yes)	Subtractive
Self Writing	(Linear)	Yes	No	Additive
Hot Embossing	Planar	No	No	Additive
E-Lithography	Planar	No	(Yes)	Subtractive
Flexographic Printing	Planar	No	No	Additive
Direct Dispensing	Linear	Yes	(Yes)	Additive
Mosquito-Method	Linear	Yes	No	Additive
Electrospinning	Linear	Yes	(Yes)	Additive
Ink-jet Printing	Planar	Yes	Yes	Additive

As several dispensers over one area are difficult to realise, these methods are considered linear.

Direct Writing and Ink-jet printing are technically also methods that create a single track. However, the laser beams of direct writing and self-writing can be moved very quickly, and multiple laser beams can be used without interference, which allows such a high degree of parallelisation, up to the point where a micromirror device is used to selectively polymerise with a high resolution over an entire area. Therefore, the technique can be considered a planar technique. Ink-jet printing also has been demonstrated to allow a high degree of parallelisation with thousands of active nozzles, which allows to employ it in roll-to-roll systems. It is therefore considered a planar technique as well.

Machine Flexibility

The second aspect is the ability for **machine flexibility**, which means that process parameters and geometries can be altered quickly. If many units of an identical item are mass-produced, this is not a critical factor. However, the ability to react quickly to customer demand, even in small batches, is an emerging trend [74]. A process with a high
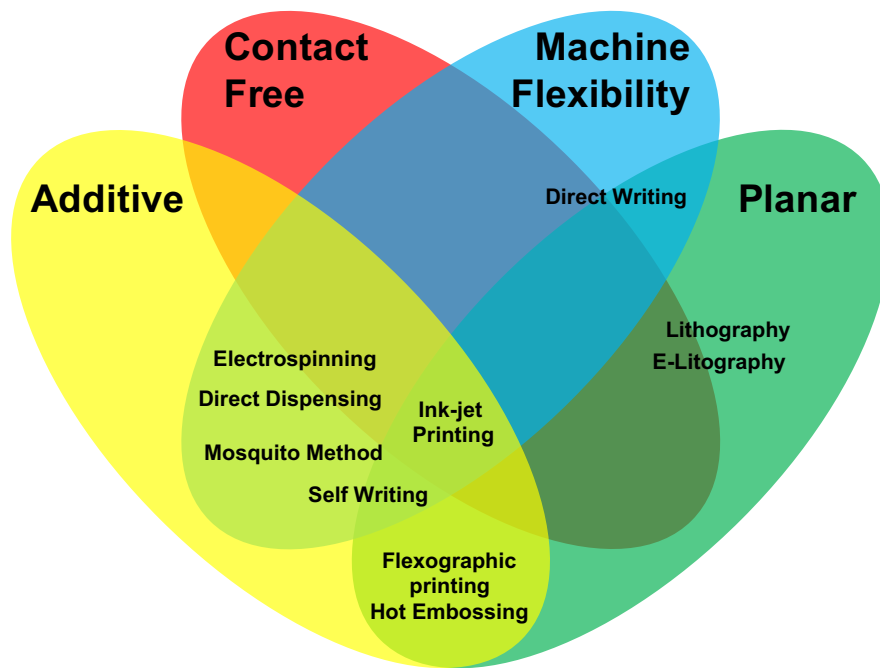
Figure 2.3: Venn-diagram to visualise the classification of the discussed manufacturing techniques. The only technique that unifies all four qualities is ink-jet printing.

degree of machine flexibility can do this without the time- and cost-intensive fabrication of corresponding tools. Additionally, the novel concept of the smart factory, which incorporates methods that measure and adapt the fabrication process autonomously in order to improve the quality of the fabricated product, increase yield, and reduce the required amount of workers in a factory, requires this ability as well.

The planar manufacturing techniques (lithography, hot embossing, E-field-lithography, and flexographic printing) all require a pre-shaped tool. The remaining techniques (direct writing, self-writing, direct dispensing, the Mosquito Method, electrospinning, and ink-jet printing) employ movable or individually active elements which are digitally controlled. This allows to alter the created structures at will, or to manufacture with incremental parameter alterations to reach a desired result.

Contact-Free

The ability to perform a manufacturing step in a contact free manner typically increases independence regarding the geometry of the manufactured part. This is beneficial for all situations where non-uniform substrates and parts are processed. Additionally, a contact-free deposition gives a high degree of flexibility in the placement of the manufacturing method in the process chain, because the method does

not interfere with preexisting structures and discrete elements on the substrate.

Hot embossing and flexographic printing both require physical contact with the substrate foil to create the structure. Lithography, direct writing, self-writing and E-field-lithography, on the other hand, don't require contact of the tool, but require a layer of dispensed material. It depends on the situation if this layer interferes with other process steps. Direct dispensing and electrospinning are technically contact-free, because the needle is moved above the substrate. However, the physical forces between the dispensed track on the substrate, the dispensed jet, and the needle, are important elements of the process, which means that it is not entirely independent of the substrate. For electrospinning, an electrically conductive substrate is additionally required. The Mosquito method again is in full contact of a dispensed layer of material. The only fabrication technique which is genuinely contact-free is Ink-jet printing. Typically, it is performed at a distance of several millimetres from the substrate, and therefore tolerates elevated structures, preexisting tracks, or a corrugated substrate.

Additive

Additive manufacturing means that only the required material is actually deposited. This has several benefits. First, no material waste is created, which makes the method both ecologically and economically attractive. A device using this method can also be placed in an environment where chemical waste disposal is not feasible. Additionally, additive manufacturing typically requires only one deposition and one material processing step, whereas subtractive methods require at least one material removal step as well. This means that additive manufacturing requires less equipment and is sometimes even faster.

In this context, lithography, direct writing, and E-field lithography are considered to be subtractive methods, because it requires a layer of photopolymerisable material, which has to be removed after the patterning step, typically in a chemical bath. This step, including the necessary cleaning and drying, makes the process unsuitable for rapid manufacturing. All other available techniques deposit the light-guiding structures only where they are desired and are therefore considered to be additive methods.

2.2.2 *Demonstrated Optical Attenuation*

To compare the achieved attenuation of the presented works, the results are listed in Table 2.2 and visualised in Figure 2.4. The data is divided into results that were achieved on a flexible polymer foil substrate, and results that were shown on a rigid substrate, either glass or FR4.

Table 2.2: Manufacturing type, dimensions, material, and attenuation for selected optical waveguides. All structures have typical dimensions of around 50 μm. The starting year of the research project described in this thesis, 2013, is indicated by a line.

	Year	Method	Attenuation (dB/cm)	Substrate	Reference
-	1993	Self Writing	< 5 (1500 nm)	rigid	Frisken et al. [24]
a	2002	Lithography	0.5 (800 nm)	rigid	Borreman et al. [19]
b	2003	Lithography	0.36 (830 nm)	rigid	Kim et al. [20]
c	2003	Hot-Embossing	0.19 (650 nm)	rigid	Mizuno et al. [32]
d	2004	Hot-Embossing	0.2 (850 nm)	rigid	Yoon et al. [33]
e	2007	Dispensing	< 0.1 (633 nm)	rigid	Leng et al. [40]
f	2008	Direct Writing	< 0.05 (850 nm)	rigid	Dangel et al. [21]
g	2009	E-Field Litography	1.97 (850 nm)	rigid	Hin et al. [34]
h	2010	Ink-jet Printing	0.47 (850 nm)	rigid	Selviah et al. [69]
i	2013	Direct Writing	0.031 (850 nm)	flexible	Dangel et al. [22]
j	2013	Dispensing	0.06 (850 nm)	rigid	Dingeldein et al. [41]
k	2013	Mosquito-Method	0.033 (850 nm)	rigid	Soma et al. [44]
l	2016	Flexo Printing	0.5 (635 nm)	flexible	Wolfer et al. [16]
m	2017	Hot-Embossing	0.09 (850 nm)	flexible	Rezem et al. [29]
n	2017	Self Writing	0.69 (850 nm)	flexible	Günther et al. [26]
z	2017	Self Writing	n.a.	flexible	Terasawa et al. [27]
o	2018	Ink-jet Printing	0.61 (650 nm)	flexible	Theiler et al. [72]
p	2018	Ink-jet Printing	0.55 (633 nm)	rigid	Alamán et al. [71]

The attenuation values range from 0.03 to 2.0 dB/cm. Until 2010, all published results were on rigid substrates. After that, a trend towards flexible substrates can be seen.
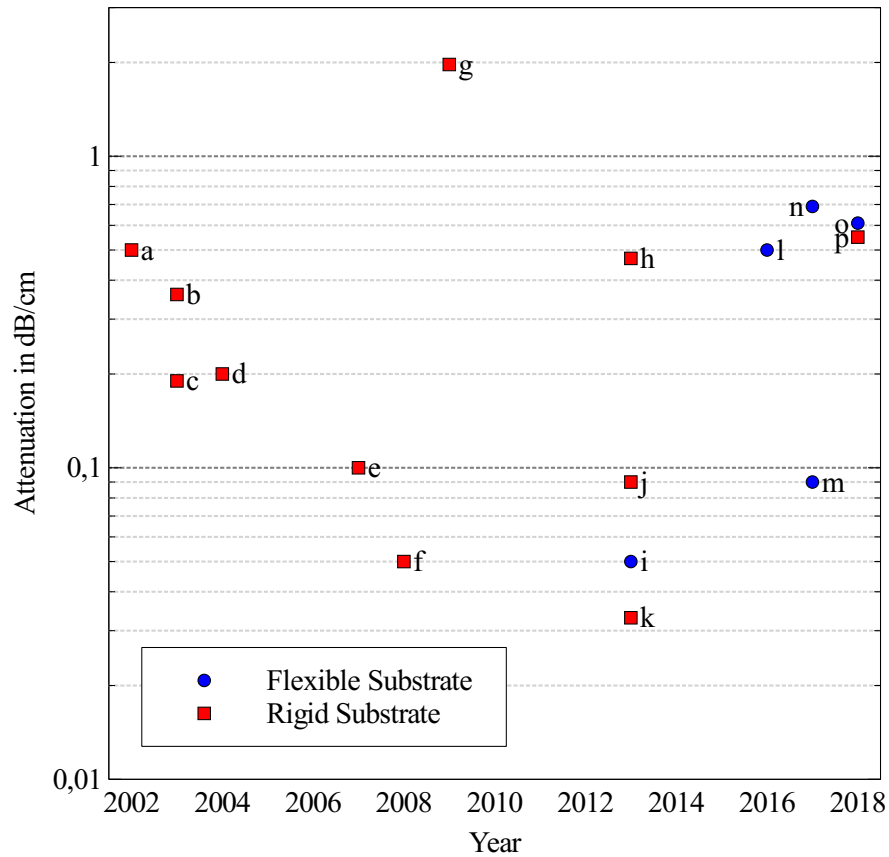
Figure 2.4: Published attenuation values of polymer optical waveguides fabricated on planar substrates by various methods from 2002 to 2017. The result by S. J. Frisken (Self-writing, <5 dB/cm, 1993) is excluded from the graph. The data is grouped in results on rigid and flexible substrates. The latter started appearing only after 2010.

2.3 INTERMEDIATE CONCLUSION AND RESEARCH GOALS

From the discussed manufacturing techniques, ink-jet printing is the only technique that unifies all advantages for mass-production which were considered. Whereas other described techniques are only feasible on a laboratory-level, ink-jet printing has a demonstrated ability to create planar patterns with high precision and through-put. Yet, only a few published results with attenuation values exists for this technique, and it can realistically expected that ink-jet printing is the most suitable technique to create networks on planar substrates. Due to this expectation, the ink-jet printing of optical waveguides is an attractive field of research which has gained interest in recent years.

Before the onset of this research project in 2013, all published results on ink-jet printing of optical waveguides were on rigid glass slabs as substrate. While glass is certainly a suitable material in regard to its optical properties and established processability for optical

applications, glass slabs are neither light nor roll-to-roll compatible. They require single-substrate processes, which places ink-jet printing in direct competition with established lithography. To avoid this, flexible, optically transparent polymer foils, which are compatible with roll-to-roll manufacturing, will be investigated as substrate material. **The theoretical and experimental demonstration of light transmission through an ink-jet printed optical waveguide on flexible polymer foil substrate** is the first research topic of this thesis. The selected attenuation limit for a practical application is 1 db/cm.

All groups reported difficulties when trying to create elevated structures. While the team from Drexel University did not address the problem in their publication at all, the researchers from Microfab solved the problem by careful tuning of the substrate temperature. This method, however, is only feasible for a hot-melt ink. The team from OPCB attempted three methods: surface energy modification, cooling the substrate, and intermediate polymerisation. The second and the third method were successful, but they are connected with several problems. The first problem is that many inks require a nitrogen atmosphere to fully polymerise. If each layer is polymerised, a nitrogen atmosphere is necessary around the print-head, which is often difficult to realise. The second problem is that many inks require a volatile solvent to be printable. This solvent has to be evaporated before polymerisation, which requires heat and time. However, heating the substrate is typically problematic for polymer substrates, because their glass transition temperature is much lower than that of glass. Choosing a lower temperature extends the time-frame that is required for full evaporation of the solvent, or prohibits it entirely. Additionally, the required cooling technology is not easily integrated in roll-to-roll printer systems. Because of these problems, an alternative **method to print elevated structures on polymer substrates** will be sought. This is the second research topic.

Additionally, none of the waveguides presented in prior publications were integrated into an optical network of light sources, optical waveguides, functional structures, and detectors. This, however, is critical to demonstrate the benefits of additive manufacturing of such structures. Naturally, the integration of all of these components would exceed the scope of this thesis, especially when considering that all elements are still under research. The first step to achieve this, however, is the **integration of light sources**. This is the third research goal of this thesis.

3

THEORETICAL BACKGROUND

Having formulated the research topics of this thesis, this chapter will cover the necessary scientific background. First, the optical phenomena that occur during the propagation of light in an optical waveguide will be presented. Then, different strategies to create inks that allow for fabrication of optical waveguides will be discussed, and the ink-jet printing of such inks for optical applications will be explained.

3.1 LIGHT

Light is born a particle, lives as a wave, and dies as a particle.

(A. Einstein) [75]

The quote by Einstein refers to the *Wave-particle duality*, the fact that certain optical phenomena can be described with a wave model, others only as with a particle model. Because of this duality, some of the following explanations will use the concept of waves, others will model light as photon particles.

3.1.1 *Light in Vacuum*

When light is propagating, the commonly used model is the electromagnetic wave, with the wave vector $\vec{k}$ and a magnitude $\vec{E}$ and $\vec{B}$ of the electric and magnetic field. Figure 3.1 shows how these properties correlate. Directly related to the wave vector $\vec{k}$ is the wavelength λ, which is responsible for the perceived colour of light:

$$\lambda = \frac{2\pi}{k} \tag{3.1}$$

Between the wavelengths of 400 nm and 800 nm, an electromagnetic wave is visible for humans as colour, as shown in Figure 3.2. Light with longer wavelengths is part of the infra-red spectrum, light with shorter wavelengths part of the ultra-violet spectrum. Both are invisible to the human eye, but are used for many optical applications.

In vacuum, the velocity of light c_0 is about $3 \cdot 10^8$ m/s. This value can be calculated following *Maxwell's Equations*, which are the mathematical descriptions of electromagnetic waves. From the velocity of
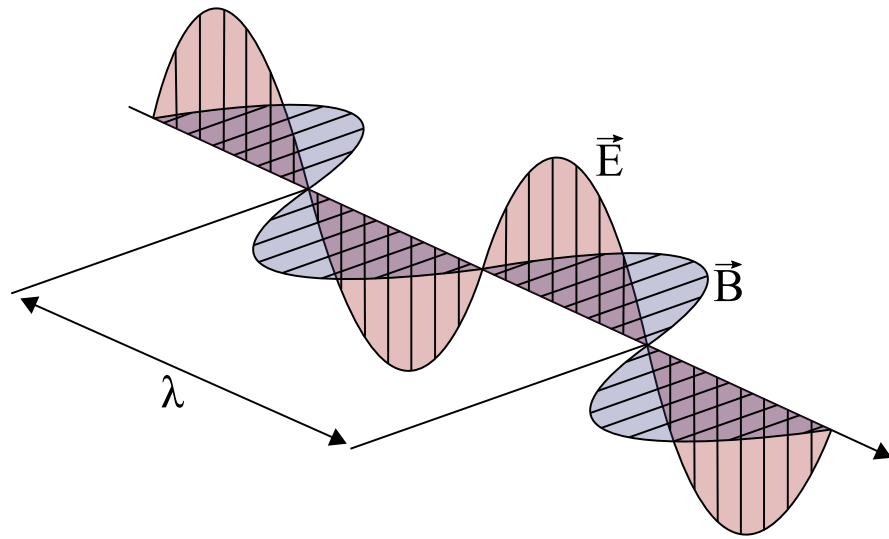
Figure 3.1: Graphical representation of a linearly polarized and sinusoidal electromagnetic wave, showing the wave vector $\vec{k}$, the wavelength λ, and the electric and magnetic fields $\vec{E}$ and $\vec{B}$
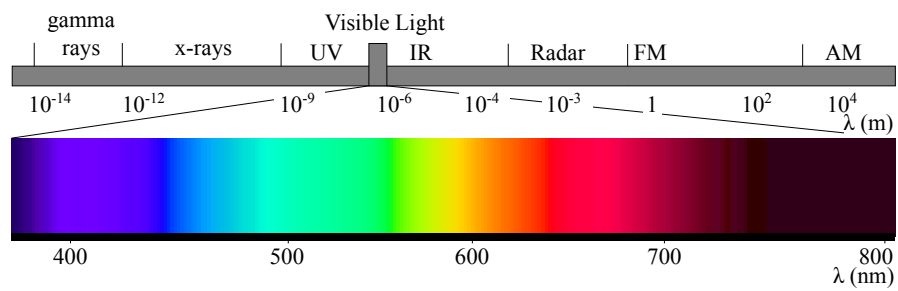
Figure 3.2: The electromagnetic spectrum from gamma rays to radio waves, with the section of visible light expanded and shown with the respective colour.

light c and the absolute value of the wave vector $\vec{k}$, the angular frequency ω of light can be defined.

$$\omega = c \cdot |\vec{k}| \tag{3.2}$$

3.1.2 *Light in Matter*

In transparent media, the alternating electric and magnetic fields E and B of an electromagnetic wave polarise the electric dipoles in matter [5], which reduces the propagation speed c. The physical explanation for this effect can again be derived from *Maxwell's Equations*. For technical purposes, it is sufficient to express a factor by which the propagation is retarded, n, called *refractive index* .

$$n = \frac{c_0}{c} \tag{3.3}$$

As the interaction with matter varies for different wavelenghts, c in matter varies over wavelength as well. As a result, a polychromatic pulse of light containing many different wavelengths *disperses* while travelling through an optical medium. A commonly used approximation tool is the *Abbe Number* ν_e, which is defined as

$$\nu_e = \frac{n_e}{n_F' - n_C} \tag{3.4}$$

with n_e, n_F', and n_C being the refractive indices at the Fraunhofer lines e (546 nm), F' (480 nm) and C (545 nm). Some researchers use an alternative definition ν_d, which uses the Fraunhofer d line at 588 nm instead of the e-line. A higher Abbe number represents a lower degree of dispersion. Typical values for polymers range between 30 and 60. For applications where a single wavelength is sufficient, a monochromatic light source is typically used to avoid any dispersion effects.

When a photon encounters electrons, atoms or molecules, it can be absorbed, if its angular frequency ω matches a resonance which is present in that material. An absorption band at the corresponding wavelength λ is the result. The superposition of different absorption mechanisms results in an absorption coefficient $\alpha(\lambda)$ at each wavelength. For a given distance d and an initial intensity I_0, the transmitted intensity I can be used to calculated with a formula known as *Beer's Law*:

$$I(z) = I_0 e^{-\alpha z} \tag{3.5}$$

With this equation, the attenuation coefficient of a material can be derived from a measurement of the transmitted intensity of a sample with a given thickness z.

A second important phenomenon that occurs when light is travelling through matter is *scattering*. Here, optical inhomogeneities in matter cause a photon to change its direction and magnitude. Depending on the size, different scattering mechanisms occur. For inhomogeneities much smaller than the wavelength, like molecules, or even atoms, *Rayleigh scattering* occurs. As it's strength varies with wavelength by λ^{-4}, it becomes much more significant at short wavelengths, and is the reason that the earths atmosphere scatters blue light stronger than red light.

Scattering at inhomogeneities that are in the same size range as the wavelength, like particles, bubbles, or macro-molecules, is described by *Mie Scattering*. This phenomenon does not scale as strongly with the wavelength, which means that inhomogeneities in this range cause a wider absorption spectrum.

In optical polymers, impurities and density fluctuations cause both Mie and Raleigh scattering [76–78]. Additionally, it is classified into *intrinsic* and *extrinsic* effects. Whereas intrinsic absorption and scattering is caused by the material itself and can only be reduced by a different optical material, extrinsic effects are caused by material contamination, gas inclusions, or surface roughness. For example, the Raleigh scattering caused by the complex structure of a polymer molecule is an intrinsic effect, whereas the Mie scattering at a gas inclusion is an extrinsic effect.

3.1.3 *Waveguide Attenuation*

Light in an optical waveguide loses intensity over distance. Because the intensity at the end facet of an illuminated waveguide is a combination of coupling and waveguide losses, it is necessary to measure the transmitted power P_1 and P_2 of two samples with a length difference Δl. The attenuation μ can be calculated with a modified form of *Beer's Law*:

$$\mu = 10 \cdot \log_{10} \frac{P_1}{P_2} \cdot \frac{1}{\Delta l} \tag{3.6}$$

3.1.4 *Light at Interfaces*

Electromagnetic waves that encounter an interface of two different media with n_1 and n_2 are partly reflected. Such reflections are called *Fresnel Reflections*. The reflected fraction R of a monochromatic wave depends on the refractive index step between n_1 and n_2 and the angle of incidence. At perpendicular incidence, it can be calculated by

$$R = \frac{n_1 - n_2}{n_1 + n_2}^2 \tag{3.7}$$

With this phenomenon, it is possible to measure the refractive index of an unknown material from the reflected intensity at an interface with a reference material. For angles of incidence other than 90°, Fresnel reflections occur as well, and the ratio of reflected and refracted light can be calculated [5].

As presented in the previous chapter, light travels slower when it enters a material with higher refractive index. The reason why this material property is not called *retardive index* although it is the factor of which light is slowed down in that medium is due to the fact that, historically, another effect of this material property was observed and applied technologically before: light refraction - a defined change of direction of light propagation. The origin of this effect becomes clear in Figure 3.3, which shows a wavefront of an electromagnetic wave that encounters a medium with a certain refractive index at a certain angle.
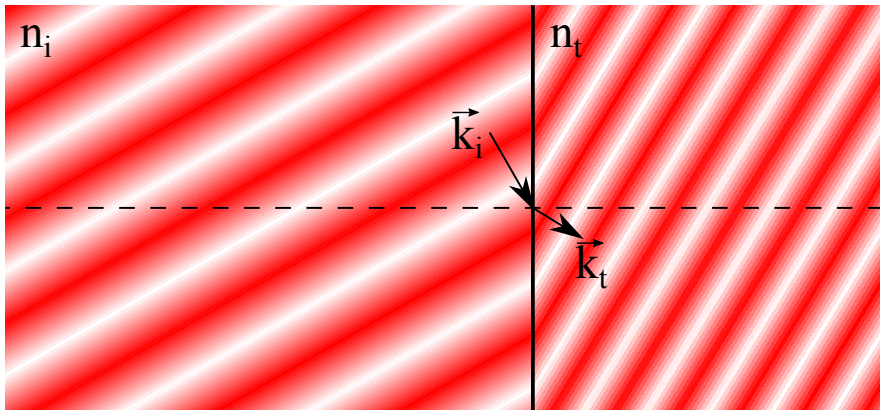
Figure 3.3: Schematic of a wave front entering a retarding material in an oblique way, drawn after a figure by R. Feynman [79].

The part of the wave inside the medium travels slower, while the part of the wave that has not yet entered the material travels at its original velocity. This causes the effective wavefront to change direction, and is the reason for the ability of optical media to refract light.

The mathematical representation of this phenomenon was published in 1621 as *Snell's law* [5]:

$$n_1 \sin \theta_{in} = n_2 \sin \theta_{out} \tag{3.8}$$

The equation applies either for an interface between a transparent material to vacuum or air, or for the interface between two optical materials with different refractive indices.

Of course, dispersion, the wavelength dependency of velocity of light c and refractive index n, is critical here, because it means that different wavelengths experience different refraction. This effect is the reason that a prism splits a white beam of light up into it's multi-coloured parts.
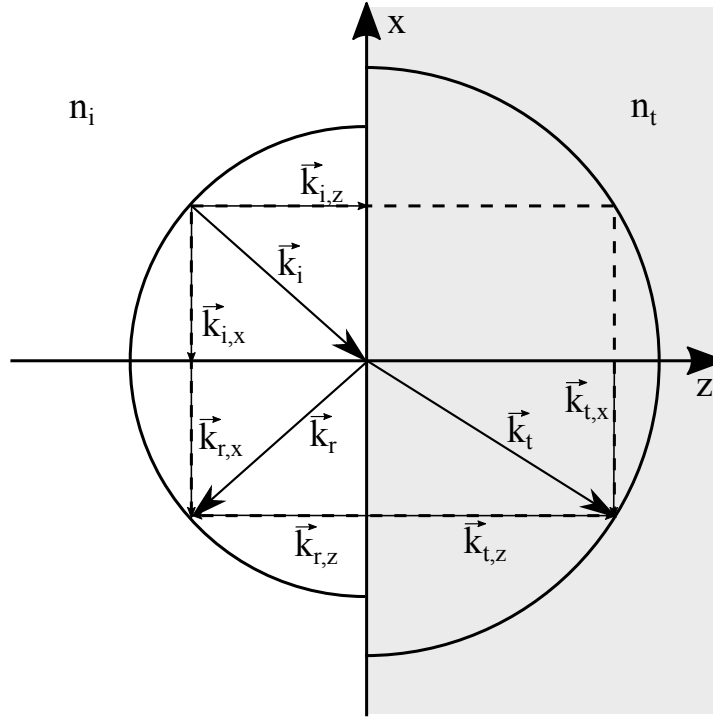
Figure 3.4: Ewald Sphere to calculate refraction of light for the situation when n_t is larger than n_i.

Naturally, an optical interface is rarely perfectly flat, and the scattering phenomena discussed in the previous chapter have to be considered here as well. Polymers often show crystalline and amorphous areas, with different refractive indices. This causes light scattering at these boundaries, increasing the effective attenuation of the material. The criterion for a "good" optical surface is typically a roughness value of 10% of the respective wavelength.

A useful tool to understand why *Snell's law* describes the directions of reflected and refracted light is the *Ewald-Sphere* [80, 81]. This model, shown in Figures 3.4 and 3.5, uses a two- or three-dimensional projection of an incident wave with a propagation vector k travelling towards an optical interface between two media with different refractive indices n_i and n_t. On both sides of the interface, a semi-circle (or semisphere) is drawn, with the radius $\vec{k} \cdot n$ and the point of incidence as shared centre. The incoming wave-vectors $\vec{k_i}$ is split up into a parallel component $\vec{k_{i,x}}$ and a normal component $\vec{k_{i,z}}$. Two situations are shown: n_t is greater than n_i, and vice versa. Magnitude is not covered by the Ewald Sphere, but can be calculated by the Fresnel Equations.

The reflected part of the wave $\vec{k_i}$ results in $\vec{k_r}$. The parallel component $\vec{k_{r,x}}$ is equal to $\vec{k_{i,x}}$, whereas the normal component changes it's direction $\vec{k_{r,z}} = -\vec{k_{i,z}}$. The transmitted part of the wave is k_t. Upon passing the optical interface, the normal component of the k-vector $\vec{k_{t,z}}$ changes its length by factor Δn. The parallel component $\vec{k_{t,x}}$ is
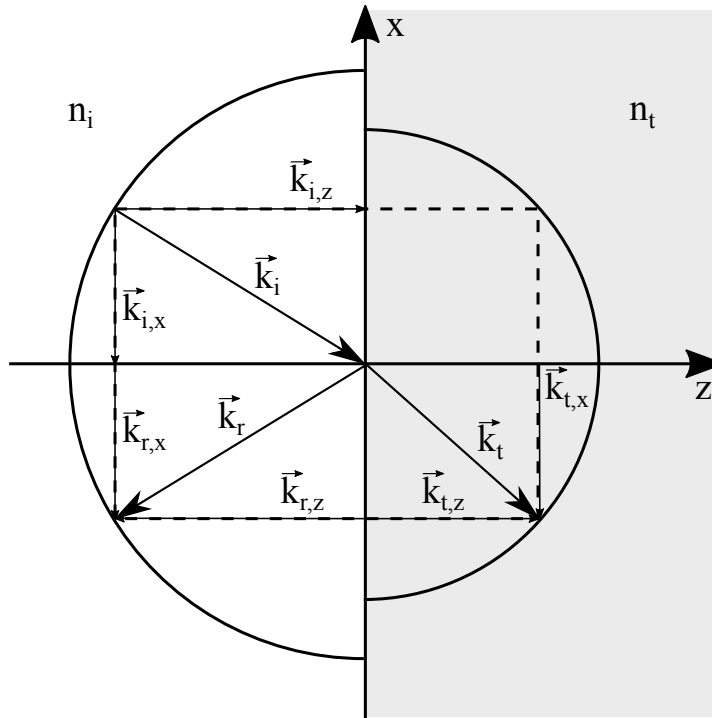
Figure 3.5: Ewald Sphere to calculate refraction of light for the situation when n_t is smaller than n_i.

unaffected by the interface, just like for the reflected part. From the two vectors or the resulting rectangle of $\vec{k_{t,x}}$ and $\vec{k_{t,z}}$, the k-vector of the propagating wave $\vec{k_t}$ can be constructed, and simple trigonometry allows to derive *Snell's law*.

3.1.5 *Reflected Light*

Under certain circumstances, the rectangle in an Ewald Sphere cannot be constructed within the radius $\vec{k} \cdot n$, and *Snell's Equation* cannot be solved. This occurs when an optical wave inside an optical medium with a given refractive index n_1 encounters an interface to a material with lower refractive index n_2, and with an incidence angle close to 90°. As the exit angle cannot exceed 90°, no propagating mode within the material with n_2 exists, and the entire wave is reflected. This phenomenon is called *total internal* or *dielectric* reflection. Figure 3.6 shows an Ewald sphere similar to Figure 3.5, but with the parallel component of k_i being so large that the transmitted vector k_t does not fit into the semicircle after the interface. For k_r, the same methods applied before are suitable.
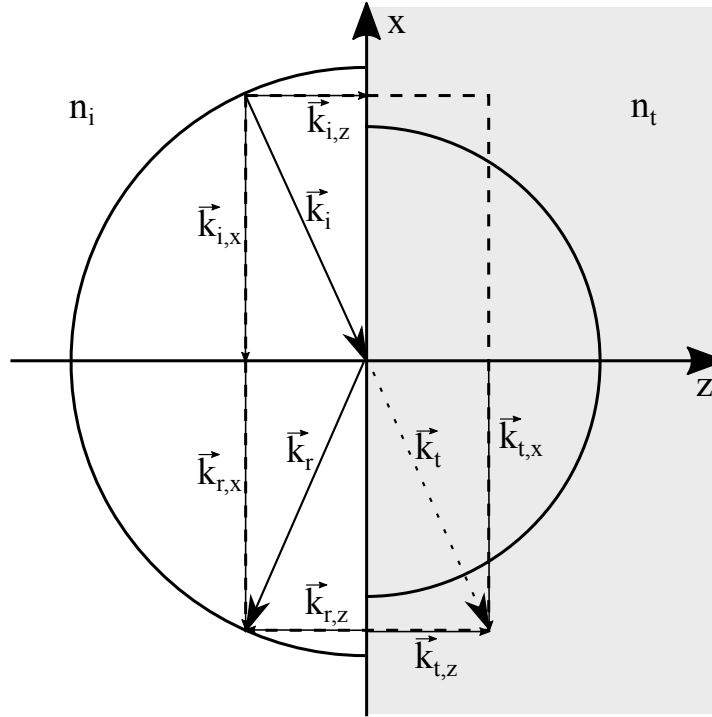
Figure 3.6: Ewald Sphere for situations where total internal reflection occurs. The k-vector of the transmitted beam does not fit into the sphere, therefore the entire light ray is reflected.

The threshold angle of this phenomenon is commonly called *critical angle* θ_c, and depends on the refractive indices present at the interface.

$$\theta_c = \arcsin \frac{n_2}{n_1} \tag{3.9}$$

During the reflection phenomenon, the energy of the photon is present as evanescent field in the medium n_2. Therefore, this material still requires to be optically transparent in order to reflect without any losses. The penetration depth of the evanescent field is in the order of a few wavelengths.

However, if both materials are optically transparent, the phenomenon of total internal reflection allows to carry light inside a transparent medium with a higher refractive index than its surroundings over a long distance. This is how optical waveguides work.

An alternative to dielectric reflection is the application of a metal interface to cause reflection. As the electrons in metals travel freely between the atoms, electromagnetic waves inside are quickly absorbed, which is why metal layers thicker than a few wavelengths are optically intransparent. However, depending on the material and wavelength, photons can be reflected at the interface. Most metals, like aluminium and silver, are reflective over the entire visible spectrum, and therefore reflect white light. Other metals, like gold or copper, absorb
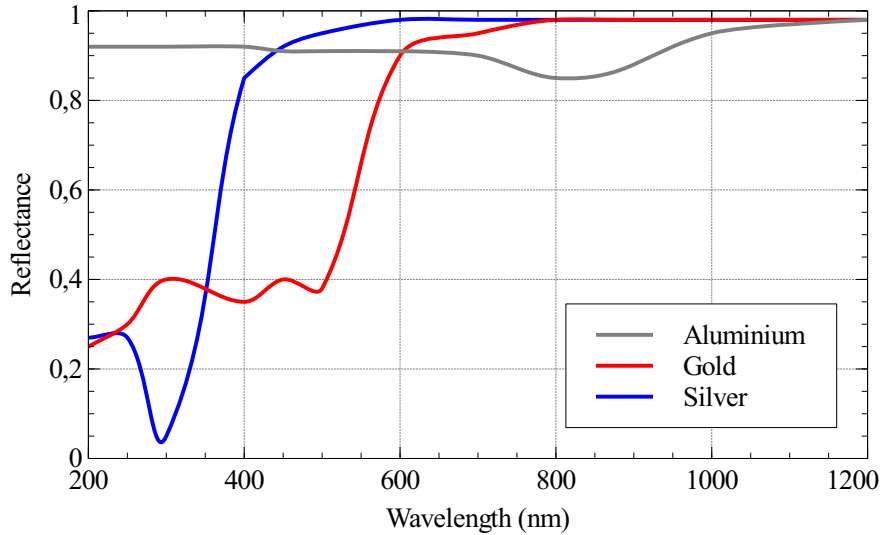
Figure 3.7: Reflection coefficient of aluminium, silver, and gold over UV, visible, and near-infrared spectrum.

blue photons, and reflect the rest of the visible spectrum, which is the reason of their colour. The reflection coefficient of different metals over the visible spectrum is shown in Figure 3.7. However, in comparison to total internal reflection, the evanescent field at reflection is always partly absorbed, so metallic reflection is always lossy. Therefore, metallic reflection is not suitable to carry light over long distances by repeated reflections. But, while dielectric reflection requires a flat angle of incidence, metallic reflection is independent of this value. The reflection angle is identical to the angle of incidence in all situations, which makes this method suitable for applications where reflection independent of angle of incidence is required, like mirrors. As a design rule, metallic reflection should be chosen when the goal is to maximise the reflection angle of a reflective surface. Total internal reflection should be chosen when the goal is to minimise the energy which is lost at the reflection.

3.2 INK FORMULATIONS

Having presented the physical phenomena that occur in optically transparent materials, the next section will show how an ink suitable for the ink-jet printing of polymer optical waveguides is created. Three requirements of such an ink will be discussed: Optical transparency, suitably low dynamic viscosity η for ink-jet printing, and a mechanism to turn into a solid after printing.

3.2.1 *Optical Transparency - Base Material*

Despite the fact that glasses are superior to polymers in terms of transparency, chemical and mechanical resistance, and available range of refractive index, they are being replaced by optical polymers in many applications. Typically, the molecular structure of polymers does not cause photon absorption at wavelengths between 400 nm and 1200 nm, which enables their application for optical structures. Additionally, polymers can be processed in the liquid liquids, and at temperatures below 200 °C [82], or even room temperature, in the form prepolymers – a term for reactive monomers or short oligomers with unreacted functional groups that polymerise upon a trigger.

To achieve good optical transparency, this polymerisation has to be controlled carefully. If crystalline and amorphous domains are created simultaneously, as shown in Figure 3.8, the polymer turns opaque, because these domains show different refractive indices, causing light scattering at each interface. The polymerisation and crystallisation can be controlled by carefully tuned process parameters, or additives that affect these processes.

Predominant in printable optical polymers are acrylate materials, of which more than 800 different types are commercially available [83]. This material class offers many advantages that are important for ink-jet printing of optics, such as good polymerisability and high optical transparency. Because the acrylate group is polar, an ink made from this material will show good adhesion on many different substrates. Additionally, combinations of acrylates with other polymers have been studied and applied extensively, which enables tailored material properties. A common co-polymer for acrylates are epoxy resins [83, 84], resulting in epoxy acrylates. Ink-jet inks based on epoxy acrylates typically have a higher refractive index than acrylates and are more resistant against solvents, but also more brittle. A good overview and example formulations of ink-jettable acrylate inks can be found in the book by Magdassi [83].

An alternative base material to acrylates are siloxanes. Typically, they are associated with a low chemical reactivity, which makes them relatively resilient against heat and ageing, but also more difficult to control on a substrate and polymerise after printing. Yet, a printable material for the fabrication of optical waveguides that combines epoxy and silane functionalities was presented recently [71].

3.2.2 *Printability - Viscosity Modification*

Piezoelectric printheads, which are the most common design in a research environment, typically operate with inks with a dynamic viscosity between 8 and 15 mPa·s [51]. Polymer resins, used to create polymer-optical structures, on the other hand, typically have a much
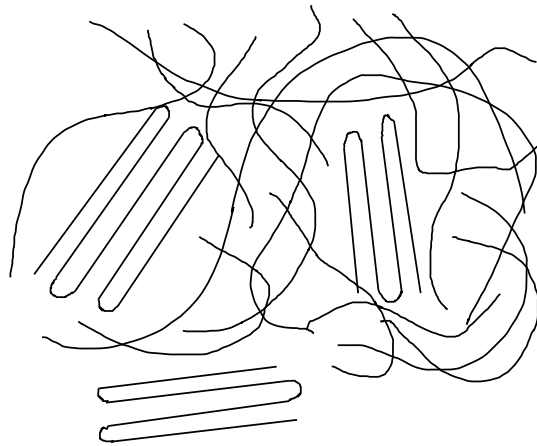
Figure 3.8: Graphical representation of an amorphous polymer with crystalline domains, shown as areas with parallel polymer chains. At the interfaces between the two regions, refraction occurs due to different refractive indices.

higher viscosity in the range of 1 Pa·s. Therefore, it is necessary to modify the viscosity of polymer resins in a way that allows ink-jet printing.

The most common method to reach the required value is to mix them with volatile solvents, typically oxygenated organic compounds, such as alcohols. A wide array of solvents is available, and several solvents can be combined to tune other parameters of the ink, like surface tension or evaporation rate. Before polymerisation, the volatile solvent has to be evaporated in a pre-bake step, which reduces the volume of the structures and often poses a source of thermal stress for the fabricated structures and the substrate. Often, the volume share after evaporation of the solvent is only a few percent, the majority of the deposited volume evaporates after printing, and flat tracks of dry material remain. The cross-sectional shape of the track is affected by convection effects like *coffee staining*, which can be exploited to achieve a desired profile [51].

To achieve elevated tracks, however, the solvent approach for the ink formulation is undesirable, as it is necessary to maintain the deposited volume and track height.

The simplest method to reach printability while maintaining the deposited volume is to heat the liquid. Between 25 °C and 75 °C, the dynamic viscosity of unpolymerised monomers and oligomers tends to show a good response to temperature change, which can be exploited to reduce dynamic viscosity and tune the drop formation process. Therefore, many printheads feature heating elements to enable this method.

If heating is insuficcient, a solvent that cures with the base material after deposition, called a reactive diluent, can be used. This ink component, typically a short monomer, features a reactive group which

can co-polymerise with the base material. As a result, a network of polymer and co-polymer that incorporates both the base material and the reactive diluent is created, with the benefit that the potentially problematic pre-bake step can be avoided, and polymerisation can be performed directly after the deposition of the material. Ethylene glycol dimethylacrylate (EGMDA) is an example of an acrylate that is commonly used as reactive diluent.

3.2.3 *Solidification - Radical Polymerisation*

To turn the liquid base material into a solid polymer network, the reactive groups of the printed oligomers need to bond together. Here, a polymerisation initiator is used, which is a substance that reacts to a photon or thermal trigger with break-up and the formation of free radicals. These free radicals - typically oxygen - have a high electronegativity and break an existing, weaker, chemical bond in the base material - typically a carbon double blond - and bind to these molecules. An unpaired electron remains from the broken chemical bond in the base material, which causes another bond to open and attach to the growing molecule. This polymerisation reaction repeats itself until it is terminated at a second unpaired electron or a free radical from a photo initiator. By tuning the concentration of free radicals, the average chain length can be controlled.

For ink-jet printing, thermal initiators are typically unsuitable, as the ink is often heated for printing, and shear forces occur during the printing process. Both can trigger preliminary polymerisation, clogging the printhead. Therefore, initiators that react to UV-light are commonly used. Although commercial materials are available, there is continuous research in the field [85, 86] which discusses common problems, such as is oxygen inhibition. Here, the oxygen from ambient air terminates the polymerisation process, resulting in an inhomogeneous polymerisation. The issue can be avoided by performing the polymerisation under inert atmosphere.

3.3   INK-JET PRINTING OF ELEVATED STRUCTURES

Ink-jet, as presented in the previous section, is a technique where liquid material is deposited on a substrate by firing individual droplets at defined positions. The process can be divided into two phases, the drop formation at the printhead, and the drop impact on the substrate. Because a commercial laboratory printer was used for the experiments, the drop formation worked reliably, and the research focus is on the second phase. In the following section, it will be discussed how a droplet behaves after landing on a substrate, and how this behaviour can be controlled to achieve an continuous track that can serve as an optical waveguide. Additionally, a set of equations to
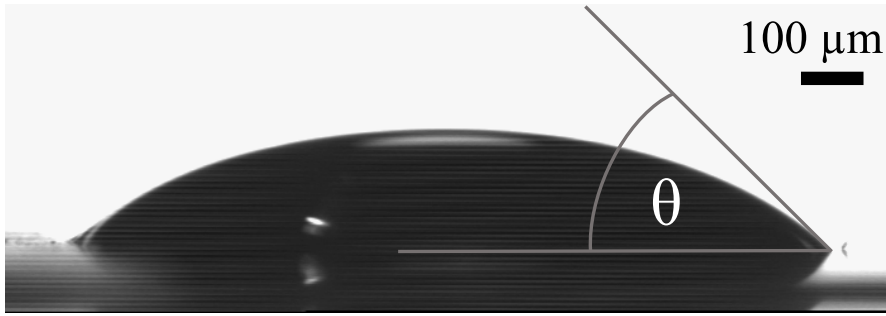
Figure 3.9: Microscope image of a deposited droplet, showing the contact angle θ.

describe the geometry of a printed track with a semi-circular cross-section are presented.

3.3.1 Contact Angle - Young's Equation

The most important parameter to describe the behaviour of a deposited droplet on a surface is the contact angle θ, shown in Figure 3.9. At small scales, the contact angle is independent of gravity and the droplet volume. A two-dimensional model of a straight liquid interface is chosen for a mathematical description of this behaviour, with length units w, parallel to the liquid interface, and l, perpendicular to the interface. The magnitude of θ is the result of the balance between the interfacial energies γ per area $\ell \cdot w$ of the solid-liquid (sl), the solid-gas (sg), and the liquid-gas (lg) interface (γ_{sl}, γ_{sg} and γ_{lg}, respectively).

For ideal surfaces, which are perfectly flat, rigid, and chemically homogeneous and inert, the contact angle can be derived from the sum of Gibbs free energy contributions $\mathcal{G}_i$ of the interfacial energies. For a small displacement $\delta\ell$ of the liquid, a variation in the Gibbs energy $\delta\mathcal{G}$ follows. At the equilibrium state, this variation equals zero [87].

Figure 3.10 shows the effect of a virtual displacement $\delta\ell$ on the interfaces. Under the assumption that the displacement $\delta\ell$ does not affect the area width w, the equilibrium state can be formulated as

$$\delta\mathcal{G} = w \cdot (\gamma_{sl}\delta\ell + \gamma_{lg}\delta\ell \cos\theta - \gamma_{sg}\delta\ell). \tag{3.10}$$

By equating $\mathcal{G}$ to 0, simple rearrangement leads to what is known as *Young's equation* [88], first formulated in the present form by Bangham and Razouk [89, 90].

$$\cos\theta = \frac{\gamma_{sg} - \gamma_{sl}}{\gamma_{lg}} \tag{3.11}$$

However, this model is only valid for ideal surfaces where the contact line is free to move by a small displacement $\delta\ell$. In reality, the
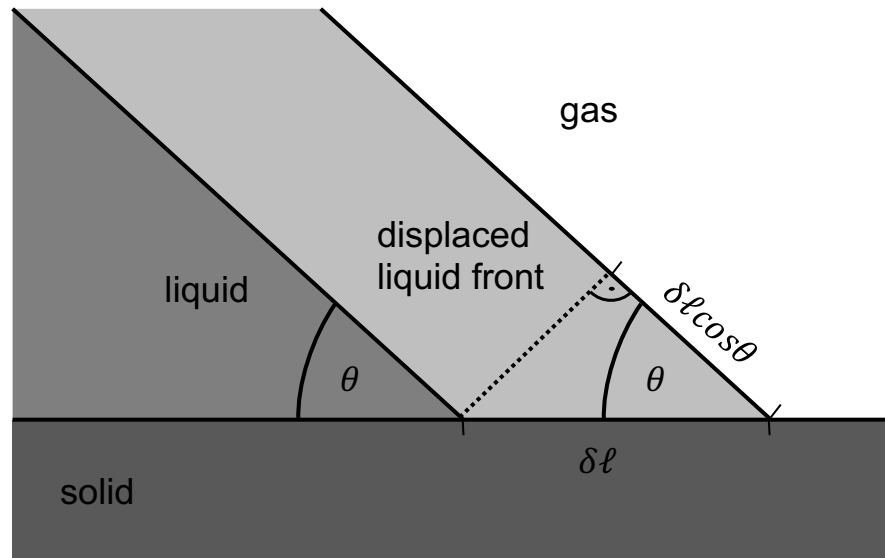
Figure 3.10: Theoretical model of a liquid front displaced by an increment $\delta\ell$. [87].

contact line tends to pin to its current position due to roughness and chemical bonds, resulting in different contact angles at an advancing contact line and a receding contact line, expressed by an advancing contact angle θ_a and a receding contact angle θ_r. The values can be measured experimentally by the sessile drop method, in which a a needle is placed within a droplet to increase of decrease the droplet volume, while measuring the respective contact angle, or alternatively the sliding drop method, where the substrate is tilted until the droplet begins to slide. This method was extensively studied by R. Tadmor [91–93], who also demonstrated in sliding drop experiments that θ_a depends on the time between the deposition and the tilting of the substrate [94].

Contact angle and surface energy are critical parameters and significantly influence the resolution of the ink-jet printing process, because the behaviour of an ink droplet upon impact defines the minimal pixel distance. If the droplet spreads out further than the droplet distance, the pixels merge. This behaviour is greatly affected by the substrate material, and can be altered with surface treatment with ozone or strong UV-radiation, or by heating the substrate.

3.3.2 *Printed Tracks*

After landing on the substrate, droplets with a given volume V_d (typically between 10 pl and 100 pl) spread out to a spherical cap shape with the contact angle θ_a. In order to create a continuous track, the drop spacing length x must be low enough for these structures to merge. For a given number of layers n, the deposited volume V_t per x is $V_t = V_d \cdot n$. Subsequently, the cross-section area $A = \frac{V_t}{x}$. For the
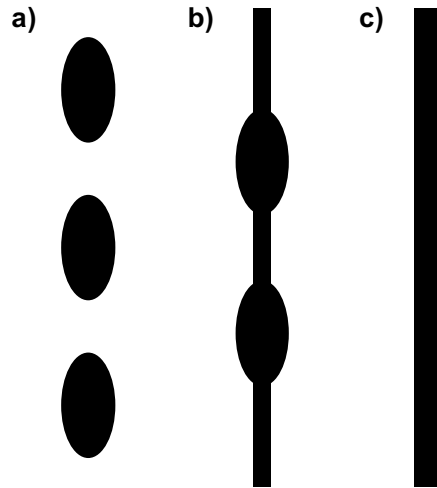
Figure 3.11: Three morphologies of a printed track, showing cases where the material forms individual droplets (a), a continuous line with regular bulges (b), or a continuous and homogeneous track (c).

calculation of the track height h, the approximation formula $h = \frac{3}{2} \cdot \frac{A}{w}$ can be used [95]. The aspect ratio $R = \frac{w}{h}$ is also an important parameter.

However, when a continuous liquid track is created on a flat surface, the droplets tend to recede into individual droplets, like rain droplets on glass. A theoretical study by Davis [96] shows that, when θ_a and θ_r are identical, and the contact line does not show pinning, a printed line is always unstable, because it is energetically favourable to form individual droplets, as shown in Figure 3.11. This was later experimentally demonstrated with printed water on flat surfaces by Schiaffino & Sonin [97], and P. C. Duineveld [98]. This means that the difference between advancing and receding contact angles, and surface pinning, are critical factors for creating continuous lines with a good contour accuracy. Ideally, the receding contact angle θ_r is zero, meaning that the ink does not de-wet the surface. Then, it can be assumed that a printed track maintains a uniform shape with straight, parallel edges.

In order to carry light, a track must not only be homogenuous and continuous, but also requires a certain height. In experiments, it shows that only a certain amount of ink per length unit can be deposited. If this amount is exceeded, a smooth track begins to show bulges. This issue is addressed in the paper by P. C. Duineveld [98].

The modelling begins with the Young-Laplace-Equation, which describes the pressure difference at both sides of a liquid interface with the radii of curvature R_1 and R_2, caused by the surface tension γ. Its

groundwork was developed by Young [88] and Laplace [99] independently, and it can be derived from the Gibbs energy as well [87].

$$\Delta p = -\gamma \cdot \left(\frac{1}{R_1} + \frac{1}{R_2} \right) \tag{3.12}$$

For a printed line, R_1 is finite, but R_2 is infinite, which alters the equation to

$$\Delta p_{Track} = \frac{-\gamma}{R_1} \tag{3.13}$$

By theoretical modelling of an infinitely small width change and the resulting change in pressure in this section, it can be shown that up to a contact angle of θ_a, the pressure in the bulge is higher, which causes material flow out of the bulge, preventing its growth. When the contact angle of the printed track exceeds θ_a, an area with a slightly larger width shows a lower pressure than the surrounding track. As a result, ink flows into this area, which results in the growth of a bulge, as shown in Figure 3.11 b. Because of this behaviour, a continuous track of liquid material (Figure 3.11 c) can only be printed up to a contact angle θ_a.

If higher structures are desired, θ_a has to be increased, either by modification of the surface energy, or simply by exploiting the *resting time effect* published by R. Tadmor, described in section 3.3.1.

An alternative strategy to achieve higher structures is to cure the ink before it can flow into individual droplets. Rapid UV-curing is quite common in printing for to achieve this, especially in roll-by-roll systems, where the substrate with freshly printed ink is moved under a UV-lamp within fractions of a second. Alternatively, the substrate can be cooled down, increasing the ink's dynamic viscosity upon impact, or even freezing it. Several available experimental methods to alter the ink behaviour on the substrate are described in Chapter 6.

METHODS AND MATERIALS

Having introduced the motivation for the chosen topic, the state of the art, and the theoretical background, the next section will discuss a process chain for the fabrication of optical waveguides by ink-jet printing and the subsequent sample preparation and characterisation. Then, the equipment which was used for these steps, and the materials which were evaluated for the fabrication of optical waveguides will be presented.

4.1 CONCEPT

The first step to create an ink-jet printed optical waveguide is to deposit many individual droplets of an ink in such a fashion that they merge on a substrate and form a continuous track (Figure 4.1 a). In the present project, photopolymerisable inks with suitable optical properties were chosen, which are liquid when printed, but can be polymerised by UV-radiation after deposition (Figure 4.1 b). A track created in this fashion would already carry light, but is exposed to external influences which disturb the light transmission. To avoid this, another material with suitable optical properties is deposited to create an upper cladding layer (Figure 4.1 c).

After this step, the waveguides are cut to defined lengths, and facets are created at both sides by polishing to allow light coupling for characterisation (Figure 4.1 d). These samples are then placed in a characterisation stage with light emitter at one side, and a camera detector at the other side (Figure 4.1 e). By taking transmission values of samples with different lengths, the attenuation by length can be derived.

4.2 EQUIPMENT

4.2.1 *Fabrication*

Printing

A commercially available ink-jet printer for a laboratory environment (DMP 2831, Fujifilm Dimatix, Santa Clara, USA) was used for the experiments. It employs a relatively cheap (< 100 €), disposable printhead integrated in a removable print cartridge system, which enables to perform research with different inks in quick succession. Figure 4.2 shows the printer system and the printhead. As all experimental re-

a) Deposition of cores — Print head

b) UV-polymerization

c) Deposition of cladding
 and UV-polymerization

d) Facet polishing — PMMA blocks

e) Measurement — Camera / detector

Butt-coupled fiber
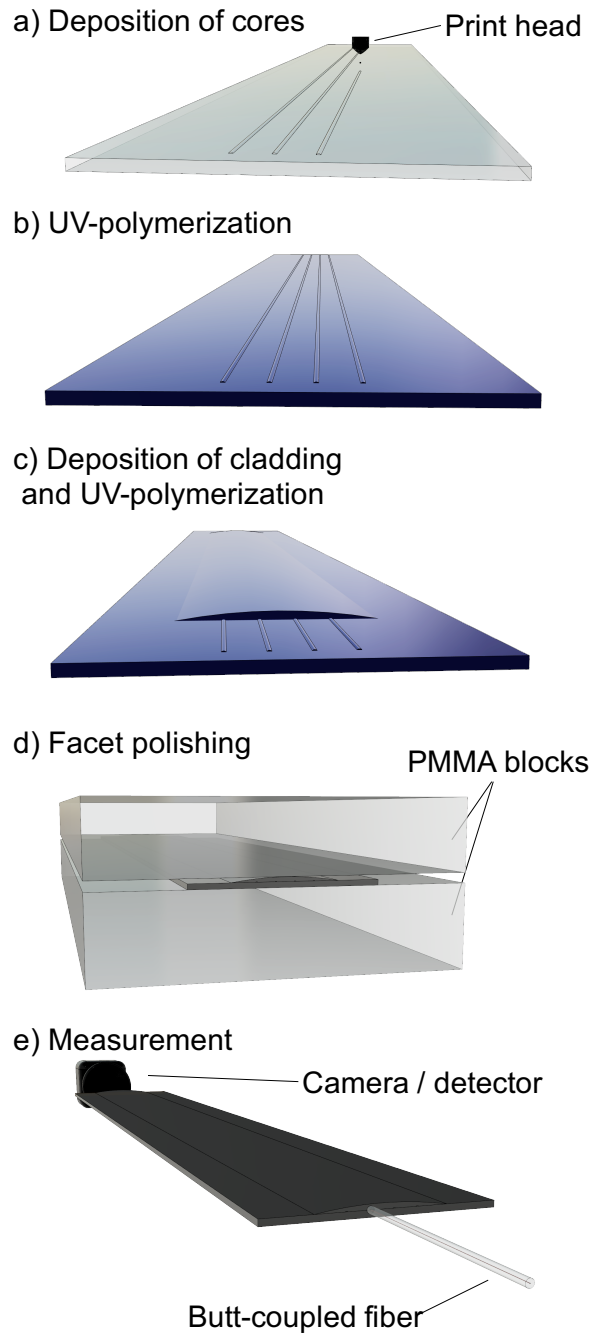
Figure 4.1: Process chain for the fabrication of waveguide core and cladding,
         preparation, and characterisation of ink-jet printed optical
         waveguides.

search presented in this dissertation was performed on this device, it
will be presented in detail on the following pages.

The heart of the printer is a microfluidic chip fabricated in MEMS-
technology that carries 16 piezo-based print nozzles with integrated
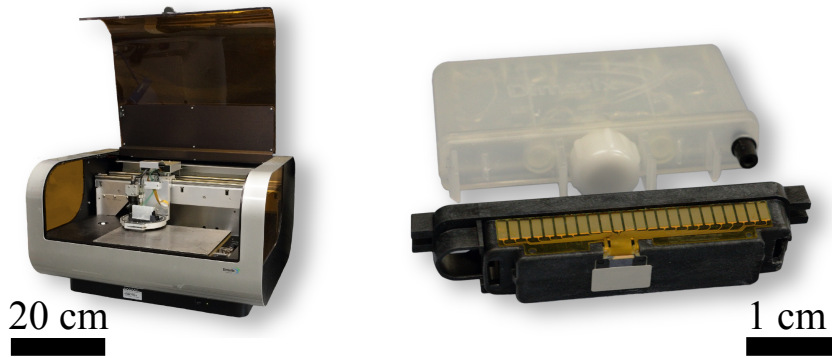
Figure 4.2: Dimatix DMP-2800 ink-jet printer and DMC-11610 cartridge. The silicon printhead is visible as a gray rectangle in the centre of the jetting module. The installed cartridge can be seen in the print carriage at the left side of the printer.

heaters. This chip is embedded in the jetting module of the cartridge with 16 electric contacts, which allow to control the pulse voltage between 0 and 40 Volts for each nozzle individually. The specified viscosity for printing is 10 ± 2 mPa·s. The integrated heaters can increase the ink temperature at the nozzle up to 70 °C to tune the printability of the ink by viscosity adjustment.

The jetting module is connected to the fluid module, which consists of a bag to carry the ink and a pressure system to control the ink flow. The bag is made from a chemically resistant polypropylene foil and has a volume of 2 ml. Around the bag is a second hard shell which can be put under either vacuum of 0 - 5 mmHg (0 - 667 Pa) to hold the ink inside the fluid module and avoid the ink leaking out of the print nozzle or pressure to flush the ink out of the nozzles for cleaning.

The print cartridge is placed in a carriage, which is moved with a belt-drive from left to right over the substrate plate with a velocity of about 1 m/s. The maximum droplet ejection frequency is 5 kHz, and the position repeatability is ± 25 µm. The maximum height of the printhead carriage is 25 mm above the substrate plate. After printing one line, the substrate plate is moved by one increment with a screw thread below the substrate plate, and the next line is printed. By printing many consecutive lines, a two-dimensional pattern is created. To alter the ink behaviour on the substrate, the substrate plate can be heated up to 60 °C.

To monitor the ink behaviour on the substrate after printing, the printhead carriage has a digital microscope camera system (*Fiducial Camera*). This camera allows to observe an area of 1.6 mm × 1.2 mm and measure the printed structures after deposition and to define where the print should start by relative alignment to any preexisting structures on the substrate before printing.

A second camera (*Drop Watcher Camera*) at the right side of the printing plate allows the user to observe and optimise the droplet
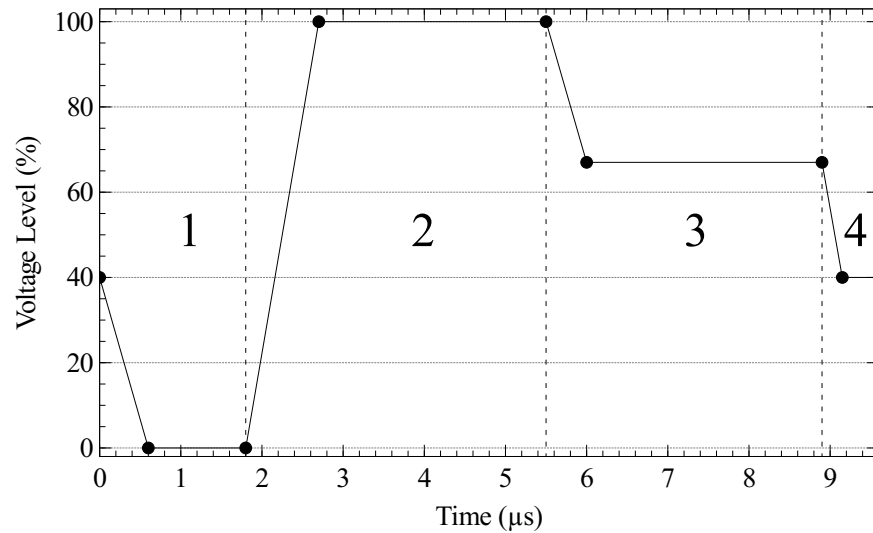
Figure 4.3: Four-phase printhead voltage pulse pattern used to actuate the nozzles. The four phases are load (1), eject (2), release (3) and reset (4). The voltage level given as percentage of the set pulse voltage. The pulse pattern has a duration of 10 µs, whereas the printhead prints with a frequency of 5 kHz. In the remaining 190 µs, the printhead rests.

formation in real time under stroboscope illumination. The effect of changing printer parameters like pulse voltage, or temperature, is directly visible with this method. Additionally, the printer has a cleaning station where the printhead can be flushed to remove any particles that block the printhead.

The droplet ejection at the nozzles is performed in four consecutive phases (load, eject, release, reset), which is shown in Figure 4.3. This pattern was suitable to print all inks that were investigated within this project.

To define where a droplet is positioned, an x-y-pattern is defined in a black/white bitmap (*.bmp) file, created in a photo editing software (MS Paint, Microsoft, Redmond, WA, USA). Each pixel in this file represents a droplet fired by the printer. By defining the droplet spacing between individual pixels, the droplet distance and pattern size is defined. The minimal droplet spacing is 5 µm.

Heating

An additional hotplate (Hot Plate 100, Labotect, Rosdorf, Germany) enables a higher substrate temperature of up to 100 °C, which is useful for inks that show a favourable substrate behaviour at elevated temperatures. With a height of only 23 mm, it is flat enough to fit under the print-carriage during printing. Additionally, it allows to perform a solvent evaporation step directly inside the printer without moving the substrate. This enables intermediate evaporation steps

between the deposition of many layers, possibly with different links, without moving the substrate.

Polymerisation

To polymerise the materials after printing, two UV-lamp systems were used. A small LED lamp (Firefly, Phoseon, Hillsboro, OR, USA) with an area of 25×10 mm emitting 4 W at 365 nm allowed to polymerise the printed structures directly in the printer without moving the substrate. A frame of intransparent PMMA holds the lamp 1 cm above the substrate and is fitted with a nitrogen supply to prevent oxygen inhibition.

For larger areas and controlled polymerisation conditions, a tabletop curing chamber with a side length of 15 cm and a 10 cm × 10 cm LED lamp (LED Cube, Hönle, Gräfelfing, Germany) was used. Two illumination units were available, with 150 mW at 365 nm and 550 mW at 405 nm. To prohibit oxygen inhibition, the chamber was fitted with a nitrogen supply and an oxygen sensor (GOX 100, Greisinger, Regenstauf, Deutschland) placed inside the chamber to monitor the atmosphere inside. Photos of both setups are shown in Figure 4.4.
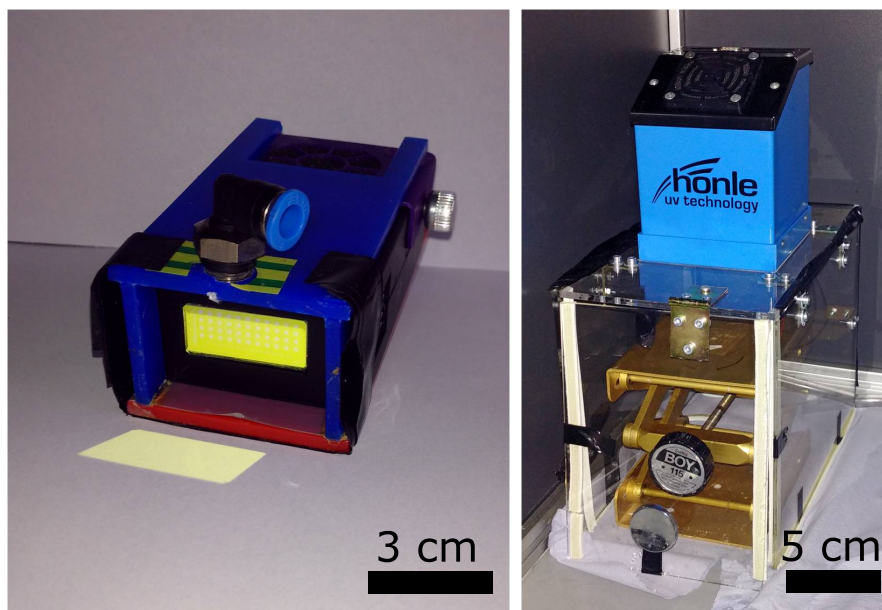
Figure 4.4: Both UV-polymerisation units. On the left, the hand-held Firefly is shown. On the right, the stationary Höhnle illumination system with a custom-built PMMA nitrogen chamber is shown.

4.2.2   *Tools for Sample Preparation*

Polishing

To couple light into and out of the structures, the waveguide facets were polished. First, the samples were cut to get substrate edges with accessible waveguide facets. Then, the edges were polished with abrasive sheets.

This was done on a rotating grinder-polisher (Beta, Buehler, Esslingen, Germany). Blocks of PMMA and thumbscrews were used to clamp the sample, and the block was manually held on rotating abrasive sheets with increasingly fine grit sizes (P180, P320, P800, P2500). Water was used as a lubricant. After the procedure, the samples were cleaned in an ultrasonic bath for 60 s.

Painting

A big problem for the characterisation and application of optical waveguides is light in the transparent cladding. When light scatters out of the core, it travels in the cladding, and for situations where the cladding is exposed to air, the light in the cladding will often reflect at this interface, as it has a very large refractive index step of up to 0.5.

Light travelling in the cladding which reaches the end facet poses a problem for light transmission measurement, as it is not possible for a photodetector to distinguish if detected light originates from the core or from the cladding. Additionally, for pulse-based data transmission, the light scattered from one pulse into the cladding could scatter back into the core, causing interference with the following pulse.

To absorb cladding modes, an absorptive layer was applied on the substrate and upper cladding. This layer was created with black spray paint (Lackspray RAL 9005 Mattschwarz, RCS-Systeme, Polling, Germany) after printing and polymerisation of the cladding layer.

4.2.3   *Optical Transmission Measurement*

For the optical transmission measurement, the samples with the polished facets were placed in a setup with a light source to couple light into the structures on one side, and a photodiode or a camera to quantify the transmitted light on the other side. Two setup variants were used.

The first variant, shown in the upper section of Figure 4.5, consists of a 637 nm diode laser light source with a power of 140 mW (Stradus 637-140, Vortran, Sacramento, USA) to create a laser beam with a diameter of 13 μm that hits the waveguide facet, and a camera detector to observe the opposite side of the waveguide. A hexapod (Newport HXP50-MECA) allows to move the sample in six degrees of freedom

and align it to the fixed laser-source. The camera can then be aligned to the sample with two linear stages. The setup is referred to as *Beam Setup*

The second variant, shown on the bottom of Figure 4.5, does not send the light in a free-space beam, but through an optical fibre in contact with the waveguide facet (HPC S0.66/K, Diamond SA, Losone, Switzerland). This setup is referred to as *Fibre Setup*. The fibre is held by magnetic clips (SM1F1, Thorlabs, Newton, USA) in an x-y-translation stage (ST1XY-D/M, Thorlabs) for alignment. The light is provided by a 785 nm laser source (S1FC785, Thorlabs) with a maximal power of 10 mW. The sample is placed on a platform held by a second x-y-z-translation stage (MS3/M, Thorlabs). To control the alignment between sample and fibre, a microscope (SMZ800, Nikon, Chiyoda, Japan) is placed above the sample. The transmitted light is captured by a camera (SMX-M83C, EHD imaging, Damme, Germany). To quantify the measured power, a photodiode (S151C, Thorlabs) was be placed in the setup.

4.3 MATERIALS

4.3.1 *Substrate*

With the goal of realising a light and flexible optical sensor system on planar foils, the substrate material has to fulfil several requirements. Roll-to-roll compatibility is benefitial for mass-production, which is the reason for choosing polymer foils as substrate. As it is the lower substrate for the optical waveguides, good optical transparency and low refractive index is critical. Several materials were investigated experimentally: Poly(methyl methacrylate) (PMMA), Poly-vinyl chloride (PVC), Cyclic Olefin Copolymers (COC), glycol-modified Poly-ethylene terephthalate (PET-G), and polyimide (PI). Also, D263, a borosilicate glass, was eveluted as substrate. The materials are listed in Table 4.1.

All polymer substrates were suitable for printing, as printed material maintained a defined shape after deposition. On the glass substrate however, the inks formed individual droplets after deposition, and no parameters were found that allowed the fabrication of continuous tracks.

First tests were performed on PVC and PET-G. However, PET-G has a refractive index of 1.57, which is above the available inks. Therefore, it is not suitable as a lower cladding substrate. PVC has a lower refractive index of 1.53, but a very low glass transition temperature of 82 °C. In contrast, PMMA Film 99524 has a glass transition temperature of 113 °C [100]. Therefore, PMMA, the material with the lowest refractive index (1.49), and a relatively high glass transition temperature, was chosen as substrate.
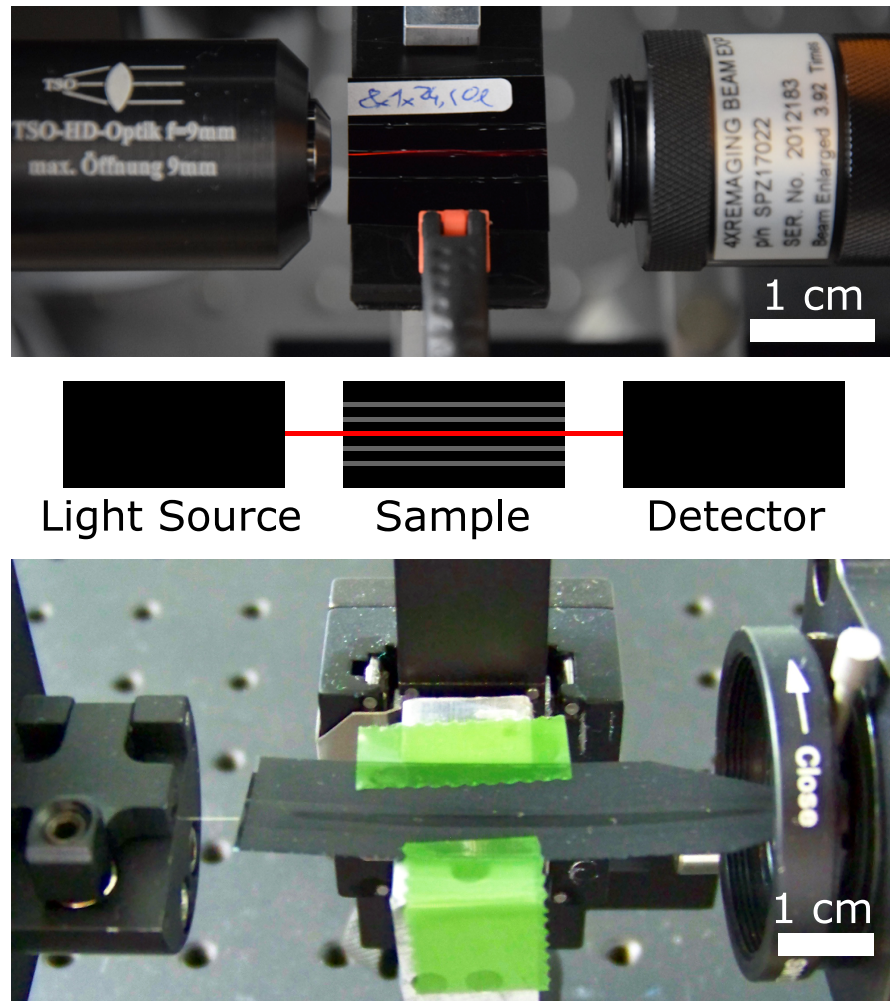
Figure 4.5: Two optical characterisation setup used for waveguide characterisation, with different methods to couple light into the waveguide facets. The first uses a free-travelling beam from a laser source with 140 mW at 638 nm and a spot size of 13 µm, and is referred to as *Beam Setup*. Two reflections along the sample are visible as bends. Because this setup was not available at times, a second, simpler setup was built, referred to as *Fibre Setup*. Here, an optical fibre, connected to a 10 mW 785 nm laser, is moved into contact with a waveguide facet to couple light into the fibre. Both setups have a digital camera at the other side of the setup to detect the transmitted light. Optionally, a photodetector is used to quantify the transmitted power.

Table 4.1: Substrates under consideration for ink-jet printed optical waveguides

Product Name	Material Type	Comments	$n_{d,20}$
Plexiglas G99524 GT	PMMA	-	1.49
Pentaprint PR M180/23	PVC	-	1.53
D 263 T eco	Borosilicate	brittle	1.53
TOPAS	COC	brittle	1.56
N/A	PET-G	-	1.57
Kapton HN	PI	opaque below 600 nm	1.70

4.3.2 *Inks with Volatile Solvent*

The only commercially available materials suitable for the fabrication of ink-jet printed optical waveguides were two experimental products called InkEpo and InkOrmo (Microresist Technology, Berlin). The inks are based on the products OrmoCore/Clad and EpoCore/Clad, which were developed for spin-coating and lithography techniques. In undiluted form, both materials have a viscosity above the specified value for the Dimatix printer (10 mPa·s). Therefore, a reactive diluent and a volatile solvent is used to achieve this viscosity.

Chemical Composition

Being an experimental product from a company, the exact material composition is undisclosed, and only the general material class is given. A research paper [101] published by the manufacturers states that the base material for InkEpo is an epoxy resin. InkOrmo, on the other hand, is based on a novel inorganic-organic hybrid polymer class named *Ormoceres* based on for organically modified ceramics and developed by the Fraunhofer Gesellschaft [102].

To reach printability, either solvents or multi-functional aliphatic epoxy groups containing reactive components as reactive diluents [101] were employed. The exact formulation of the reactive diluents is undisclosed. Gamma-butyrolacton (GBL) was used as volatile solvent. The photo-polymers are undisclosed as well. An important detail, however, is that neither material shows oxygen inhibition.

Processing Guidelines

To evaporate the volatile solvent, both materials require a pre-bake step at 80-90 °C for 5-15 minutes. As this is too hot for many polymer substrates, a lower temperature can used in combination with a longer evaporation time, but no data is provided in this context. After the solvent evaporation step, the materials are polymerised with UV-light (365 nm). The required exposure dose to reach polymerisation is 350-500 mJ/cm^2. As neither of the two inks shows oxygen inhibition, they can be polymerised in air. For InkEpo, a post-exposure bake at 90-100 °C for 5 minutes is required. For InkOrmo, this is not necessary.

Optical Properties

Being commercial products, the optical properties of InkEpo and InkOrmo are provided by the company in the material data sheets [103]. The refractive indices are given in Figure 4.6. InkEpo has a much higher refractive index, which makes it better suited as core material. The values are stated for the polymerised material. The refractive index of the unprocessed inks are much lower because of the GBL solvent, which has a refractive index (n_d20) of 1.43. For InkEpo, the value is 1.476, for InkOrmo, 1.459.

Table 4.2: Refractive indices of InkEpo and InkOrmo at the Fraunhofer lines e, F′ and C, which are used to calculate the Abbe numbers.

Fraunhofer Line	Wavelength	InkEpo	InkOrmo
e	546 nm	1.559	1.516
F′	480 nm	1.567	1.521
C	656 nm	1.550	1.510
Abbe number ν_e		33	47

No data on the optical attenuation of the inks is given. However, there is data on the attenuation of related materials [104]. OrmoCore and OrmoClad show <0.06 dB/cm at 630 nm, EpoCore and EpoClad <0.2 dB/cm at 830 nm. The effect of the reactive diluents on the refractive index, however, is unknown.

To quantify the dispersion properties of the materials, the Abbe number ν_e was calculated for InkEpo and InkOrmo. For this, the refractive indices at the Fraunhofer lines e, F′ and C were taken from the graph. These values are listed in table 4.2. The Abbe numbers for
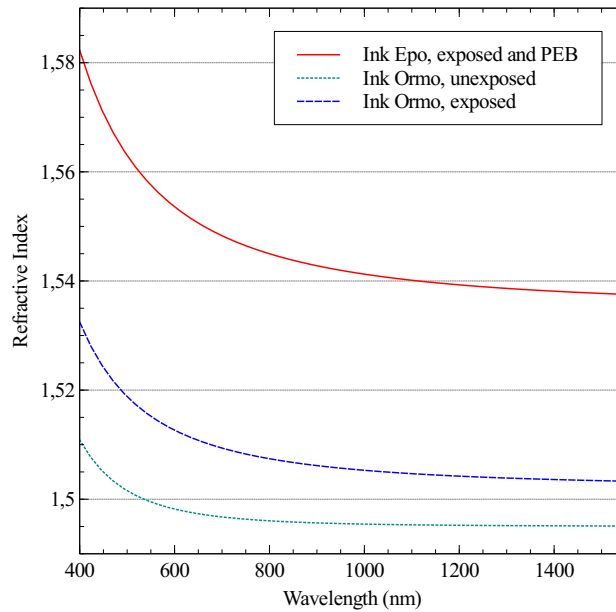
Figure 4.6: Refractive index of InkEpo and InkOrmo, reprinted with the interpolation equations provided in the data sheet. For InkEpo, data is available for the material after UV-exposure and post-exposure bake (PEB). The refractive index is 1.58 at 400 nm, 1.55 at 650 nm, and 1.54 at 1000 nm. For InkOrmo, data is available for the unpolymerised and polymerised material, with polymerisation increasing the refractive index. For polymerised InkOrmo, the refractive index is 1.53 at 400 nm, 1.51 at 800 nm, and 1.505 at 1200 nm.

InkEpo and InkOrmo are 33 and 47, respectively, which are typical values for polymers.

4.3.3 *Solvent-Free Inks*

A solvent-free, in-house developed ink was evaluated for its suitability to print optical waveguides as an alternative to the commercially available materials. This ink was prepared, manufactured and characterised by U. Gleissner at the Laboratory for Materials Processing, led by Professor Dr. T. Hanemann [105], and the data from these measurements was used to create the figures of this section.

Similarly as the materials described in the previous chapter, the viscosity of the base material is above the printable regime, and requires to be lowered to 10 mPa·s in order to reach printability. Unlike InkOrmo and InkEpo, the material uses no volatile solvent, but only a reactive diluent for this viscosity modification. This has the advantage that no solvent evaporation step is required between printing and polymerisation. The material is called SynthEG, after the two main components (Syntholux and EGDMA). A subsequent number indicates the wt% content of the reactive diluent.

Chemical Composition

The materials consists of three components: A base material, a reactive diluent, and a photo-initiator. The base material for the inks is Syntholux 291 EA, a commercially available polymer varnish based on an epoxy acrylate, diluted with 80% tripropylene glycol diacrylate [105, 106].

To reduce the viscosity of the base material, ethylene-glycol dimethacrylate (EGDMA) was used as a reactive diluent [107]. This material is a diester formed by two equivalents of methacrylic acid and one equivalent of ethylene glycol. Having two acrylate groups, it can fully co-polymerise with the base material. The amount of additive that copolymerises in the polymer matrix affects the resulting refractive index, which can be used as a tool to tune the refractive index of the ink. As photo-initiator, diphenyl(2,4,6-trimethylbenzoyl)phosphine oxide (DPO) was used [108].

Processing Guidelines

As SynthEG does not use a volatile solvent, no pre-bake step between deposition and polymerisation is necessary. However, the used photo-initators are sensitive to oxygen, which is why the materials have to be polymerised under nitrogen atmosphere. To compensate for any traces of oxygen inhibiting the polymerisation, a generous exposure dose of $15 J/cm^2$ is given with an intensity of $500 mW/cm^2$ over 30 seconds.

Dynamic Viscosity

To characterise the effect of the diluent on the dynamic viscosity, the ink was analysed in a rheometer (CVO50, Bohlin/Malvern Instruments, Malvern, UK). The results of this characterisation are shown in Figure 4.7. At room temperature, pure Syntholux 291 EA has a dynamic viscosity of about 50.000 mPa·s, pure EGDMA 5 mPa·s. When heated to 60 °C, the value of Syntholux reduces to about 800 mPa·s, EGDMA shows about 2 mPa·s. The ideal value for printing with the available system is 10 mPa·s, which means that mixtures between 50 wt% and 80 wt% EGDMA can be considered for printing when heated to a suitable temperature.

Refractive index tuning

The use of EGDMA as a reactive diluent also has an effect on the refractive index, which is a valuable tool when printing micro-optical structures. This effect was measured in an abbe refractometer (DR-M2/1550, ATAGO, Tokyo, Japan). The results, shown in Figure 4.8, indicate that for the given viscosity constraints, a refractive index be-
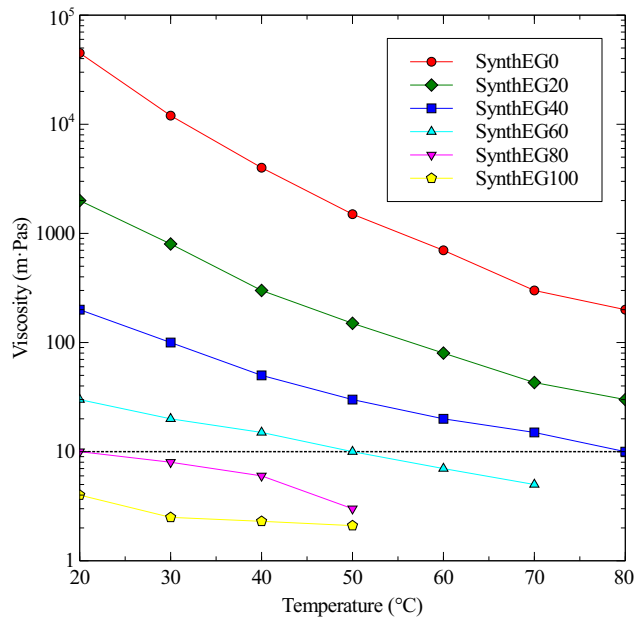
Figure 4.7: Viscosity between 20 °C and 80 °C of different mixtures of Syn-thEG [105]. The high viscosity of pure Syntholux is reduced by the addition of EGDMA. A content between 40% and 80% allows to reach the ideal viscosity for the Dimatix printer, indicated by the dotted line.
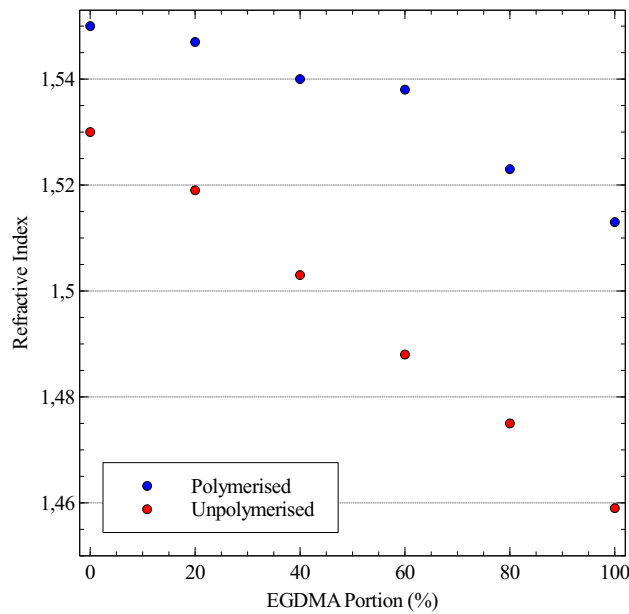
Figure 4.8: Influence of addition of EGDMA on the refractive index of the unpolymerised and polymerised material [105].

tween 1.535 and 1.52 is possible. The refractive index change and EGDMA percentage follow a linear behaviour in this window.

Transmission Spectrum and Attenuation
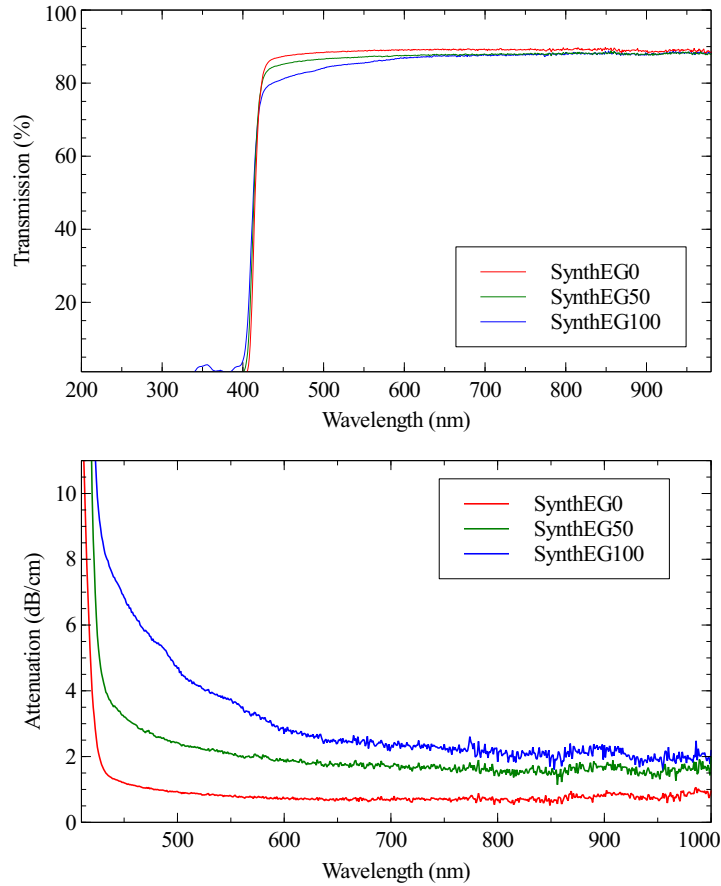
Figure 4.9: Top: Transmission spectrum of SynthEG0 (pure Syntholux), SynthEG50, and SynthEG100 (pure EGDMA), taken in a UV-Vis-spectrometer. Bottom: Derived attenuation after considering the fresnel-reflections at both interfaces.

The transmission characteristics of SynthEG0 (pure Syntholux), SynthEG50, and SynthEG100 (pure EGDMA), were measured in a UV-Vis spectrometer (Cary 50 UV-Vis, Varian-Agilent, Santa Clara, USA). For this, samples with a thickness of 1 ± 0.05 mm were prepared. All materials are transparent down to 430 nm, the addition of EGDMA reduces the transmission, especially in the blue spectrum.

From these measurements, the bulk attenuation was derived. The data is shown in Figure 4.9. After taking the Fresnel-reflections into account, pure Syntholux shows an attenuation in the range of 1 dB/cm, the addition of EGDMA increases this value to about 1.5 dB/cm. This value is about 1 order of magnitude higher than the data given for InkEpo and InkOrmo, and above the attenuation criterion of 1 dB/cm, which was set in the research goals. The material was used for printing experiments nonetheless in order to compare the bulk attenuation to the waveguide attenuation.

Dispersion

For SynthEG, the dispersion was evaluated by measuring the refractive index at three wavelengths (450 nm, 589 nm, 680 nm). The results are shown in Figure 4.10. For SynthEG50, a quadriatic fit is plotted, which allows to estimate the refractive index in the red spectrum and the refractive indices at the e, F' and C Fraunhofer lines. These values are required to calculate the Abbe number, listed in Table 4.3. The calculated Abbe number for SynthEG50 is 49, which means that this material shows weaker dispersion than the solvent-based inks.
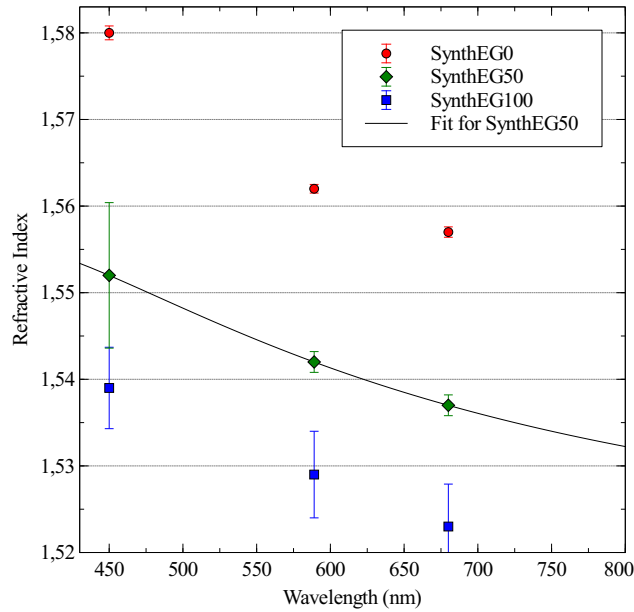
Figure 4.10: Refractive index of SynthEG in the visible spectrum, showing the optical dispersion.

Table 4.3: Refractive indices at the Fraunhofer lines e, F' and C, as derived from the quadratic fit. This values were to calculate the Abbe number ν_e

Fraunhofer Line	Wavelength	Derived refractive index
e	546 nm	1.5443
F'	480 nm	1.5494
C	656 nm	1.5382

4.4   SUMMARY OF AVAILABLE METHODS AND MATERIALS

The selected printer was found to be suitable to investigate the research goals, as it allowed to evaluate different inks and substrates experimentally. Although many different ink concepts for optical waveguides have been proposed, only one commercial product was available, because the concept is not widely in use yet. The solvent-free in-house alternative has a higher attenuation, but can be processed much more flexibly, as no solvent evaporation step is required. With no solvent-free material with lower attenuation available, it was selected as an alternative to the commercial material with the goal to evaluate and compare the printability of these two ink types. The optimisation of the material attenuation should be seen as a research goal on its own.

RAY-TRACING SIMULATION

To investigate the concept of ink-jet printed optical waveguides and the influence of different factors on the attenuation, a commercial ray-tracing tool (OpticStudio, Zemax LLC) was used. Although Snell's law might suggest that any continuous track of an optically transparent material with positive refractive index difference to its environment would guide light, this is by no means guaranteed. The typical cross-subsection of a continuous track deposited by ink-jet printing is a flat circular segment with sharp edges. Such edges do not exist in round or rectangular waveguides, but can be found in wave absorber structures, like light traps made from stacks of razor blades. Therefore the most important question is if the flat circular segment shape has a negative influence on the light transmission, and how it performs in comparison to a conventional round optical waveguide, especially when bulk scattering, which is present in any polymer optical material, is considered.

5.1 SIMULATION MODEL
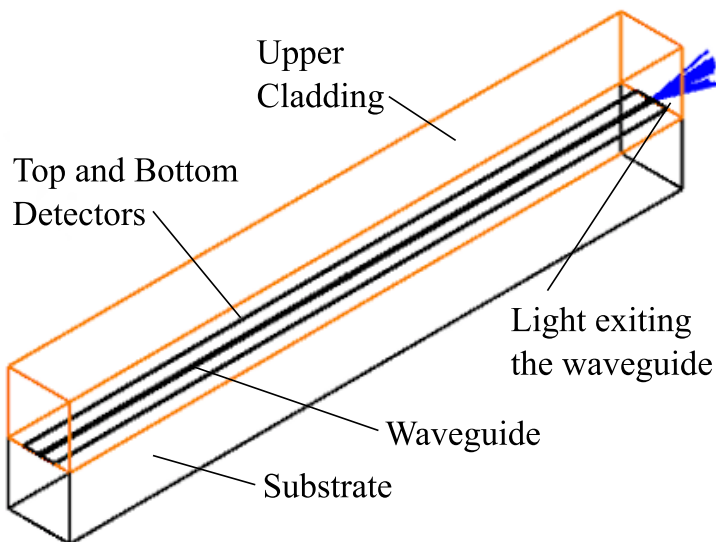
Figure 5.1: Model waveguide used for the simulations. On the left side, light enters through a point source. The light is visualised as blue rays on the right, where it exits the waveguide. The orange cuboid is the optional upper cladding, which encloses the upper waveguide interface.

The simulation was performed on waveguide models with dimensions which are typical for ink-jet printed tracks, with a width of 100 μm, a height of 10, 15, or 20 μm, and a length of 1 cm, limited by a front and back facet. This waveguide model is placed on a cuboid, which serves as lower cladding, and optionally within a second cuboid, which serves as upper cladding. On the front facet, light is generated by a 1 W point source and sent towards the waveguide as a cone-shaped beam with an opening angle of 1 degree. Detector rectangles within the waveguide, positioned just after the front facet, in the waveguide centre, and just before the end facet, count each ray that passes through them and summarise the total power. If light is contained perfectly, the three areas along the waveguide will count a similar amount of light, otherwise the measured power will drop. Detector areas above and below the waveguides are used to track the scattered light. By comparing the total power of the top, bottom and rear detectors to the light source power, the validity of the simulation is ensured. The simulation model with upper and lower cladding is shown in Figure 5.1.

The simulation wavelength was 550 nm, which is a standard for ray-tracing simulations because it is in the centre of the visible spectrum. Several simulation series were performed to investigate the influence of the refractive index step between core and cladding, bulk scattering caused by the material, aspect ratio of the waveguide core, and an upper cladding layer. The results of the simulations are expressed as the power measured by the detector rectangles. Additionally, the beam patterns in the front, centre, rear, top and bottom detectors (F, C, R, T, B) are shown for selected parameters to show how the light is scattered.

5.2   SIMULATION RESULTS

5.2.1   *No Scattering*

In the first simulation, a waveguide core of 100 μm width and 10 μm height was placed on a substrate, and the effect of the refractive index step between substrate and core on the light transmission was investigated. The refractive index of the substrate was defined at 1.49, modelling the selected PMMA substrate foil. To find out what refractive index step is actually necessary for waveguiding, refractive index steps Δn between core and substrate of 0.000, 0.001, 0.005, 0.010, 0.020, and 0.100 were simulated. The results are shown in Figure 5.2. In the x-y graph, the detected power of the front, centre, and rear detectors are plotted versus the refractive index difference. Following Snell's law, a refractive index difference of zero causes the waveguide to lose its ability to confine light. The lost light is picked up by the bottom detector, as the lower cladding has the same refractive index as the

core and optically merges with the core. But already a refractive index step of 0.001 causes a significant improvement of the light guiding capabilities, and rays are reflected within the waveguide. At a refractive index step of $\Delta n = 0.005$, the intensities of front, centre and rear detector are collectively at 1W, which equals the input power, and the detectors above and below the waveguide count no rays. On the right of Figure 5.2, the intensity profiles as measured by the front, centre, back, top, and bottom detector are shown for selected refractive index steps. These graphs show that the off-axis rays distribute evenly within the waveguide core.

The results indicate that for an optically transparent track with a circle subsection shape at 100 um width and 10 um height, a refractive index step from 1.49 to 1.495 is sufficient to ensure complete light confinement at 550 nm, and the suitability of this shape to guide light is demonstrated successfully.
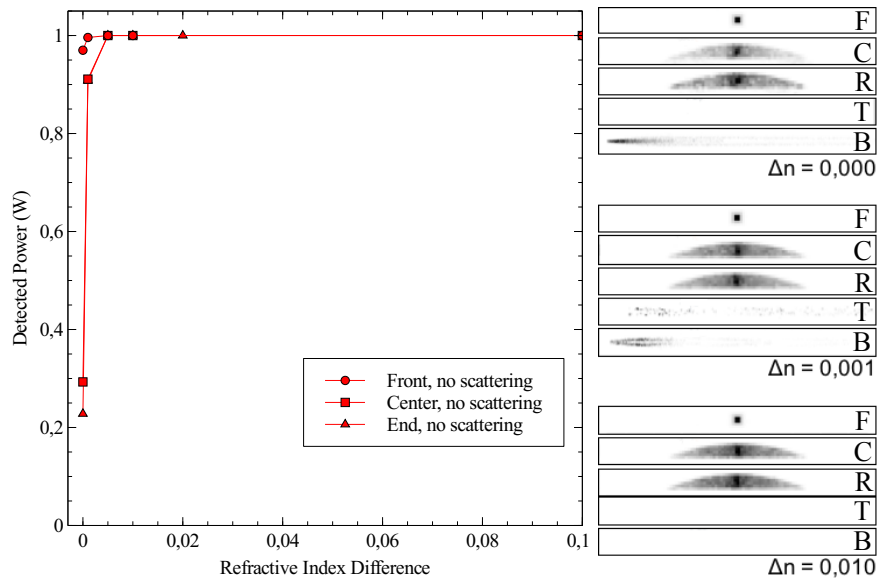
Figure 5.2: Results of the simulation without scattering, showing the power counted by the three detectors. The results show that a refractive index step of only 0.05 is sufficient to reach light confinement in a waveguide with the cross-subsection of a flat circular segment. The detector plots for the front, centre, rear, top and bottom detectors (F, C, R, T, B) show that the off-axis rays that do not travel straight trough the waveguide distribute evenly in the waveguide, and that light is only scattered from the waveguide right at the beginning.

5.2.2 Scattering

As described in Chapter 3, all optical polymer materials show relatively strong bulk scattering, which is why fibres for long distance communication are made of glass. Unfortunately, the actual scatter-

ing properties of the used materials are unknown and difficult to measure. Therefore, a simple angle scattering model provided by OpticStudio was employed, which uses an integrated probability p for scattering over a distance x given by

$$p(x) = 1 - e^{-x/M}$$

. The symbol M is the mean free path that a ray can travel before encountering a scattering event. As x increases, the probability that the ray has scattered approaches 1. [109]

As no data for the material scattering of the actual inks was available, parameters were chosen in such a way that the simulation of the scattered beams showed significantly lower values at the detector. The mean length of the scattering model was set to 1 mm, and the scattering angle was set to 5°. The aim of this investigation was to evaluate how the bulk scattering can be counteracted by aspect ratio or refractive index step. With this scattering model activated, the simulation was performed again for refractive index values up to 1.55, which is refractive index of InkEpo, and the highest available value. The results are shown in Figure 5.3.
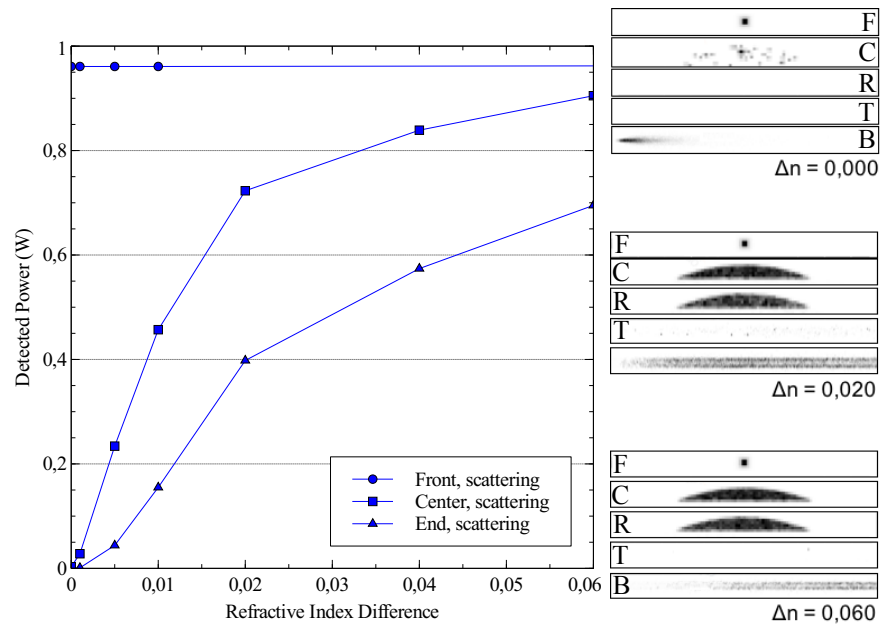
Figure 5.3: Results of the simulation with activated bulk scattering for a circle-section waveguide. The end detectors count less light than the front detector, which means that even a relatively high refractive index step of 0.06 is unable to inhibit scattering losses. The scattered light appears on the bottom detector, and a higher refractive index step reduces the intensity in this detector.

Now, the power collected by the centre and end detector deviates significantly from the power at the waveguide front, which does not collect 1 W created by the light source as in the simulation without

scattering. By increasing the refractive index of the core in increments of 0.01, up to a refractive index of 1.55, the light confinement improves, but the effect of the scattering is never fully compensated. This lost light is detected on the bottom detector, and the image shows that a higher refractive index pushes the area where most light is scattered towards the waveguide end. Although the selected scattering parameters are not related to a real material, the results are still very valuable. Whereas the model without scattering reached full confinement at a small refractive index step of 0.005 was sufficient to reach full light confinement, this was not possible with activated scattering even at a high refractive index step of 0.06. Yet, a high refractive index step significantly improved the waveguide performance. This means that a material that scatters light can be used for printed waveguides, but a high refractive index step between substrate and waveguide core should be aimed for as it counteracts the negative influence of scattering.

5.2.3 *Aspect Ratio*
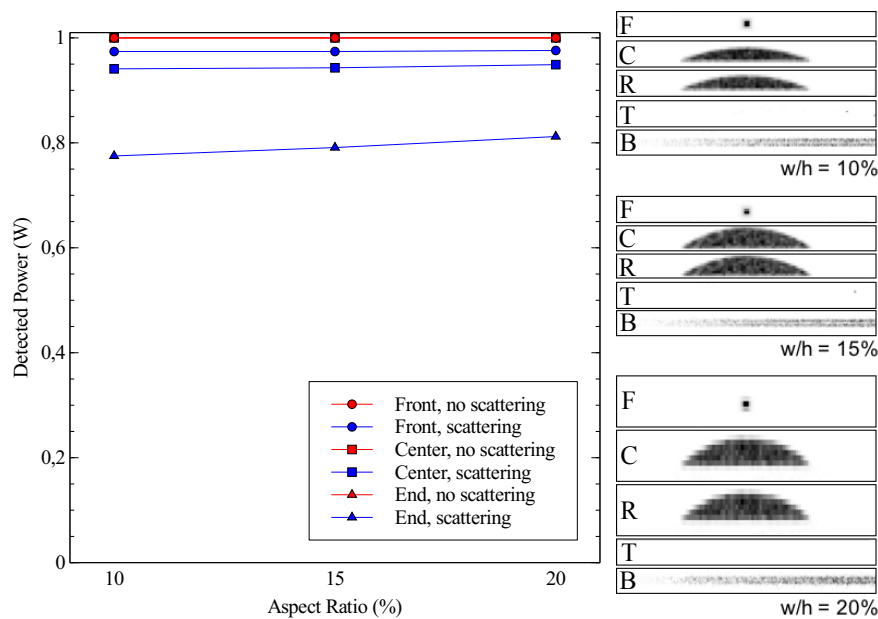
Figure 5.4: Ray-tracing simulation that investigates the influence of width and height ratio (aspect ratio) on waveguides with a refractive index of 1.54. Without scattering, no effect is visible, because all detectors report 100% transmission. With activated scattering, it becomes visible that a higher aspect ratio slightly improves the light confinement. The detector patterns show the same phenomena, independent of the aspect ratio.

In the third simulation, the influence of the waveguide aspect ratio on the attenuation was investigated. For this, samples with a width of 100 μm, and heights of 10, 15 and 20 μm, representing aspect ratios of
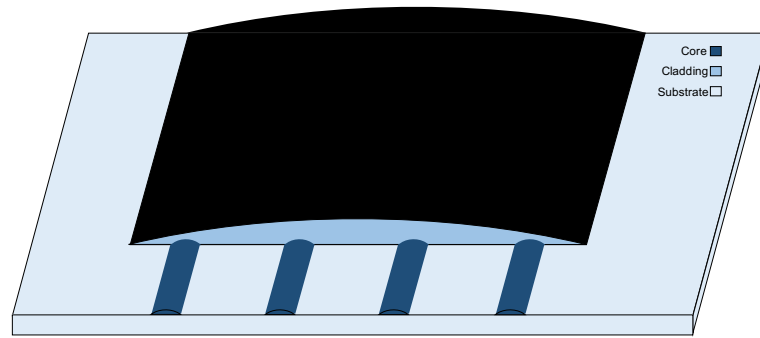
Figure 5.5: Drawing of printed optical waveguides with a printed upper cladding. The substrate acts as lower cladding.

10 %, 15 %, 20 %, and a fixed refractive index of 1.54 for the core and 1.49 for the substrate, were investigated. These values are realistic for the application - a lower aspect ratio makes it very difficult to couple a circular fibre or light beam into the facet, higher aspect ratios could not be fabricated reliably. The simulation results with and without scattering are shown in Figure 5.4.

Similar to the previous result, all waveguides perform excellently when scattering is deactivated, and the measured power of all detectors is uniformly at 1 W. With scattering activated, the performance drops, and the measured power of the end detector is just below 0.8 W for the waveguide with an aspect ratio of 10%, which represents an attenuation of about 1 dB/cm. The light is, as before, detected below the waveguide. When the aspect ratio is increased, the value increases slightly, so that a waveguide with an aspect ratio of 20% shows slightly more than 0.8 W at the rear facet, or an attenuation of 0.8 dB/cm. Compared to the refractive index step, the effect of the aspect ratio is relatively small. Yet, an aspect ratio of 20% gives a lower attenuation than an aspect ratio of 10%, so a higher aspect ratio should be aimed for.

5.2.4 *Cladding*

In the previous simulations, the waveguide cores were unprotected to their environment, and the upper cladding was modelled as vacuum. While there are some applications where this situation might apply, most require the waveguide to be protected by an upper cladding to avoid damage to the waveguide core. A sketch of the cladded waveguides is shown in Figure 5.5.

In the simulations, the upper cladding was modelled by a second cuboid placed above the waveguide substrate. The waveguide core model was defined to be within the second cuboid, which solved the modelling problem of ensuring a close interface between the waveguide core and the upper cladding. The simulation was done with several values for refractive index in the upper cladding, ranging

from 1.49, which was the value of the substrate, to 1.55, which was the value of the core.
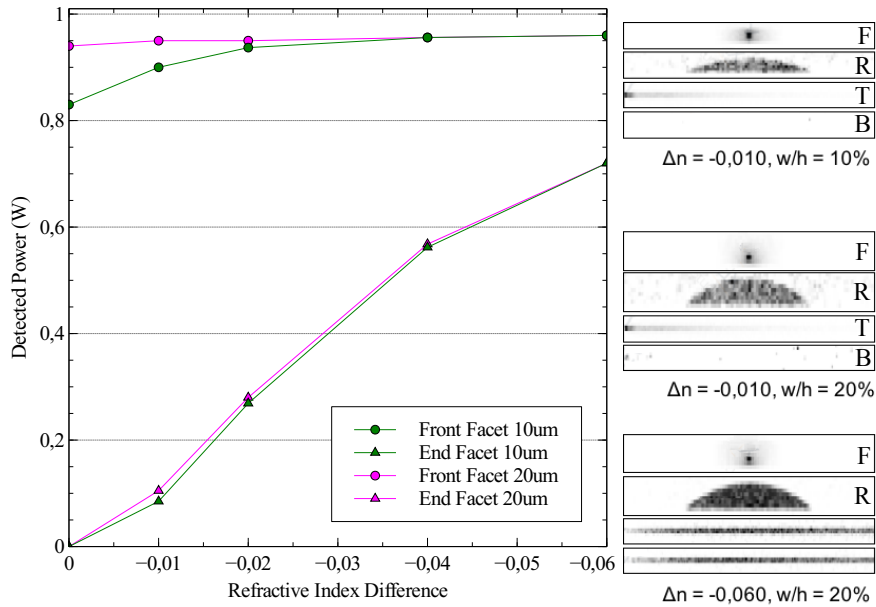
Figure 5.6: Ray-tracing simulations for cladded waveguides with varied negative refractive index step between a core of 1.55 and the cladding. The results show that, just as before, the refractive index step has a significant influence, whereas the aspect ratio of the material has a neglible influence.

The results are shown in Figure 5.6, with the x-axis showing the refractive index step from core to cladding. For the cladded waveguides, the simulations imply that the refractive index step between core and cladding is most important for a good light transmission. Compared to that, the influence of the aspect ratio on the waveguide attenuation is negligible.

5.2.5 *Derived Attenuation*

To visualise the simulation results, the transmitted power values from the simulations were used to derive a waveguide attenuation value in dB/cm, shown in Figure 5.7. The simulated attenuation of a round polymer waveguide with a diameter of 50 μm was added to assess the effect of the waveguide shape on the attenuation. The data shows that the attenuation of printed waveguides is typically about factor 2 worse than that of round waveguides, but still in the same order of magnitude between 3 dB/cm and 0.3 dB/cm. The printed waveguide without upper cladding has an even lower attenuation than the round waveguide with cladding. This shows again the strong influence of the refractive index step at the interface – for the printed waveguide, it is about 0.50 at the upper interface to vacuum.

5.2.6 *Intermediate Conclusion for Simulations*

The ray-tracing simulations of optically transparent structures that resemble ink-jet printed tracks attest the feasibility of the concept to use ink-jet printing for the fabrication optical waveguides, and show which parameters are important to reduce attenuation. However, the complex optical properties of polymers are not represented by the simple scattering model provided by a ray-tracing software – especially with estimated parameters. Additionally, diffusion processes and refractive index gradients are not considered, although these are certainly present in polymer optics. Here, a more realistic simulation of the waveguides with a tool that can model these interfaces realistically would improve the significance of the simulations.
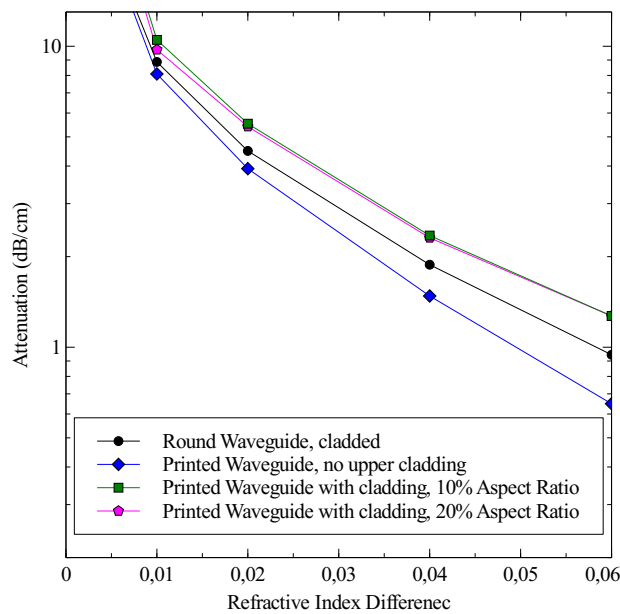
Figure 5.7: Simulation results plotted as attenuation. The round waveguide has the lowest value, the printed waveguides are comparable.

Yet, the results are valuable because they allow to evaluate certain parameters and their relative influence on the attenuation. Increasing the refractive index step by 0.02 generally reduced the attenuation by half, which means that this parameter is the most relevant one.

The core result of the ray-tracing simulations is that the circle-section shape of ink-jet printed optical waveguides does not lead to an unacceptably high waveguide attenuation, which would render the concept unfeasible. Although printed optical waveguides were published before, this question persisted in the community and was not answered conclusively with evidence yet. The simulations show that the influence of the shape on the waveguide attenuation is in the same order of magnitude as other parameters like refractive index step and material attenuation.

INK-JET PRINTING OF OPTICAL WAVEGUIDES

With a theoretical proof of principle and a selection of materials available, the next step was to perform printing experiments. First, the selected materials were qualified via a proof-of-principle. Then, methods to control the wavegide cross-section were investigated, as the simulations suggested that a high aspect ratio correlates with lower attenuation values. The last section will present results on the fabrication and characterisation of printed optical waveguides with an upper cladding.

6.1 COMPARISON OF WAVEGUIDE MATERIALS

To assess the suitability of the different materials presented in the preceding chapter for printing optical waveguides, tracks were printed with varying parameters on different substrates, and the ability to carry light was evaluated. An experimental proof of principle could be demonstrated for both selected materials.

6.1.1 *Inks with volatile solvent*

6.1.1.1 *Ink-jet printing evaluation*

InkEpo and InkOrmo were reliably printable in the Dimatix printer with a standard pulse pattern (Figure 4.3) and printhead heated to 45 °C to reduce the viscosity from 12 mPa·s to 10 mPa·s. A pulse voltage of 20 V was optimal for printing with good resolution and reliability, although droplet formation could be achieved at lower voltages down to 15 V, which improved resolution, but didn't show the required reliability. Higher voltages led to larger droplets and therefore reduced resolution.

The substrates listed in the previous chapter (Table 4.1) were tested on their suitability for the inks with two test pattern shown in Figure 6.1. The purpose of the patterns is to evaluate how the ink maintains the shape of a printed pattern, either for a combination of a rectangle and thin tracks, or for for curved tracks.

The first evaluation showed that, generally, InkEpo maintained the shape well, whereas InkOrmo would contract to a circular shape. The effect is shown in Figure 6.2.

The contraction effect of InkOrmo could be counteracted by substrate heating. By using a temperature of 60 °C, InkOrmo, could be deposited on many substrates as well. This phenomenon is shown in

Figure 6.1: Two test patterns to evaluate the behaviour of inks on substrate.
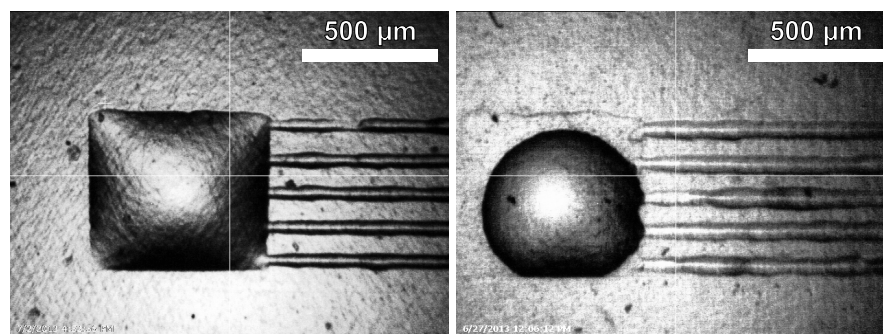
Figure 6.2: Test print of InkEpo (left) and InkOrmo (right) on PVC substrate at room temperature. While InkEpo maintains the shape it was deposited in, InkOrmo contracts to a spherical cap.
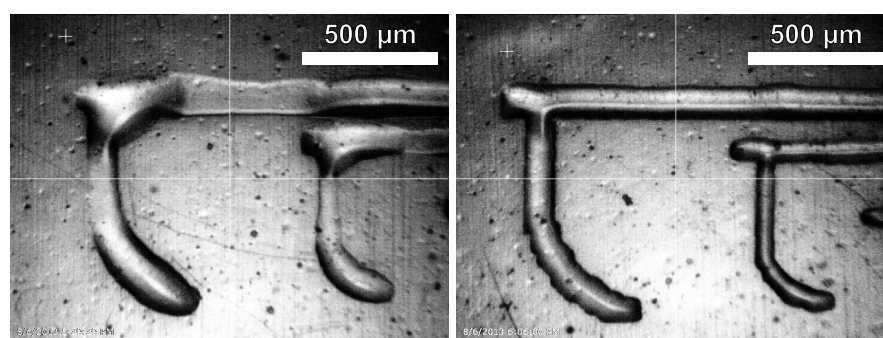
Figure 6.3: Effect of heated substrate for InkOrmo, shown exemplarily on PET substrate. On the left, the substrate is at 30 °C, and the ink contracts. On the right, the substrate is heated to 60 °C, leading to much better contour accuracy and equal track width.
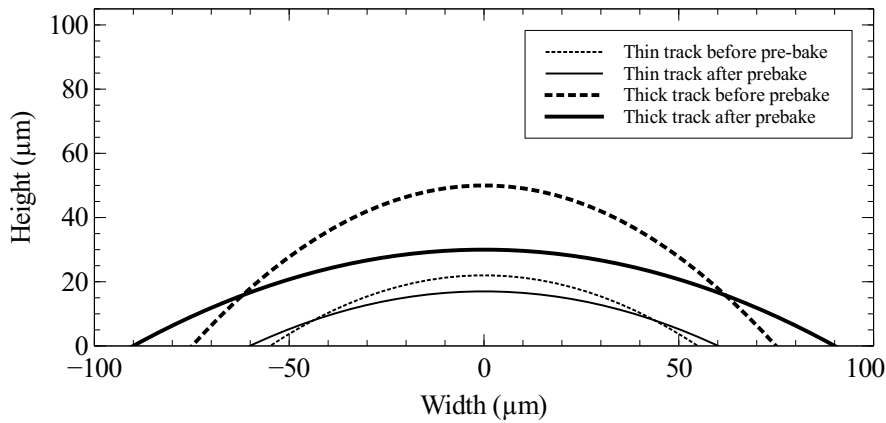
Figure 6.4: Waveguide cross-subsection of printed tracks, measured in a white light interferometer. The image visualises the effect of the pre-bake step on the track shape.

Figure 6.3 with the second test pattern. However, the pattern shows that curvatures are difficult to print with this pattern, as the edges show distinct steps that originate from the individual droplets.

Even though the problems that occurred when printing tracks of InkOrmo could be counteracted, the material was dismissed. InkEpo was selected for further tests because of its higher refractive index, which was shown in simulations to reduce attenuation, and was less problematic handling on the substrate. The method of heating the substrate, however, was adopted for InkEpo as well because it allowed much better height and width homogeneity across the structures.

To evaluate the effect of solvent evaporation on waveguide shape and track height, lines with a nominal track width of 1 and 3 pixels were printed on PMMA foil. The pulse voltage was 23 V, the substrate was heated to 75 °C, which is the maximum processing temperature for this substrate to promote a good contour accuracy and evaporate the solvent after printing. Above this value, the polymer foil starts to buckle and turns opaque. 12 layers could be printed before bulges appeared.

The tracks were polymerised once directly after printing, and once after a 15 h pre-bake step at 75 °C, which was performed on the hotplate in the printer. Then, the track cross-section of both samples was characterised in a white-light interferometer (NewView 100, Zygo, Middlefield, USA). The effect of the pre-bake step is shown in Figure 6.4.

For InkEpo, the volume difference between the immediately polymerised samples, and the samples which were left over night at a temperature of 75 °C to ensure solvent evaporation is about 20 %.
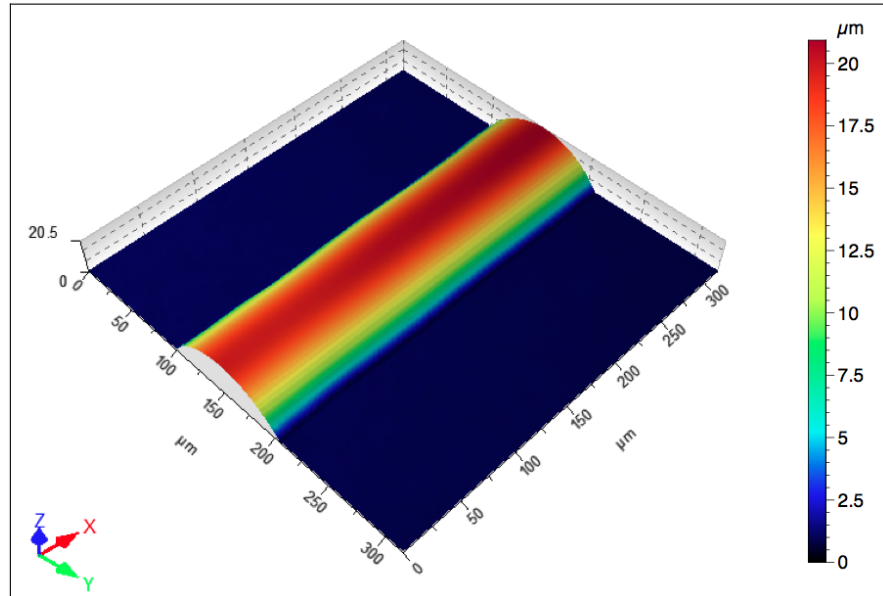
Figure 6.5: Scan of the track used for optical characterisation, taken in a confocal microscope (μsurf custom, (NanoFocusAG, Oberhausen, Germany). The track is 110 um wide, and 20 micron high. The surface roughness, shown below, was measured to be below 50 nm. Reprinted from [35] with permission.

6.1.1.2 *Optical evaluation of InkEpo*

To evaluate the ability of a deposited track of InkEpo to carry light, a test structure (5 pixels wide, 5 layers) was printed. Figure 6.5 shows a scan of the printed track, taken in a confocal microscope (μsurf custom, NanoFocusAG, Oberhausen, Germany). The track is 110 μm wide, and 20 μm high.

After preparing the facets by polishing, a sample with a length of 3 cm was placed in the *Beam Setup* characterisation stage. Figure 6.6 shows the front and rear facet of the sample. The waveguide core of the rear facet is clearly visible in the centre of the photograph, which proves that the waveguide carries light. However, the substrate appears almost as bright as the waveguide, which means that a significant part of the light is scattered into the substrate. Closer observation of the substrate reveals a distinct brightness pattern correlating with the position of the printed structures above, with the area under the waveguides darker. This suggests a significant scattering from the waveguide into the substrate.

A high magnification image of the waveguide facet, shown in Figure 6.7, reveals a possible explanation for the strong scattering. The image reveals that the interface between the deposited track and the substrate is not clearly defined, but rather a diffuse area almost as high as the printed track itself, where the ink appears to merge with the substrate. A scan of a similar sample with the refractive-index-profiler, shown in the bottom of that figure, supports this hypothesis.
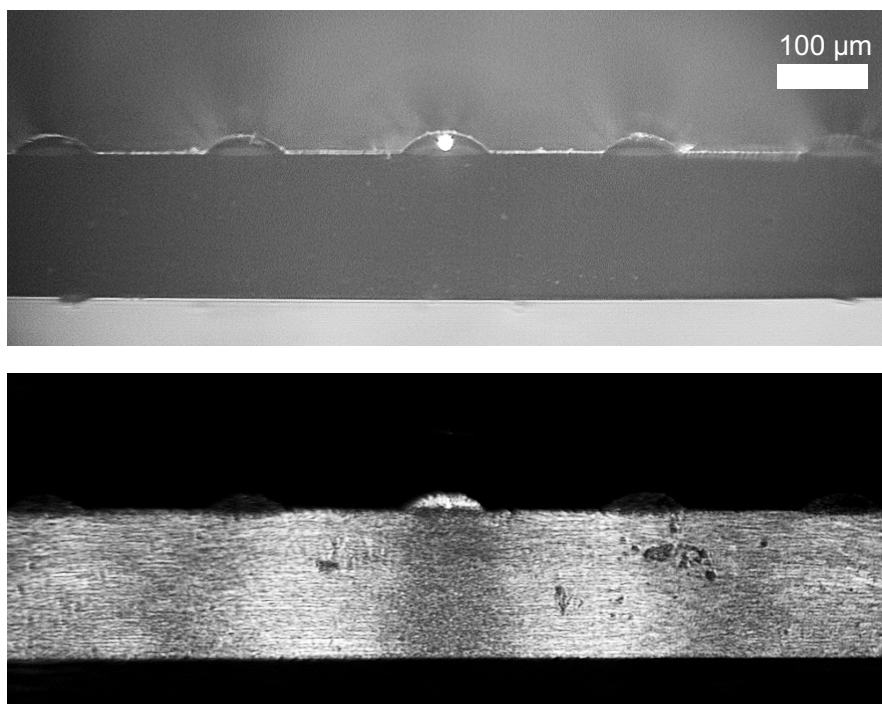
Figure 6.6: Images of front and back facet of a 3 cm long track of InkEpo. The front facet shows a clear laser spot to couple light. The rear facet shows a glowing waveguide, but also a distinct light pattern that correlates with the printed waveguides. This suggests strong light scattering from waveguide to substrate.

The area where the refractive index is homogeneous has a lune-shape. Below, there is an area with a refractive index gradient, which suggests that the ink or the solvent dissolves the substrate and causes an interface layer with unknown optical, probably diffuse, properties. A likely cause for this is the agressive solvent (GBL), which was shown to dissolve PMMA at elevated temperatures.

6.1.2 *Solvent-free ink*

6.1.2.1 *Ink-jet printing experiments*

SynthEG70 was prepared for experiments and was well printable in the Dimatix printer with a standard pulse pattern (Figure 4.3), similar to InkEpo and InkOrmo. The printhead was heated to 50 °C to reach the required viscosity, and no pre-bake was required before polymerisation. However, because the chosen photo-initiators are inhibited by oxygen, the polymerisation had to be performed in nitrogen atmosphere. A UV-exposure dose of $15\,J/cm^2$, given with an intensity of $500\,mW/cm^2$ over 30 seconds ensured full polymerisation.
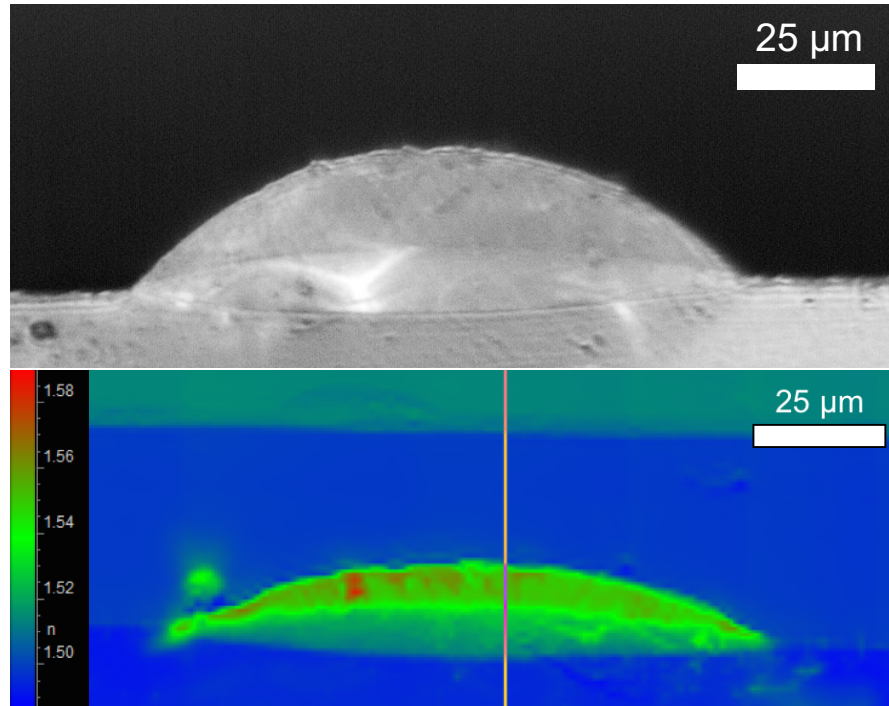
Figure 6.7: Top: A close-up view of the deposited facet of InkEp0, which reveals that there is an intermediate layer between a lune-shaped core. Bottom: Scan of a similar (flatter) facet with a refractive-index-profiler. The colour indicates the refractive index. The image reveals that there is a refractive index gradient, which suggests diffusion between core and substrate material.
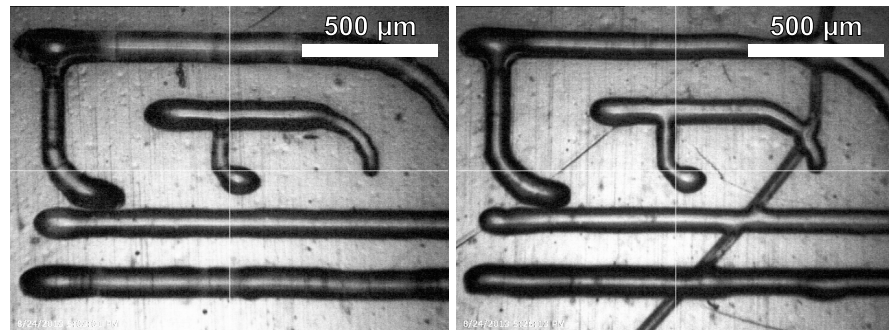
Figure 6.8: SynthEG70 printed on PET foil. On the left, the substrate was at room temperature. On the right, the substrate was heated to 60 °C. A slight influence on print homogeneity and line width is visible.

6.1.2.2 *Ink-jet Printing Evaluation*

Figure 6.8 shows a typical result of SynthEG70 printed on PET foil with good contour accuracy. Similar to the other inks, heating the substrate to elevated temperature improved this behaviour. For SynthEG70, printing 25 layers of a 1-pixel wide track at a voltage of 20 V allowed a track width of 130 micron, at a height of 23 μm on a sub-

strate heated to 70 °C. Generally, the printing performance is comparable with InkEpo. The test patterns show that curves can be printed with a reasonable contour accuracy and smooth edges, without the steps that occurred when printing curves with InkOrmo.

6.1.2.3 *Optical Evaluation*

To evaluate the light-guiding capabilities of the SynthEG materials, samples for a transmission measurement were prepared by polishing to a length of 3 cm and tested in the *Fibre Setup*. Figure 6.9 shows the rear facet of the sample used for evaluation, once with external white-light illumination, and once with laser illumination directly at the facet through the optical fibre. The experiment shows that a track of SynthEG ink gives a good light confinement on PMMA, and no stray light pattern, as it was seen in samples made from InkEpo, appears in the substrate. Close observation of the facet created by a SynthEG ink shows that the ink also dissolves the material, similarly to InkEpo, but the effect is less distinct. The concept of printing curves was not evaluated optically.
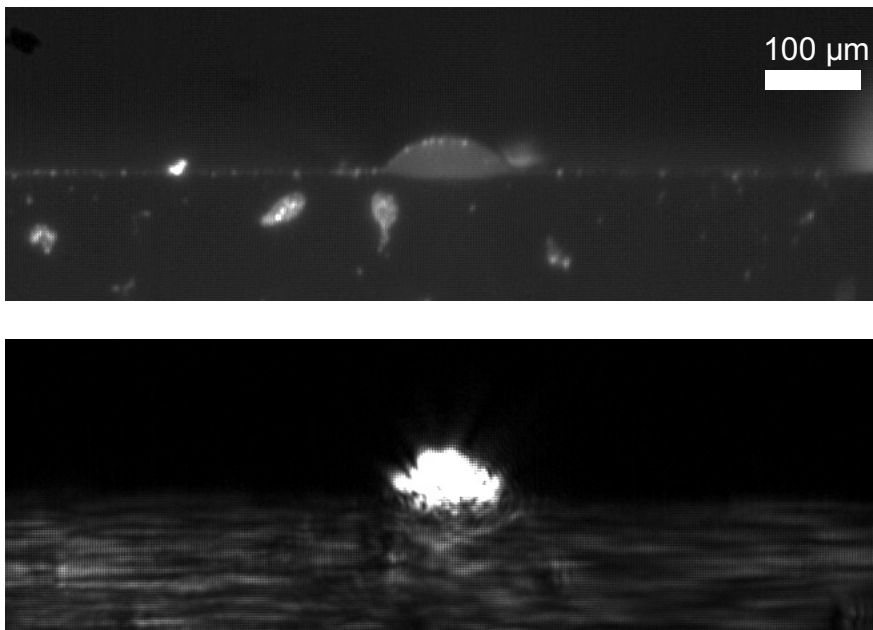
Figure 6.9: Optical evaluation of the rear facet of the polished SynthEG70 waveguide. On the top, the facet is shown with external white-light illumination. On the bottom, waveguide light transmission is shown. Unlike the sample of InkEpo, the substrate is dark, and the light is confined to the optical waveguide.

Occasionally, the printed tracks of SynthEG showed bubbles in the printed tracks, as can be seen in Figure 6.10. These appeared before polymerisation, but were not visible in the bulk material before it was filled into the printhead. This suggests that they are created during the printing process. However, it was not possible to find the cause of

this phenomenon, and it is unknown if the bubbles are gas, or liquid reactive diluent that accumulates within the ink. To avoid this issue, all waveguides which were tested for light transmission were checked under the microscope for these particles before.
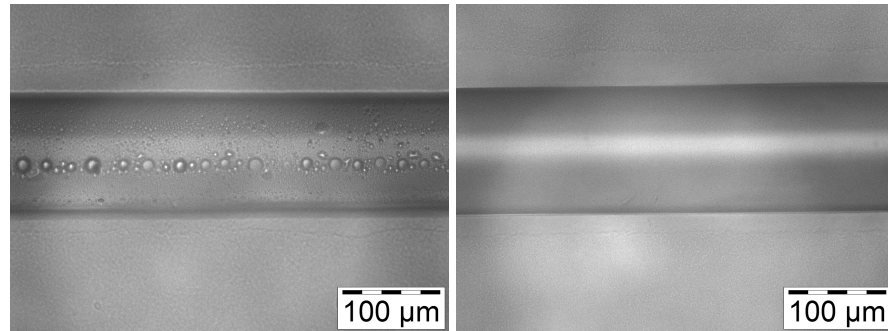
Figure 6.10: Track of SynthEG50 printed on PMMA at a substrate temperature of 60 °C. On the left, the unpolymerised track shows particles or bubbles with diameters ranging from 20 µm to below 1 µm. The origin of these imhomogeneities is unknown. On the right, the track is clear, and no particles are visible.

6.1.3   *Intermediate Conclusion of Material Comparison*

The experiments showed that InkEpo and InkOrmo are well printable. Sufficient contour accuracy is possible by heating the substrate, which is also required for solvent evaporation. However, the solvent is very problematic, as it requires heat and time to evaporate, during which it dissolves the substrate, which is suspected to cause light to scatter into the substrate. Because of the problems related to the solvent, InkEpo and InkOrmo were dismissed for printing optical waveguides on PMMA, which was the only material that combined a suitably low refractive index and a high optical transparency. Because of its low chemical and thermal resilience, a solvent-based ink could not be used.

SynthEG could be qualified as similarly well printable as InkEpo and InkOrmo in the Dimatix printer, and the aspect ratio was in a similar range. It was found out that the printing could be performed in ambient air, although the ink polymerisation mechanism is sensitive to oxygen. Inert gas was only necessary for the actual polymerisation. Without a solvent, the material required only two processing steps, deposition and polymerisation, and potentially harmful influences of an agressive solvent and thermal stress from solvent evaporation can be avoided. A big benefit of the material is that the refractive index is tunable within a certain range and therefore can be adapted to other used materials. Most importantly, SynthEG is able to carry light through a printed waveguide without causing significant scatter-

ing into the substrate. This quality makes the material the best choice for fabrication of optical waveguides from the available options.

There are, however, two disadvantages to the material. The first problem is the very high bulk attenuation, reported in Chapter 4, which is one order of magnitude above the values of InkEpo and InkOrmo. This reduces the maximal length where optical waveguides are still feasible for a given illumination power and detection limit. The second problem is the occasional particle formation after printing, whose origin could not be identified in the experiments and means that each manufactured sample needs to be checked rigorously for this phenomenon. Here, further research and subsequent material optimisation is required to reach the performance of the commercial products. Yet, the experimental comparison of the results showed that a solvent-free acrylate-based ink gave the best results on the selected PMMA substrate.

6.2 PRINTING ELEVATED STRUCTURES ON POLYMER SUBSTRATES

6.2.1 *Approach I: Thermally Induced Pinning and the Resting Time Effect*

In the proof of principle, it was shown how a heated substrate enabled a better contour accuracy of the printed structures (Figures 6.3 and 6.8). This phenomenon was used as a tool to increase the contact angle θ of the deposited ink on the polymer foil substrates, leading to higher structures, which were shown to have lower attenuation values in the simulations. Additionally, higher waveguides with larger facets enable better light coupling from a point source, which makes them more suitable for experimental characterisation.

Upon characterisation of the relation between temperature and θ, it became apparent that not only the temperature, but also the time frame between deposition of individual layers is a critical parameter for this tool.

6.2.1.1 *Phenomenon of Thermally induced Pinning*

The printer which was used in this thesis creates a two-dimensional droplet pattern by printing many subsequent lines. When more than one layer is deposited, the printer finishes one entire pattern, and then deposits the first line of the next layer. This leads to a varying time interval t_p between the deposition of the individual layers, depending on pattern size.

For situations where the deposited ink interacts with the substrate over time, this effect can lead to a different printing result depending on the pattern size. For example, a solvent-based ink deposited on a heated substrate will lose a fraction of its solvent before the next layer is deposited, and the diffusion process between an ink that dissolves

the substrate will be affected as well. Depending on t_p, and therefore on pattern size, the print result will be different.

For the present case with solvent-free materials, a longer t_p enables a certain number of printed layers to form a straight and homogeneous line, whereas the same number of layers would form bulges with shorter time intervals. Evidence for this phenomenon is shown in Figure 6.11.
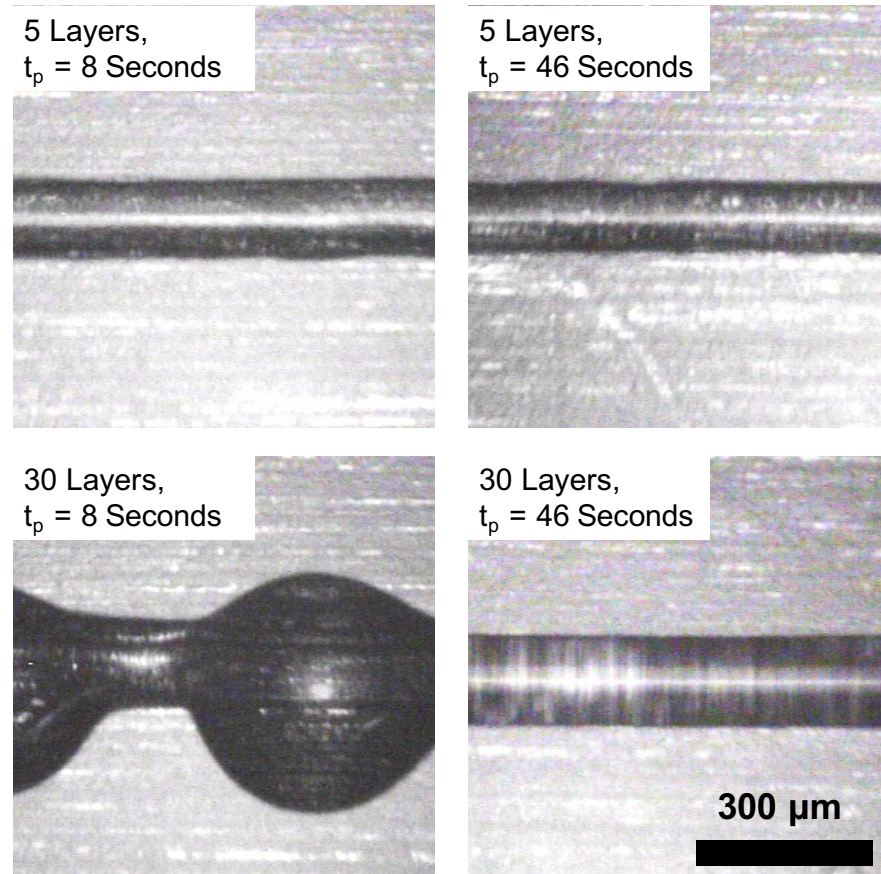
Figure 6.11: Influence of resting time between deposition of individual layers when printing on a heated substrate on the morphology of a track printed of several layers. For a given temperature and number of layers, the time between deposition reduces the line width and the maximum number of layers before bulge instabilities occur. Reproduced with permission from [15], © IOP Publishing. All rights reserved.

In this experiment, two different patterns were printed with SynthEG50 at 18 V on PMMA foil heated to 60 °C. The different patterns led to two different values for t_p of 8 s and 46 s. All other printing parameters were identical.

When printing five layers, both patterns resulted in homogeneous tracks without any interruptions. The print with a t_p of 8 s showed a track width of $135 \pm 3\,\mu m$, whereas a t_p of 46 s resulted in a track width of $123 \pm 3\,\mu m$. As the same material was deposited, a higher

track height can be expected. When depositing 30 layers, the result is much more striking. The pattern with a t_p of 8 s no longer shows smooth and continuous lines, but bulges. This means that the contact angle θ exceeded the threshold that allows smooth lines. The pattern with a t_p of 46 s, on the other hand, still results in homogeneous lines, with a line-width of $163 \pm 3\,\mu m$. This result shows that the effect of the resting time t_p is a valuable tool when printed structures with a high aspect ratio are desired.

6.2.1.2   *Characterisation of the thermal pinning effect*
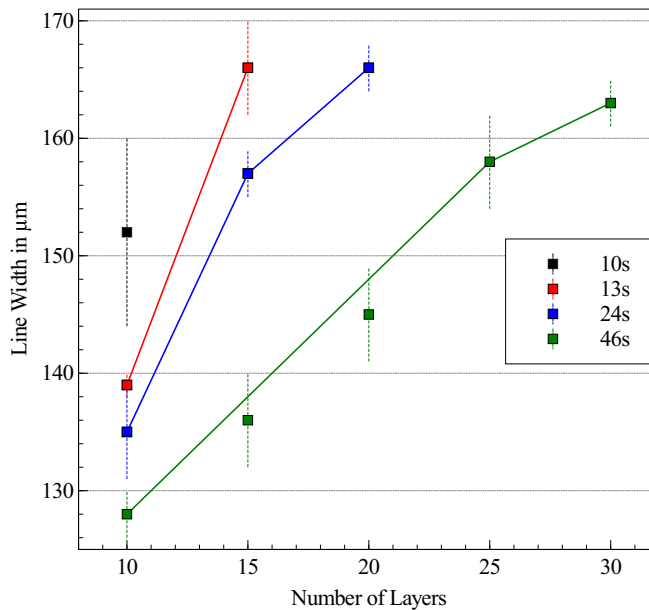
Figure 6.12: Results of evaluation of thermal pinning, showing the measured line width depending on the time interval t_p and the number of deposited layers. Reproduced with permission from [15], © IOP Publishing. All rights reserved.

To characterise the thermal pinning phenomenon, lines with increasing numbers of layers n and four different time intervals t_p (10 s, 13 s, 24 s, 46 s), with a fixed drop spacing x of 25 μm, a fixed voltage of 18 V, and a fixed substrate temperature of 60 °C, were printed. The track width w was measured before polymerisation, directly in the printer. This data is shown in Figure 6.12.

The results show that for 10 deposited layers, even a comparatively small increase of t_p from 10 s to 13 s has a significant influence on the track width, which was reduced from $152 \pm 8\,\mu m$ to $139 \pm 1\,\mu m$. A further increase of t_p to 24 s and 46 s continued to reduce the line width, but the effect was less pronounced.

The second effect of increasing t_p is the increased amount of deposited ink before bulge instabilities occur. For a resting time of 10 s, only 10 layers could be deposited. A slightly longer resting time al-
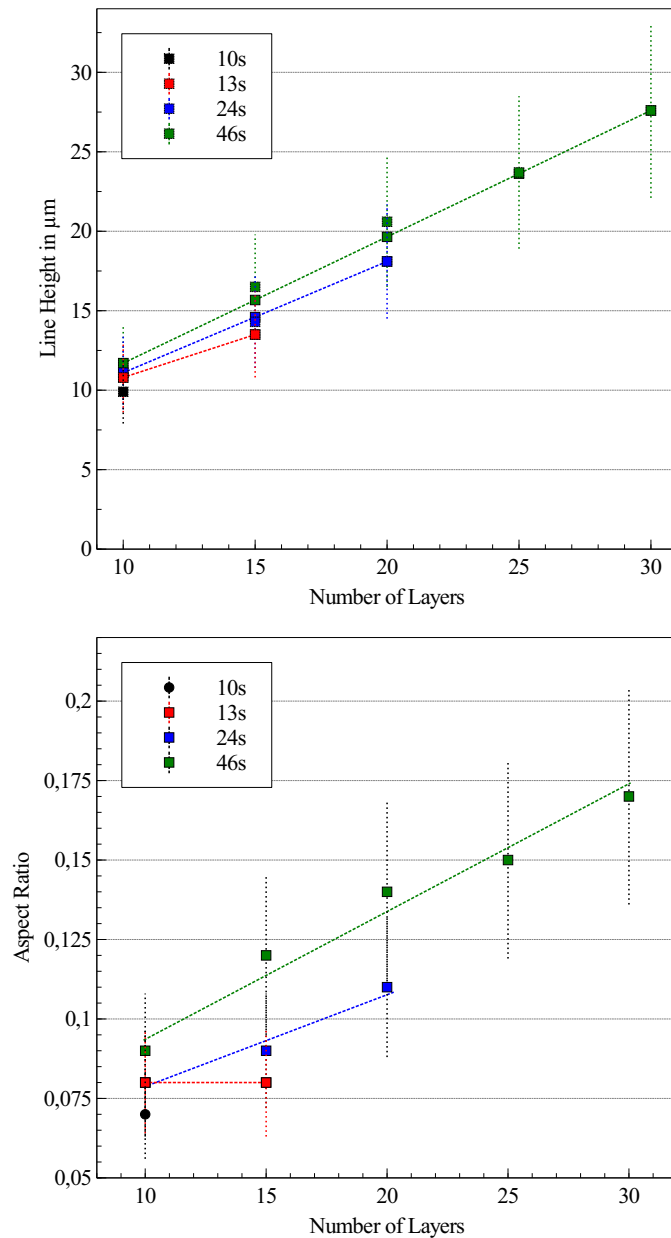
Figure 6.13: Track height and aspect ratio for the evaluation of the resting time effect at thermally induced pinning, derived from the measured track width, measured droplet mass, and given density. Reproduced with permission from [15], © IOP Publishing. All rights reserved.

ready increased the number of possible layers to 15, and the trend continued, up to 30 layers at a resting time t_p of 46 s. Just before bulge instabilities occurred, the track width increased less with additional deposited layers. Before this, the track width per deposited layer can be approximated with a linear function.

From the width values and the amount of deposited volume, the track height and aspect ratio were derived. To calculate the deposited

volume, the mass of 10^6 droplets was measured, giving a droplet mass of 2.8 ± 0.5 ng. This value was divided by the ink density of 1.10 g/cm^3, which was taken from literature [106, 107]. As a result, the droplet volume V_d of 2.5 ± 0.5 pl was derived. From this value and the geometry described in Chapter 3, the track height h and the aspect ratio R was calculated. The data is shown in Figure 6.13.

The results show that the track height and aspect ratio increase in a similar fashion as the track width, but the direct effect of the t_p on the gradient is weaker. The maximum values are mainly caused by the increased amount of layers that can be deposited before bulge instabilities occur. Due to the large uncertainty of the droplet volume measurement, the derived values of track height and aspect ratio show large error bars.
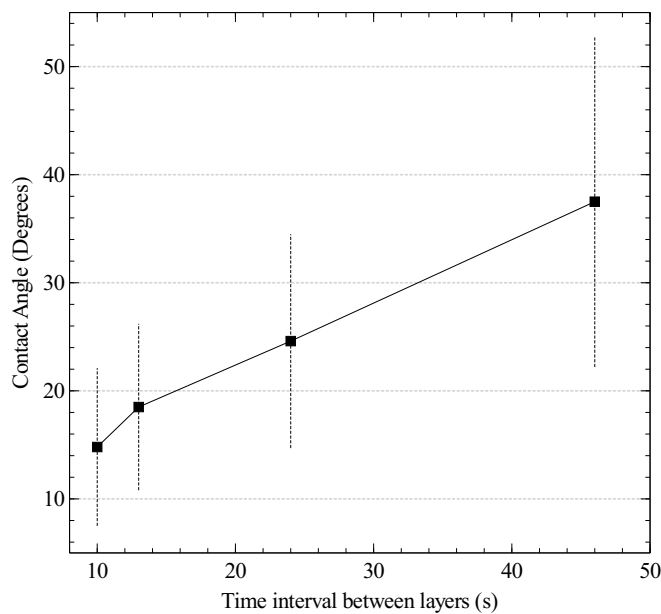
Figure 6.14: Effect of resting time t_p at thermal pinning on the maximum contact angle θ. Reproduced with permission from [15], © IOP Publishing. All rights reserved.

To visualise the effect from a second angle, the contact angle θ at the three-phase interface was plotted as a function of the increasing t_p. This value can be calculated by $\theta = \arcsin \frac{4 \cdot h \cdot w}{4 \cdot h^2 + w^2}$. The data is visualised in Figure 6.14, and shows that the contact angle of the printed structures could be substantially increased from $15 \pm 7\,°$ to $38 \pm 15\,°$, simply by increasing the resting time t_p from 10 s to 46 s.

6.2.2 *Approach II: Lightplate*

Conventionally, photopolymerisable ink-jet printed structures are exposed to UV-light after printing by an external source placed above the sample. However, in the time frame between deposition and poly-
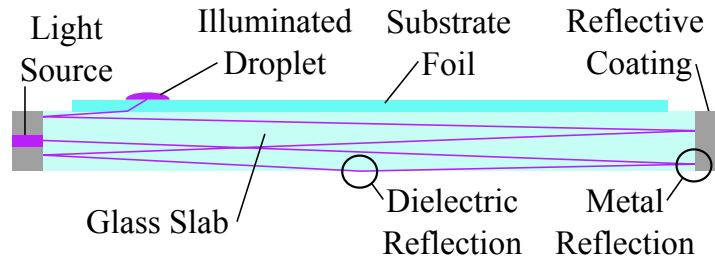
Figure 6.15: Cross-sectional schematic of the Lightplate. The purple line in-
          dicates a single beam of light. In reality, an LED with a cone-
          shaped emission is used.

merisation, the ink can spread out on the substrate, which is typi-
cally more energetically favourable, but undesired when the aim is
to maximise the track height and aspect ratio. To solve this problem,
an alternative polymerisation method was devised which exposes the
printed ink to UV-light immediately in the moment when it lands on
the substrate.

The basis for this concept is the phenomenon of total internal reflec-
tion in a material with higher refractive index than its surroundings.
If a transparent sheet of material is illuminated by a small light source
at the edge, most of the light will follow Snell's law and travel within
the sheet, similar as in an optical waveguide or Colladon's light pipe
shown in Figure 1.2. If the entire edge area of the slab is covered with
a reflecting metal (with the exception of the area covered by the light
source), most of the light will be contained and continue to travel
inside until it is eventually scattered or absorbed. A UV-transparent
substrate foil with similar refractive index can be placed on the illumi-
nated slab and pick up the light. If a liquid drop is deposited on the
surface of the illuminated substrate, the refractive index step is sud-
denly much lower, causing the light to enter this droplet. To maintain
an air interface and total internal reflection at the bottom interface,
the device has to be held by support structures.

With a suitable UV wavelength and material, this concept can be
used for photopolymerisation of printed ink. A deposited material
will be exposed to the UV-light as soon as it is in contact with the
illuminated sheet, and receive the radiation dose required for poly-
merisation. It is expected that this has an influence on linewidth and
aspect ratio of the printed structures, similarly as thermal pinning.
A schematic of the concept, which is called *Lightplate*, is shown in
Fig. 6.15.

6.2.2.1 *Theoretical Considerations*

For a simple estimation of the light intensity within the Lightplate,
two approaches are presented, with identical results. Both assume
that all light is completely confined by total internal reflection, and

only lost upon absorption on the metal at the edges. The reflective coating has a reflectively R and an absorbance A ($A + R = 1$).

The first approach models the path of the light starting at the source. If a pulse of light is emitted with a given radiant energy Q_0 and travels along the Lightplate, it has the chance of A to be absorbed, and R to be reflected at the metallic edge. In the second pass, after the first reflection, the pulse energy is $Q_1 = Q_0 \cdot R$. Upon the second reflection, the same fraction is absorbed again: $Q_2 = Q_1 \cdot R = Q_0 \cdot R^2$. The $n_t h$ element of this series can be expressed with $Q_n = Q_0 \cdot R^n$. At any given time, there is the sum of all those passes in the glass slab.

$$Q_{total} = \sum_{n=0}^{\infty} Q_0 \cdot R^n \tag{6.1}$$

For a reflectivity of 93%, which is the value for aluminium at 365 nm, the value becomes

$$Q_{total} = 14.29 \cdot Q_0. \tag{6.2}$$

This approach suggests that the Lightplate concept can in fact be used to create an illuminated substrate, and that the reflective coatings significantly increase the light intensity.

An alternative model follows the approach that the emitted power Q_0 and the absorbed power $A \cdot Q_{total}$ quickly reach equilibrium and maintain it.

$$Q_0 = Q_{total} \cdot A \tag{6.3}$$

With a reflectivity of 93%, 7% of the light in the Lightplate is absorbed at the edges. The result is

$$Q_0 = Q_{total} \cdot 0.07 \tag{6.4}$$

and

$$Q_{total} = 14.29 \cdot Q_0 \tag{6.5}$$

This value is identical to the first result. The model suggests a considerable increase of intensity can be expected by the reflective coatings, and that a higher reflection coefficient significantly increases the power in the Lightplate.

6.2.2.2 *Design and Materials*

The main element of the Lightplate is a UV-transparent sheet. For this, two glasses were available for experiments (N-BK5 and N-FK7, Schott AG, Müllheim, Germany). For the substrate foil, it was assumed that the refractive index should not be lower than the refractive index of the plate to allow the light to pass into the substrate.

Table 6.1: Suitable materials for the Lightplate. The refractive index of InkEpo is in unpolymerised state with solvent.

Element	Material Name	Material Type	$n_{I,20}$
Plate			
	N-FK5	Glass	1.504
	N-BK7	Glass	1.536
Substrate			
	"Plexiglas Spezial"	Polymer	1.49
	D263	Glass	1.53
	TOPAS	Polymer	1.557
Ink			
	InkEpo	Polymer + Solvent	1.476

Here, three UV-transparent materials were available: Thin borosilicate glass (D263, Schott AG, Müllheim, Germany), a cyclo-olefin co-polymer resin as foil (TOPAS COC, TOPAS Advanced Polymers GmbH Frankfurt-Höchst, Germany), and "Plexiglas Spezial", which is a custom fabricated PMMA foil without the UV-stabilisers typically found in PMMA foil. The materials and their refractive indices are listed in Table 6.1. The reflective coating was created by chemical vapor deposition of aluminium, as it has the highest UV reflection coefficient of commonly available metal coatings [110].

As light source, high-power UV-LEDs (OCU-440 UE365, OSA Opto Light, Berlin) were selected, each with a power of 75 mW at 365 nm (I-line). The diodes were placed on a PCB in a row, wired in series, and the complete element was supplied with a current of 350 mA and a voltage of 16 V.

As ink, InkEpo was selected because it is the only available ink that does not show oxygen inhibition, although the volatile solvent poses a problem as it should be evaporated before polymerisation. Additionally, the volatile solvent significantly reduces the refractive index to 1.476, which reduces the amount of light that couples into the deposited material.

6.2.2.3 *Ray-Tracing Simulations*

For the theoretical consideration, an idealised model was assumed where all light is perfectly confined in the plate until it is absorbed by the edges. For a more realistic model of the Lightplate, ray tracing simulations were performed with all combinations of available materials. Two hypothetical inks with refractive indices of 1.51 and 1.60 were simulated. The simulation model is shown in 6.16. It consists of a glass slab measuring 75 mm x 75 mm x 4 mm, and a thinner substrate slab measuring 60 mm x 60 mm x 0.1 mm. At one edge, a light emitting area with a power of 300 mW and dimensions of 3.8 mm x 15.2 mm is placed. To model the reflective coating, the edges of the plate were defined to have a reflection coefficient of 95%, which was, from the range of available simulation parameters, closest to the reflection coefficient of Aluminium. To detect the light in the different parts of the Lightplate, detector rectangles were placed in the glass slab, in the substrate, and above the substrate.
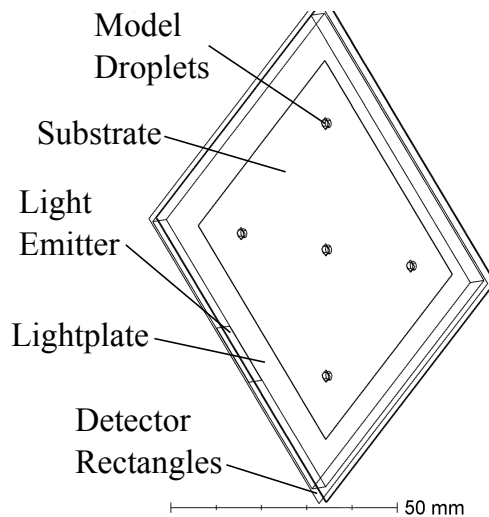
Figure 6.16: CAD model of the Lightplate as displayed in ZEMAX

In the first simulation, the power in the Lightplate was investigated and compared to the theoretical model from the previous section. With a reflectance of 95 %, the detector inside the plate counted about 7 W, which is 23 times the power of the light source. The theoretical model would predict a factor of 20 for this reflectivity value, which is a justifiable deviation from the analytical model of 15 %. To verify this result, a reflectance of 50 % was simulated, resulting in a power of about 0.7 W, which is 2.3 times the entered power. This is also in accordance with the theoretical model.

In a second simulation, the effect of a refractive index difference between plate and substrate was simulated, with the expectation that the refractive index of the substrate should be above the refractive index of the plate to ensure that the light from the plate progresses into the substrate. The results are visualised in two graphs, shown in Fig-
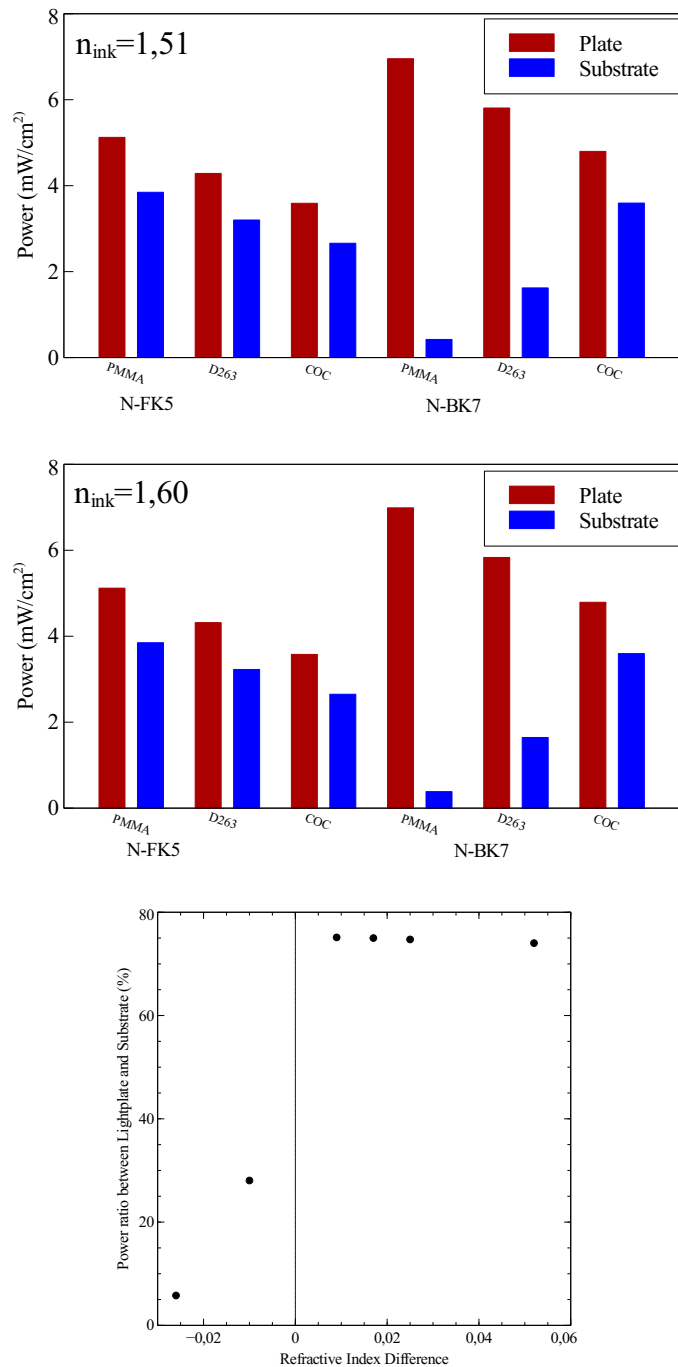
Figure 6.17: Simulation of the power inside the Lightplate, and inside the substrate. The first two graphs show the absolute values of each dataset, and reveal that the ink does not have an influence on the power in plate or substrate. The bottom graph shows the ratio of power that couples from the Lightplate into the substrate, plotted against the refractive index difference, and reveals that any positive index difference gives a good coupling, whereas negative values cause a significantly worse performance.

ure 6.17. The left graph shows the absolute power measured by the two area detectors in plate and substrate, the right graph the power ratio between substrate and plate versus the refractive index step. It can be seen that generally, a high refractive index in the plate gives a higher absolute power in the plate, but a lower power that is passed onto the substrate. Additionally, the power in the substrate is very low if the refractive index of the plate is higher than the refractive index in the substrate. This is visible in the right plot. Therefore, the simulation confirms the prediction that a positive refractive index step from plate to substrate increases the power in the substrate. However, as soon as the refractive index step is positive, the ratio stays constant, which means that any substrate material is suitable as long as its refractive index is above the refractive index of the Lightplate.

In a third simulation, the intensity within the deposited droplets was simulated. For this, five cylinders with a radius of 1 mm and a height of 1 mm to model five deposited droplets were placed at the centre of the Lightplate and in the four corners of a square measuring a side length of 40 mm. To detect the light in the cylinders, detectors with a side length of 1 mm were placed at each one. The simulation results for the combinations of both available plate materials, three available substrate materials, and two inks, are shown in Figure 6.18. The left figure shows the absolute power measured in the droplets. Typically, the droplet in the centre had twice as much power as the droplets at the edges, which means that the light distribution is not even. The right figure shows the ratio between average droplet power and substrate power plotted versus the refractive index step from substrate to ink. This result is surprising. While there is a clear correlation between refractive index step and power ratio between plate and substrate, for the ink material there is no correlation visible. This means that a positive refractive index step from substrate to ink is not necessary.

The result of the simulation is that the substrate should always have a higher refractive index than the Lightplate. On the other hand, it appears that the refractive index of the inks is not critical.

6.2.2.4 *Experimental Results*

To test the Lightplate experimentally, a prototype was built. Although FK5 showed slightly higher power in the simulations, BK7 was chosen as material for the plate because it was readily available off the shelf in a suitable size. After polishing the edges by hand in a grinder-polisher until they appeared as optically clear, the aluminium coating was created by CVD (Minicoater, Tectra, Frankfurt (Main), Germany). To lift the Lightplate from the ground and allow total internal reflection at the bottom interface, laser-cut PMMA legs were attached to the Lightplate at the corners. The four diodes were placed on a carrier substrate of FR4, contacted in series, powered by a desktop power
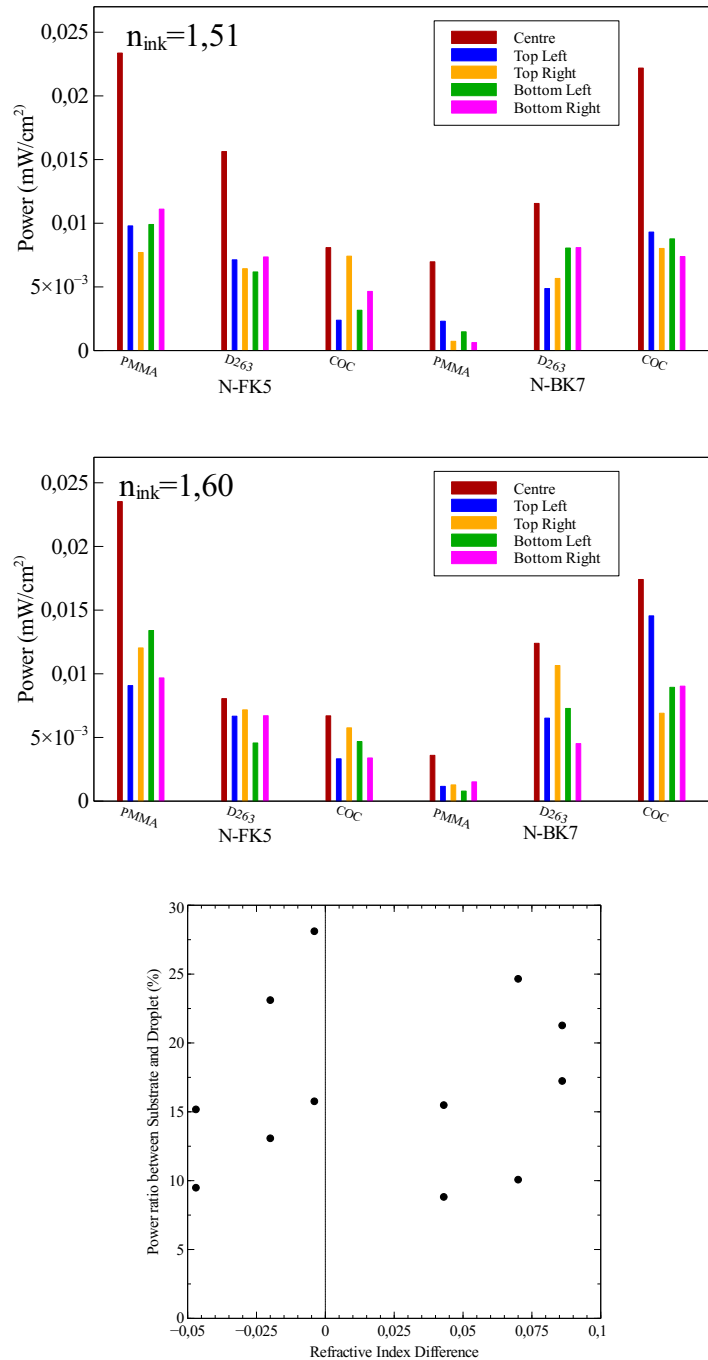
Figure 6.18: Simulation of the intensity inside the droplets on the Lightplate for all possible material combinations. The first two plots give the absolute values and reveal that the droplet in the centre typically receives the double amount of power than the other droplets. The bottom graph shows the ratio of power between average droplet and substrate plotted against the refractive index difference. Here, no correlation is visible, which suggests that the refractive index of the ink does not affect the intensity of the interface significantly.

supply and then glued to the Lightplate with an UV-transparent optical adhesive (NOA 63, Norland Products, Cranbury, USA). The prototype is shown in Figure 6.19
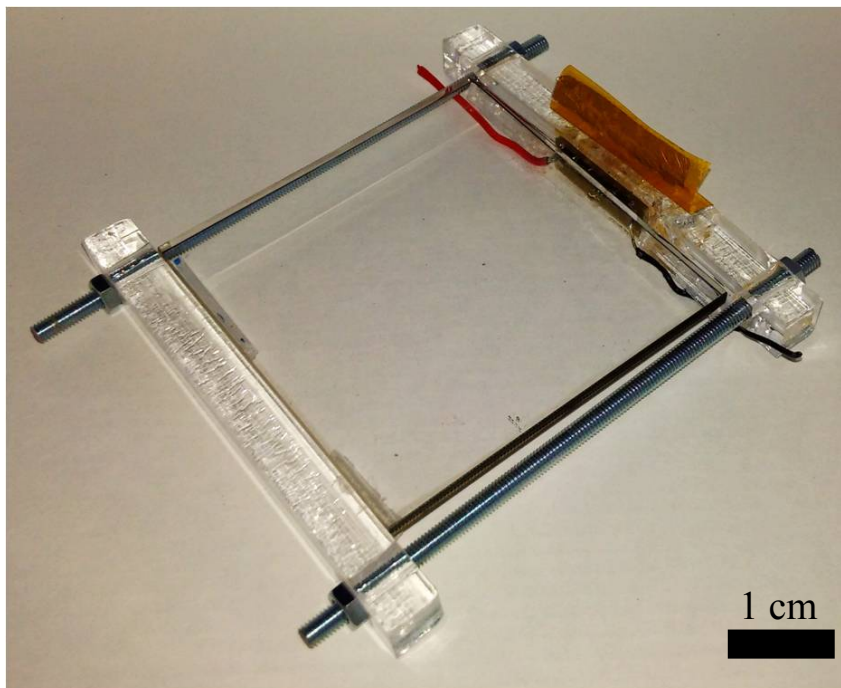
Figure 6.19: Photograph of the assembled Lightplate prototype. A glass-slide with aluminium-coated edges was fitted with an LED-bar with 5 elements at the top right. Threaded rods and blocks of PMMA were used to build a frame that held the glass slide above ground.

All three substrate materials were tested, but only TOPAS was compatible with InkEpo for printing tracks at room temperature. To remove the air gap between the glass slab and the substrate, ethanol was dispensed on the Lightplate before placing the foil.

Figure 6.20 shows how a syringe filled with fluorescent ink from a marker pen reacts to the Lightplate. On the left, the syringe is held just above the Lightplate, and the dye does not fluoresce, while the droplets on the substrate are glowing brightly. On the right, the syringe is in contact with the Lightplate, and the syringe lights up brightly at the tip. This shows that the UV-light is confined inside the Lightplate until the ink is in direct contact, and hereby confirms the functionality of the Lightplate concept.

To investigate the effect of the Lightplate on ink-jet printed tracks, an experiment was performed in the Dimatix printer. A test pattern of single droplets and printed tracks was printed with and without activated UV-light. Directly after printing, an image was taken with the fiducial camera, and the track width was compared. After printing, the illumination of the Lightplate was maintained for one minute to allow fore full polymerisation. After this time, the deposited tracks
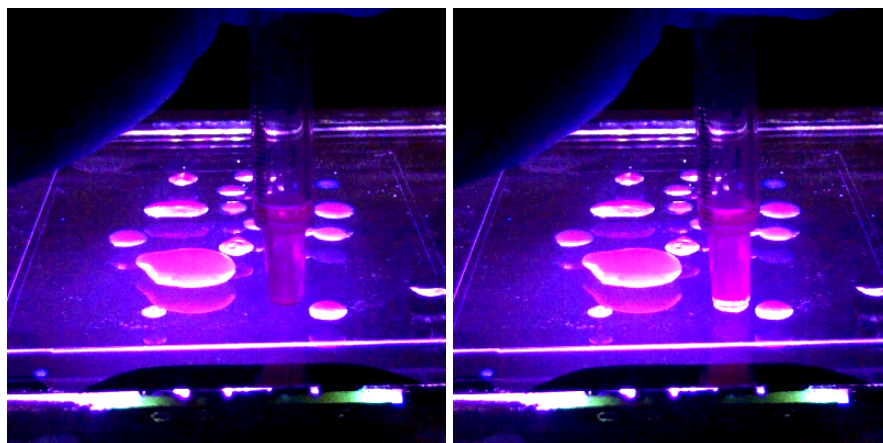
Figure 6.20: First experimental demonstration of the Lightplate. On the left, the syringe is held slightly above the surface, and the fluorescent ink inside is dark. On the right, the syringe is brought down, and the fluorescent dye lights up.
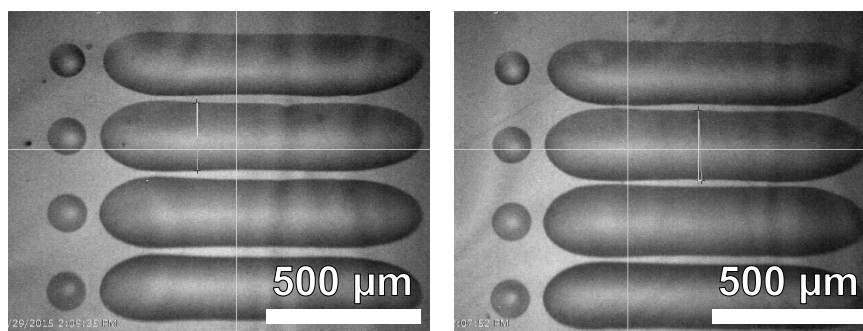
Figure 6.21: Images of printed structures taken in the Dimatix printer, without (left) and with (right) UV-light. The structures look similar, which indicates that the Lightplate has no effect on the ink at this point on TOPAS.

were polymerised, but still contained the solvent, as the Lightplate prototype did not have any heating elements.

However, the Lightplate prototype appears to have no significant effect on the morphology of the printed structures, as the structures shown in Figure 6.21 are identical. Without light, the droplet had a diameter of 130±10 μm, and the track a diameter of 219±10 μm. With UV light the droplet had a diameter of 117±10 μm, and the track a diameter of 224±10 μm. The slighty lower diameter of the droplets printed with activated polymerisation can be attributed to polymerisation shrinkage.

6.2.3 *Discussion of presented methods to print elevated structures*

6.2.3.1 *Thermal Pinning*

The finding that ink-jet printed structures can reach higher aspect ratio values if they are created more slowly is an important addition to the repertoire of tools which are commonly used in the field of ink-jet printing and not yet reported in the literature. On the other hand, the effect requires further characterisation to evaluate benefits and disadvantages. The time needed to exploit the effect are in conflict with industry's requirement of a fast process, and the interaction between ink and substrate has to be evaluated for other inks before it can be generalised. Regarding the application for optical waveguides, the diffusion processes during t_p at the optical interface between substrate and printed core have to be studied in regard of their influence on the optical attenuation of the waveguide.

6.2.3.2 *Lightplate*

The most likely explanation for the missing effect of the Lightplate on line width is that the light intensity on the Lightplate was too weak to enable a rapid polymerisation. Although a highly increased intensity was predicted by theory, it appears that the ink still flows into equilibrium before the polymerisation occurs. This hypothesis could either by investigated theoretically by comparing the time scale of polymerisation and ink flow, or experimentally by using a sufficiently fast camera.

Following Haitz's law [111], which can be considered to be the LED counterpart to Moore's law [112], the amount of light created by an LED grows by a factor of 20 every decade. This means that a higher intensity can be expected to be available in the future. Additionally, more sophisticated reflectors, like photonic crystals [113], would greatly enhance the intensity within the Lightplate.

On the other hand, the Lightplate poses strong design rules on the substrate material, as the refractive index has to be higher than the Lightplate material. Also, the material has to be UV-transparent, which rules out most polymer foils. Ultra-thin glasses appear as an alternative choice and should be further investigated to find an ink with compatible surface behaviour.

As modification of surface wetting is critical for process control of ink-jet printing, there are other methods which could be used to achieve elevated structures for optical waveguides.

The most common method to create elevated structures with ink-jet printing is to polymerise each layer of deposited material is polymerised directly after printing. This concept is commercially applied, for example under the name *PolyJet* (Stratasys, Rechovot, Israel).

The advantage of this method is its simplicity, as UV LED lamps are compact and can be integrated in printing systems easily. However, for inks that show oxygen inhibition, the entire setup must be put under inert atmosphere [114], or a material that polymerises despite the presence of oxygen must be found. Additionally, inks with a solvent require an evaporation step for every layer, which increases processing time. However, the method of layer-by-layer polymerisation was not investigated in this project.

Instead of heating, substrate cooling can also be used to affect the behaviour of the ink on the substrate. However, cooling the substrate is much more difficult to achieve in a mass-production facility than substrate heating, as latter can be achieved in a non-contact fashion by simple infrared radiators, whereas cooling requires a liquid cooling system.

Another common tool for surface behaviour modification is oxygen plasma [115]. Here, the plasma ions interact with the chemical bonds on the surface of the substrate material, which are normally saturated with ambient oxygen. As a result, the wetting behaviour is altered. Depending on the ink, the contact angle either increases or decreases. This is typically done for an entire substrate in a plasma chamber under low pressure. However, the effect can also be created locally by so-called plasma torches, which are able to operate under normal atmospheric conditions [116, 117]. Such a system (µPlasma for PixDRO LP50, Meyer Burger Technology AG, Gwatt, Switzerland) is already available commercially for ink-jet printing [118]. Unlike the variant that employs a plasma chamber, such plasma torches allow to create individual tracks with a tailored surface behaviour, which could potentially be used to increase the contact angle of printed structures.

A similar technique is the deposition of conditioning lines [36–39]. Here, a track which confines the deposited material later is created by two tracks of a different material which were printed before. If a suitable material is chosen, the materials of the deposited core and the conditioning lines avoid contact, which helps to increase the contact angle.

All of the listed methods have certain benefits, depending on application and materials, which makes it difficult to reach a general comparison. It is attempted in table 6.2.

The Lightplate can be seen as a comparable method to intermediate polymerisation. The benefit of polymerisation by a Lightplate has to be verified, because intermediate polymerisation can happen in similarly quick time frames with an integrated lamp. An important benefit is that the printhead is not exposed to UV-light with a Lightplate, which could improve process reliability.

Both the plasma torch and conditioning lines generate locally altered surface properties. Conditioning lines can be fabricated with

an area-processing technique such as flexographic printing, whereas the plasma torch has to be moved in a linear fashion, ideally directly attached to the print-head.

Table 6.2: Classification of different methods to alter the wetting behaviour of printed structures.

Method	Planar/Linear	Complexity/Effort
Substrate heating	Planar	Low
Substrate cooling	Planar	High
Intermediate Polymerization	Planar	Low
Lightplate	Planar	High
Oxygen Plasma	Planar	High
Plasma Torch	Linear	High
Conditioning Lines	Linear	High

6.2.4 *Intermediate Conclusion for Methods to Print Elevated Structures*

By increasing the resting time t_p between the deposition of individual layers on a heated polymer foil, the aspect ratio of printed structures could be increased significantly. This finding implies that for any elevated structure created from a low-viscosity material, as it is used by ink-jet printing, the resting time has to be considered when characterising the behaviour of the ink on the substrate. If elevated structures are desired, a longer resting time on a heated substrate contribute to this goal. The method therefore represents a very valuable tool for creating elevated structures on polymer foils.

The expected effect of the Lightplate could not be demonstrated successfully. While the light created by the Lightplate was sufficient to polymerise the printed material, the dimensions of the tracks printed with and without UV light are identical. This means that the goal to affect the track width with the Lightplate was not reached. However, it could be shown that the principle works. If the light intensity could be increased significantly, the effect on the morphology of the printed structures will likely show. Therefore, the concept should not yet be dismissed, but kept in mind when selecting a method to create elevated structures by ink-jet printing.

6.3 CLADDED WAVEGUIDES

For many applications, it is necessary to protect the wave-guide core that carries light from the environment. Common round optical waveguides have a tubular transparent cladding around the cylindrical core, which serves both as an optical interface for total internal reflection and as first protection layer from the environment.

To provide a solution for these requirements for printed optical waveguides, different designs of printed cladding layers were tested. The most suitable design was fabricated and characterised.

As the structures presented in this thesis are flat and fabricated in layers, it is better to understand the cladding as a lower and upper cladding layer. These two elements will be investigated separately in this section.

6.3.1 *Printed lower cladding*

In the experimental assessment, the substrate foil acted as a lower cladding for the printed waveguide. Although this is an elegant solution because it reduces the required number of processing steps, it poses a design constraint for the substrate, as the material needs to be optically transparent and show a lower refractive index to ensure light confinement. To become independent of these constraints, a printed layer that acts as lower cladding was investigated.

6.3.1.1 *Ink-jet printed lower cladding*

At a wavelength of 800 nm, Ink Ormo has a refractive index of 1.51, Ink Epo a refractive index of 1.54. Therefore, Ink Ormo was chosen for the lower cladding, and InkEpo for the core. After printing and polymerisation of a 20 pixel wide track of InkOrmo, a single line of InkEpo was printed as core. At room temperature, a distinct bulge formation along the track was observed, which indicates that the advancing contact angle of this interface is very low. Similar to earlier experiments, heating the substrate to 70 °C allowed to print continuous lines. With a heated substrate, it was possible to print continuous tracks on a printed lower cladding, as shown in Figure 6.22. By printing three subsequent layers of Ink Epo at 20 V, a waveguide core with a width of 100 µm and a height of 10 µm, as shown in Figure 6.23, was created. Aspect ratios above 1/10 could not be achieved, and light transmission measurements were not possible with the available setups at such low aspect ratios.

6.3.1.2 *Flexographic printing*

In a second study, flexographically printed tracks of an acrylate varnish [35] were employed as lower cladding. Similarly to the previ-
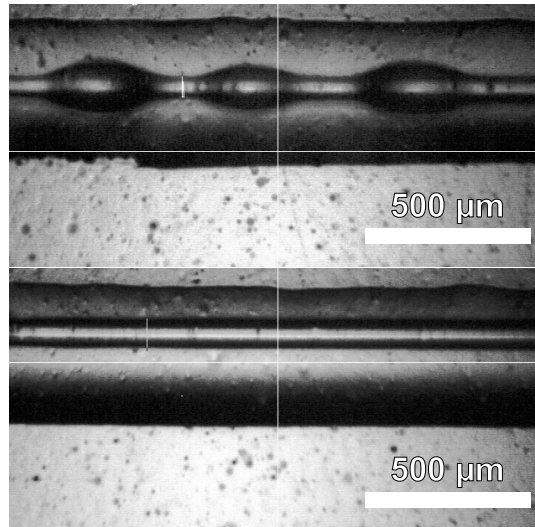
Figure 6.22: Thin track of InkEpo on a printed area of InkOrmo as lower cladding. On the upper picture, at room temperature, on the bottom, at 70 °C.
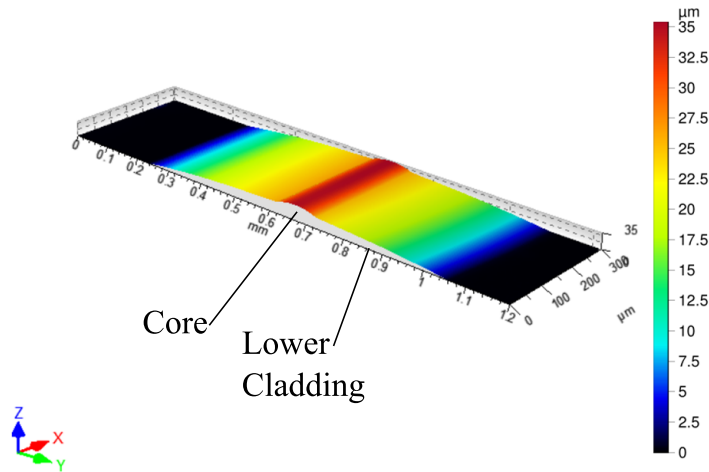
Figure 6.23: Experimental result for an ink-jet printed core on an ink-jet printed lower cladding. The picture shows a confocal scan of a waveguide printed with InkOrmo as lower cladding and InkEpo as core. Reprinted from [119].

ous study, Ink Epo was used as core material. For the flexographically printed tracks, the previously applied method to use heat to improve the ink behaviour was not sufficient to create continuous tracks. Therefore, 60 s of oxygen plasma treatment at a power of 100 W in combination with heating the substrate was used. This method led to wetting conditions suitable for continuous tracks. However, the line formation process was still very unstable and allowed only an aspect ratio below 10 %, and some sections of the printed tracks still showed bulge formation.
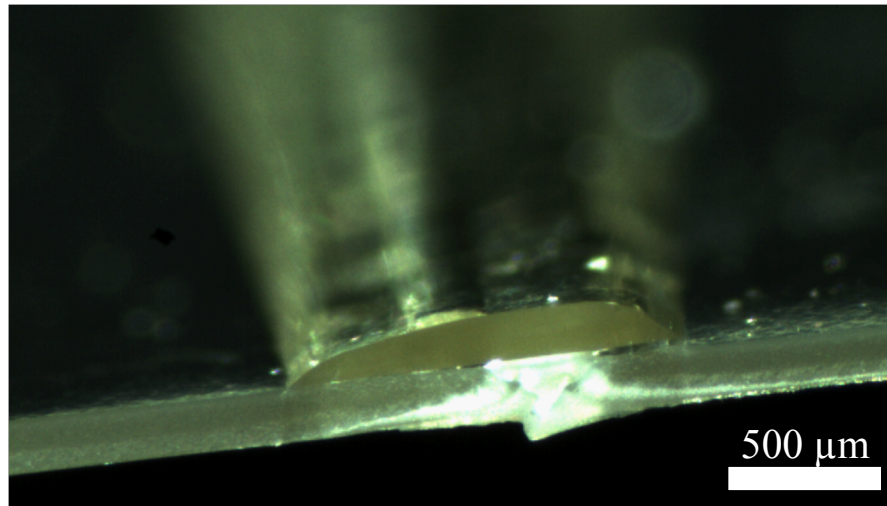
Figure 6.24: Experimental result for an ink-jet printed core made of InkEpo on a flexographically printed lower cladding fabricated by flexographic printing. Reprinted with permission of IS&T: The Society for Imaging Science and Technology, sole copyright owners of Printing for Fabrication 2016 (NIP32) 32nd International Conference on Digital Printing Technology[120].

Figure 6.24 shows the experimental assessment of a sample fabricated by this method, with the waveguide core is visible on top of the large cladding layer. The optical proof-of-principle with the illuminated waveguide core is shown in Figure 6.25. However, a significant amount of light is also visible in the cladding. Because of the low reliability of the process and the low aspect ratio, an attenuation characterisation was not possible, and the approach of using flexographically printed tracks as lower cladding was abandoned.
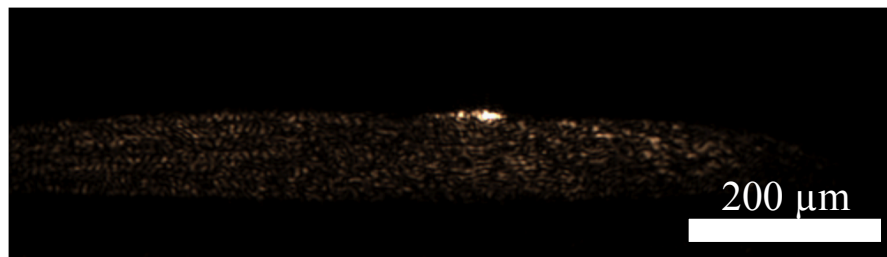
Figure 6.25: Proof of principle for light transmission of a printed core of InkEpo on a flexographically printed cladding. Reprinted with permission of IS&T: The Society for Imaging Science and Technology, sole copyright owners of Printing for Fabrication 2016 (NIP32) 32nd International Conference on Digital Printing Technology[120].

6.3.2 *Printed upper cladding*

All previously described waveguide designs use an air interface as the upper optical interface. By this method, the refractive index step is maximised, which improves the light-guiding capabilities of the waveguide. However, this design also leaves the exposed waveguide cores vulnerable to mechanical and chemical influences from the environment, causing light scattering at dust particles or scratches on the surface, and a material layer with undefined chemical properties caused by increased humidity or oxidation. Especially the polishing step to prepare waveguides with clear facets, which relies on clamping the samples between two blocks of PMMA, can be expected to cause significant damage. To resolve this problem, the waveguide cores were given an upper cladding layer. Although spin- or spray coating is a feasible and easy technique for this, the upper cladding layer was created by ink-jet printing in the same manner as the printed lower cladding. This way, the entire sample could be created with one single fabrication method.

As materials for core and cladding, two variants of SynthEG were used. SynthEG50, with a refractive index of 1.54, was chosen as core material, and SynthEG70, with a refractive index of 1.53, for the upper cladding. The inks were printed at 70 °C and 50 °C, respectively, to tune their viscosity to a printable value of 10 mPa·s.

Waveguide cores were printed from SynthEG50 at a pulse voltage of 18 V and 20 layers. A resting time t_p of 46 s for the printing of the waveguide cores resulted in tracks with an average height of $20 \pm 4\,\mu m$, and an average track width of $145 \pm 5\,\mu m$. After polymerisation, the cladding was deposited as a printed rectangle with sufficient size in 20 layers to overlap all cores. To ensure that the cladding fully encloses the cores, a pulse voltage of 40 V was used, and the substrate temperature was kept at 60 °C to restrain the ink from spreading out on the surface. The resulting structure fully enclosed the printed cores. After deposition and polymerisation of the cladding, both sides of the sample were sprayed black to filter cladding modes caused by light scattered from the core.

Figure 6.26 shows this structure after facet polishing in the *Fibre Setup*, both under ambient light (a) and illuminated by a 705 nm laser (b). The rear facet of the illuminated waveguide is clearly visible, which demonstrates the light transmission. Upon close observation of the interface in Figure 6.26, it becomes apparent that the deposited SynthEG70 under-etches the polymerised cores. This phenomenon even caused buckling of the polymerised cores inside the unpolymerised cladding, if given enough time. This suggests that the EGDMA perpetrates the polymerised material and causes swelling. To avoid the underetching phenomenon, the polymerisation of the printed cladding was performed quickly after printing.
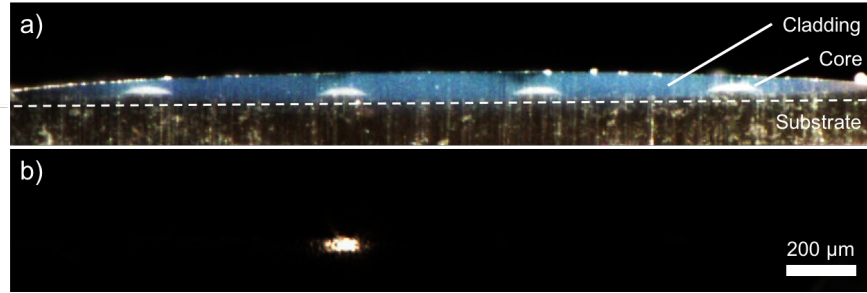
Figure 6.26: Microscope image of the rear facet of an optical waveguide printed with SynthEG. Each of the four embedded cores is 145 µm wide and 20 µm high. Figure (a) shows the sample under ambient light illumination. The under-etching of the printed cores by the cladding, resulting in a curved interface, is indicated by a dotted line. Figure (b) shows one waveguide illuminated by laser light at 785 nm.[15] © IOP Publishing. Reproduced with permission. All rights reserved.

To assess the attenuation of these waveguides, samples with two different lengths were fabricated and evaluated in the *Fibre Setup*. First, cladded waveguides were printed as described in the previous section. Then, samples with two different lengths were cut by scissors and polished to a length of 49.4 mm and 28.6 mm, respectively.

Table 6.3: Measured power from the two characterised waveguide samples at 785 nm, which were both measured three times. From eight waveguides, three carried only little light. The data from the other five was used to derive an attenuation value. Reproduced with permission from [15], © IOP Publishing. All rights reserved.

Length	1	2	3	4	Average
49.4 mm	(<1 µW)	5.1 ± 3.6 µW	4.7 ± 1.9 µW	(<1 µW)	4.9 ± 2.7 µW
28.6 mm	9.7 ± 1.2 µW	11 ± 2.6 µW	8.4 ± 3.5 µW	(<2 µW)	9.7 ± 2.5 µW
Result					1.4 ± 0.4 dB/cm

The samples were characterised in the *Fibre Setup* by manual alignment. To compensate for alignment errors, the transmitted power of each waveguide core was measured three times, resulting in 24 data points. The results are shown in Table 6.3. The data shows a considerable degree of uncertainty, and it is unclear if this large deviation between the individual measurements stems from the characterisation setup or from the samples. Yet the data is sufficiently consistent to rank the optical attenuation above 1 dB/cm, which was the chosen limit for practical short-distance applicability.

However, when comparing the attenuation value to the measured attenuation of the bulk material, it becomes clear that the majority of the attenuation can likely be attributed to the bulk attenuation of the material at this wavelength. This means that the first step to reduce the attenuation and get the concept ready for application in data transmission or sensing should be towards reduction of the bulk attenuation.

Two samples with different lengths could be measured, each of them with four waveguides. From these eight waveguides available for characterisation, only five allowed to take a value. The fact that the three waveguides that do not carry light are at near the edge of the cladding is striking. A way to evaluate if their position caused their failure would be to print an array with a different amount of parallel waveguides.

The process of sample fabrication, polishing, and characterisation required numerous steps, many of them by hand. Additionally, the yield was very low. While it is justifiable to achieve a first transmission value, it renders the study of individual process parameters unrealistic. To overcome this problem, an alternative characterisation method with less process steps should be sought. For the facet preparation, hot-cleaving [121, 122] appears as a promising alternative to the expensive and time-consuming polishing process. For the measurement of transmitted power, a collimated laser beam for illumination and a beam profiler for visualisation and power measurement should be considered. By using a collimated laser beam, it would no longer be necessary to align the fibre as close as possible to the sample under the microscope manually. A beam profiler would render the characterisation faster as it combines the abilities of the CCD camera to align the light source and detector with the sample and the photodiode to take the actual transmitted power. In combination with a digitally controlled sample holder, this would enable an autonomous characterisation setup. Alternatively, integrated light sources and detectors would allow to derive an attenuation value.

6.3.3 *Summary and Intermediate Conclusion for Cladded Waveguides*

Several available materials were used to print cladded optical waveguides. To become independent of the optical properties of the substrate material, a printed lower cladding was investigated. The experimental assessment shows that a printed lower cladding layer leads to difficulties when printing a waveguide core on top. In the experiments, printing directly on untreated PMMA foil allowed a higher aspect ratio, and higher reliability. Therefore, the feature of being independent of the substrate by printing a lower cladding layer could not be realised, and the concept had to be dismissed.

To protect the waveguide cores, an upper cladding was deposited. This method worked well, and allowed to fabricated waveguides with protected cores, which could then be characterised.

The measured attenuation of the cladded waveguides is above the previously defined attenuation goal of 1 dB/cm, and therefore not yet ready for an application. However, this can be explained with the high bulk attenuation of the selected material, which should be seen as the main cause of this high value.

Despite the high attenuation value, the concept to use ink-jet printing for the fabrication of optical waveguides was successfully demonstrated, because the attenuation of the printed waveguides can be explained with the bulk attenuation of the material, and not by the fabrication method. On the publication date in 2017, the results represented the first scientifically published result [15] on ink-jet printed optical waveguides on flexible polymer foils.

To reduce the attenuation and reach the target value for the attenuation, the developed methods to control the waveguide shape should be applied in combination with a material with lower bulk attenuation.

INTEGRATION OF LIGHT SOURCES

For the experimental characterisation of printed waveguides, it is sufficient to have a passive waveguide structure that is illuminated by an external light source. For an application, however, it is beneficial to integrate a light source directly into the waveguide.

Two concepts for the integration of light sources and printed optical waveguides were investigated: The integration of a state-of-the-art semiconductor-based light source as surface-mount device (SMD), and the additive deposition of fluorescent materials as light-emitting layers on top of a printed waveguide.

7.1 INTEGRATION APPROACH 1: SMD ELEMENTS

7.1.1 *Concept*

In the semiconductor industry, LED or laser diode light sources as SMD elements are widely used on rigid and flexible substrates [123]. As these devices typically have sub-mm dimensions, it is possible to mount them on flexible foils. There are, however, several challenges which need to be addressed in order to apply this concept. The first problem is that the chips require electric power. Therefore, electrically conductive tracks need to be created in addition to the optical waveguides. In the present work, this was achieved by ink-jet printing of a silver-nanoparticle-based ink [124]. Because conventional sintering at 200 °C was not possible with the PMMA substrate due to temperature constraints, Ohmic curing [125] was applied. Although these steps are state-of-the art and manageable, they pose additional fabrication steps, which counteracts the benefits of ink-jet printing as a manufacturing technique.

The second problem is the orientation of the diode, shown in Figure 7.1. Typically, the SMD light sources emit light from a ridge of optically active material on the top of the chip. As SMD diodes are several hundred micrometers high, and the printed waveguides typically less then 50 μm high, the light is emitted above the waveguide, and an optical coupling structure is required. If the chip is flipped, the light is emitted right at the surface of the substrate. Here, only half of the light is coupled into the waveguide, the rest is lost into the substrate. In the present case, the first design was selected, because the bottom of the diode was embedded in conductive adhesive. A printed coupling structure was used to bridge the optical gap between the chip light source and the optical waveguide.
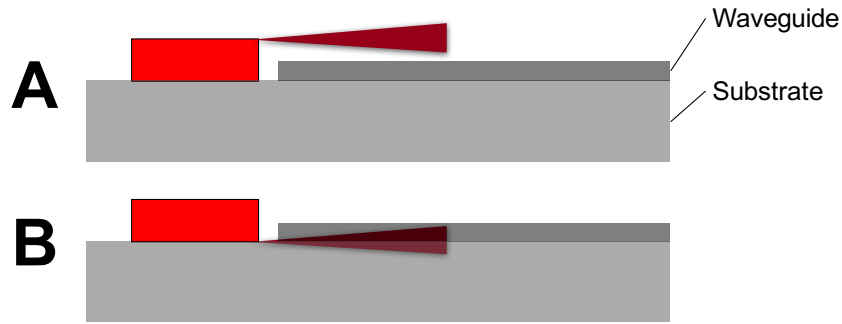
Figure 7.1: Schematic representation from the side of an ridge-emitting SMD diode used as a light source. In situation A, the diode is oriented with the emitting ridge on top. Here, the height difference between SMD chip and printed optical waveguide is problematic. In situation B, the ridge is emitted at the bottom, which causes 50% of the light to be emitted into the transparent substrate.

The third problem is thermal management. The energy density of an SMD light source is in the range of $1\,W/mm^2$, and polymer substrates to not conduct heat as well as PCBs, which is the typical substrate for SMD light sources. As a consequence, the thermal energy can damage the substrate, hereby causing failure of the system. Additionally, the resonance of a laser diode breaks down at elevated temperatures due to thermal expansion. To solve this problem, the light source has to be operated in pulsed mode.

7.1.2 *Experimental Assessment*

For an experimental assessment, a prototype of an optical waveguide with an SMD light source was built. As optical waveguides, flexographically printed waveguides were used. On this substrate, an electrically conductive adhesive was distributed at the edge of a waveguide by hand. Then, a laser diode chip (CHIP 650ps, Roitner Lasertechnik, Vienna, Austria) that emits light at a wavelength of 650 nm was placed on the substrate manually by means of an optical microscope and tweezers. Then, the samples were placed in the oven at 75 °C for 12 h to sinter the adhesive. To print the optical taper between diode and waveguide, a rectangle of 25×25 droplets of SynthEG70 was printed in 25 layers in the area between the diode and the waveguide.

To provide electrical current for the diode, a pogo pin was used for the upper contact, and a clamp at the conductive adhesive for the lower contact. Upon application of 2.5 V and 25 mA, the diode emitted light, which was visible at the end facet of the waveguide. A photograph of the demonstrator is shown in Figure 7.2. However, the setup was very sensitive mechanically, and no power measurement could be performed because the diodes were often damaged by the pogo pin.
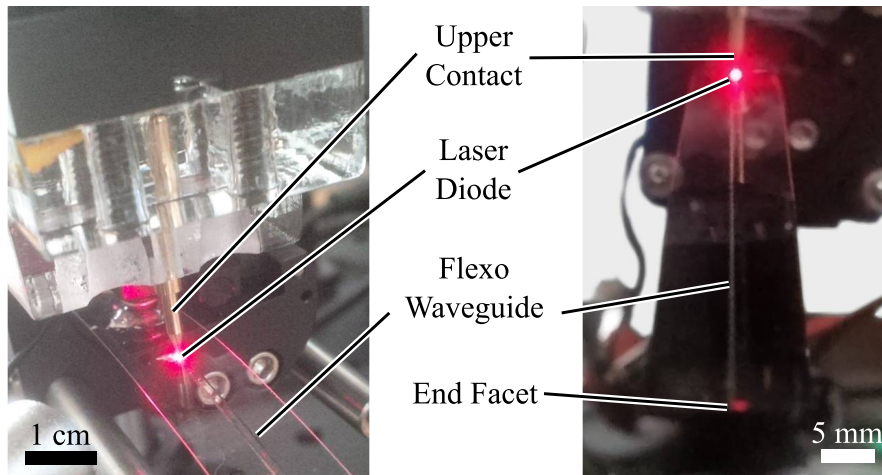
Figure 7.2: Photograph of a glowing SMD laser diode integrated into a flex-ographically printed optical waveguide. On the right, the illuminated waveguide facet is visible.

7.1.3 *Discussion*

Although the experimental proof-of-principle was successful, the concept was abandoned due to difficulties in sample assembly and characterisation. The manual placement of diodes took much time, and the yield in the individual process steps was relatively low. Additionally, the upper contact by the pogo-pin was only feasible in experiments, and often caused mechanical stress that damaged the laser diode and destroyed the sample. A more reliable fabrication and characterisation would have required a printed upper electrode and a pick-and-place device for reliable positioning of the diodes.

From an industrial standpoint, this approach is certainly feasible, but it could not be realised within this project. Generally, it should be considered that the concept to integrate SMD elements and the necessary electrical tracks might counteract the benefits of ink-jet printing as a single-step process. For future work, a flipped diode, as is shown in Figure 7.1 B with a metallic layer on the substrate, could have several benefits. The metallic layer would simultaneously serve as electric contact, heat sink, and reflective layer to reflect the light which is emitted towards the substrate.

7.2 INTEGRATION APPROACH II: FLUORESCENT ELEMENTS

The second light source concept presented in this thesis is to print a fluorescent material to create a light source for the waveguides. This is achieved by mixing fluorophores into a transparent ink. By depositing a layer of this ink on top of a waveguide, a simple light source that does not require any electrical parts on the substrate can be created. The light emission is stimulated by an external laser beam. The result

is a light, all-polymer micro-optical system that can be manufactured entirely by ink-jet printing. Additionally, it maintains the benefit of an all-polymer, metal-free system.
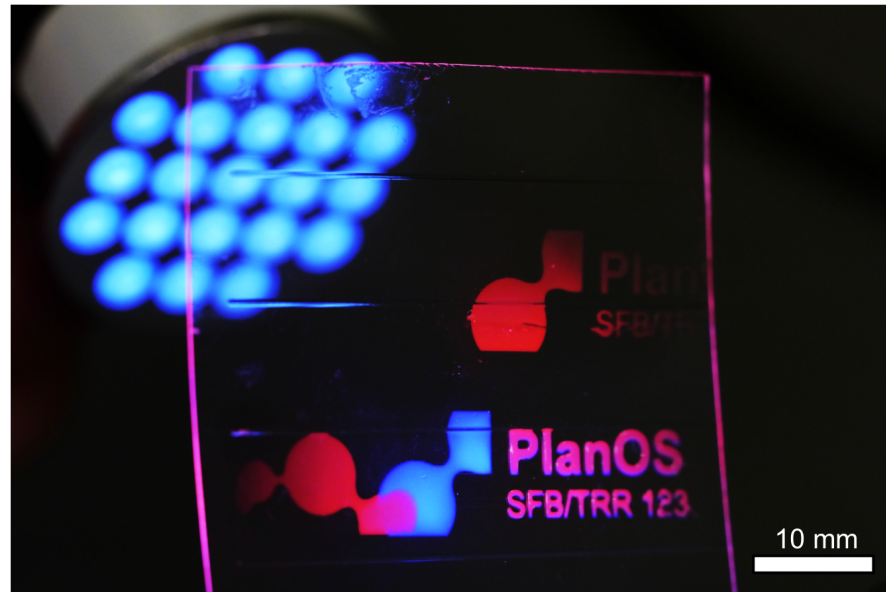
Figure 7.3: Test pattern of both fluorescent inks under UV-light. Areas where both inks were applied appear pink. Reprinted with permission from[16].

7.2.1 *Fluorescent Inks*

From a range of suitable fluorophores [126], two were selected and evaluated: (Eu(DBM)$_3$ Phen), a europium-based rare-earth complex that fluoresces red, and 9,10-diphenylantracene (DPA), a poly-cyclic aromatic hydrocarbon, which is commonly used in light-sticks, and fluoresces blue. The materials are shown in Figure 7.4. An experimental study revealed that BEEG50 [16], which is a 50/50 mixture of Bisphenol-A-Ethoxylate-Diacrylate (BE) as base material, and Ethylenglycol-dimethacrylate (EGDMA) as reactive diluent, was most suitable to dissolve the fluorophores in a printable ink. In BEEG50, the maximum concentration that still allowed printing was 2.5 wt.% for the europium complex, and 0.5 wt.% for DPA. At these concentrations, the printability of the inks was not affected, and printing with the standard waveform at a pulse voltage of 20 V at an ink temperature of 50 °C worked well. The materials are referred to as Antraceneink and Europium-ink. A printed test pattern with both materials is shown in Figure 7.3.

Eu(DBM)₃Phen   9,10-diphenylantracene
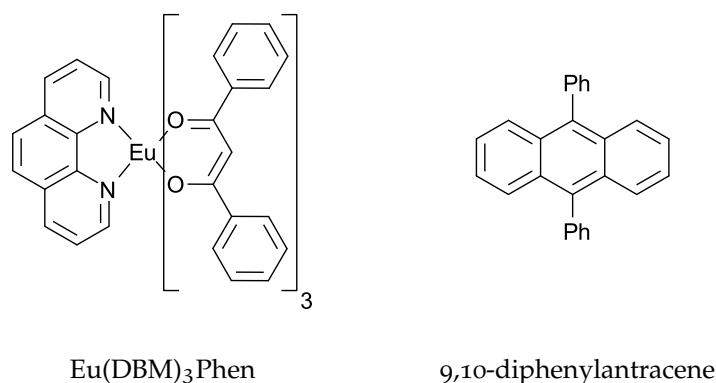
Figure 7.4: The two fluorophores which were used in the project. Reprinted with permission from [16].

7.2.2 *Characterisation of fluorescent ink*

To analyse the emission spectrum of the fluorescent inks, polymerised samples of the material were measured in a fluorescence spectrometer (LS 55, Perkin Elmer, Waltham, USA). The results of this measurement are shown in Figure 7.5.
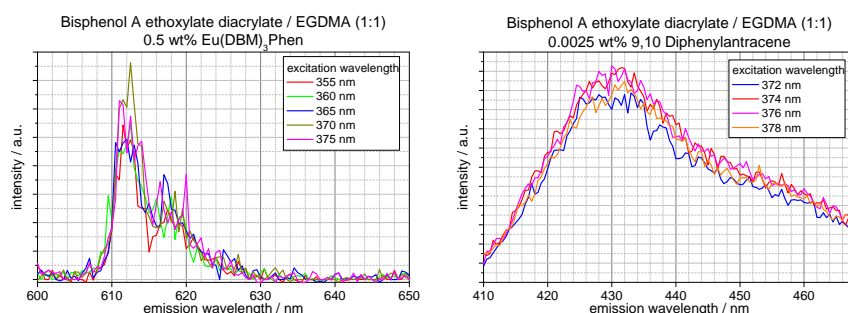
Figure 7.5: Emission spectra of Europium-ink and Antracene-ink after printing and polymerisation. Reprinted with permission from [16].

To measure the intensity of the inks after printing and polymerisation, rectangles of 400×400 droplets with a drop spacing of $25\,\mu m$ were printed in 3 and 9 layers and polymerised under UV with $1.5\,W$ for $30\,s$. This resulted in squares with a side length of $10\,mm$ and a thickness of $13 \pm 1\,\mu m$ per layer. These samples were directly placed on a photo-diode (S151C, Thorlabs), with the fluorescent layer facing up. The fluorescence was excited with a UV lamp (LED Spot 100, Hönle) at an intensity of $100\,mW/cm^2$ and a wavelength of $405\,nm$ for the Europium-ink, and $365\,nm$ for the Antracene-ink. The $365\,nm$ excitation light was blocked from the detector by the PMMA substrate, which acted as a filter. For the europium ink excited at $405\,nm$, an optical long-pass filter (FEL0450, Thorlabs) was necessary. For an additional isolation of the light emitted by fluorescent material from

the excitation, the measurement was taken once with fluorescent material, and once without, and the measured values were subtracted. The results of the measurement are shown in Figure 7.6.
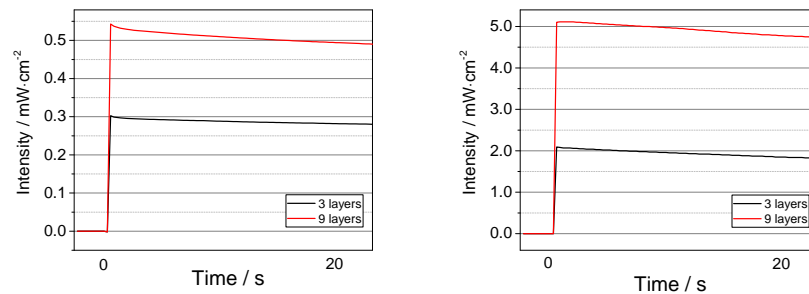
Figure 7.6: Intensity of printed squares of Europium-ink (left) and Antracene-ink (right) over time. The intensity drops over time, which suggests that there is some photonic bleaching of the materials. Reprinted with permission from [16].

The results show that generally, the materials emit light in the mW-range, with Antracene-ink showing an intensity about one order of magnitude higher than Europium-ink. The samples with nine layers are about twice as bright as the samples with three layers. The reason why a layer with three times the fluorescent material is only twice as bright is that the excitation light is absorbed by the host material of the fluorescent inks, and the lower layers are exposed to a lower excitation intensity. When measuring over time, it became apparent that the materials lose intensity due to photonic bleaching. To counteract this for an application with a reliable intensity, a pulsed excitation should be considered, and the expected lifetime of the material should be evaluated.

7.2.3 *Application as fluorescent light source*

Although the intensity of the materials is several orders of magnitude below the intensity of typical SMD light sources, the application as light sources was successfully demonstrated. For this, an optical waveguide fabricated by flexographic printing was used. The sample was 80 mm long. A square of europium-ink with side-length of 0.7 mm was printed on the waveguide at one end and polymerised. The bottom of the substrate was sprayed black to absorb the light in the cladding.

For excitation, a 405 nm laser source (S1FC405) was used at a power of 10 mW. A collimation lens allowed to create a laser beam with a spot size of approximately 1 mm. This beam was then pointed to the fluorescent area from a distance of 1 m. After quick alignment by hand, the fluorescent area lit up, and the end facet of the sample was visible with the bare eye. This successful experimental demonstration

is shown in Figure 7.7. A photodiode (S151C, Thorlabs) furnished with a 1 mm aperture and an additional 450 nm long-pass filter to absorb the blue laser light was used to measure the intensity directly at the end facet. Between ambient light and activation of the excitation laser, a power difference of 28 nW was measured.
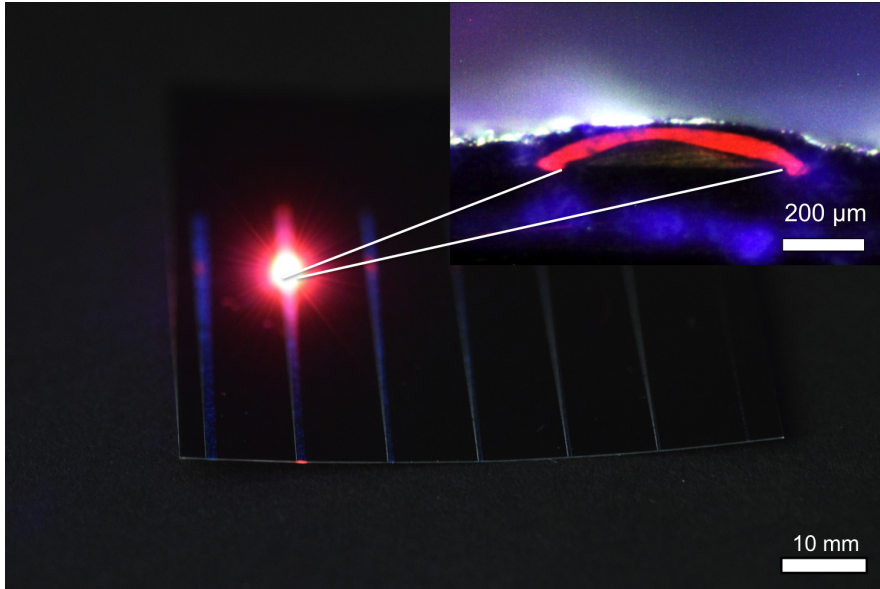
Figure 7.7: Application as fluorescent light source of europium-ink. A small square on top of the waveguide allows to create light within the waveguide from a considerable distance, visible at the end facet at the bottom. The system does not require any electrical elements on the substrate. The inset shows a cross-section of the printed waveguide, with the fluorescent material printed above. Reprinted with permission from [16].

7.2.4 *Discussion*

In comparison with established light source technologies, the measured intensity of the printed fluorescent layers is quite low. However, it is intrinsically coupled into the waveguide and sufficiently bright to create light within a printed waveguide, which means that the low intensity is sufficient for certain applications where a light-weight, cheap system is required. The observed photonic bleaching requires further characterisation to understand the long-term effects, as this phenomenon would render the concept unsuitable for applications where the light source is not easily replaced. On the other hand, the concept is very simple, and the expected benefit of not requiring any electrical elements or discrete parts could be demonstrated in a simple, light, and flexible demonstrator, which was fabricated entirely with printing techniques. Compared to direct light coupling, simple

alignment of the laser collimation lens by three screws was sufficient for activation of the fluorescent light source.

7.3   INTERMEDIATE CONCLUSION FOR INTEGRATED LIGHT SOURCES

Two techniques were shown, an integrated laser diode, and a fluorescent layer. The integrated laser diode is able to give high intensity, but requires electrical tracks and defined positioning, which poses additional manufacturing steps and was the cause of low yield. The concept is certainly feasible, but requires an automated fabrication process which was not within the scope of this project.

The fluorescent layer, on the other hand, was created with a single step, and could be reliably fabricated. Although the intensity was much lower, it was sufficiently bright for a practical demonstrator. Compared to external coupling from a laser, the method is much more robust against minor misalignment, and does not require sophisticated coupling optics. This makes the concept feasible for devices where the optical device is positioned with a simple alignment method, like a clip mechanism. Additionally, the absence of any metal makes the concept attractive for situations where electrical power is not available or possible due to high fields or a second measurement technique sensitive to electric fields. The concept was published [16] and is ready for application.

CONCLUSION AND OUTLOOK

Having presented and discussed the experimental results, the last chapter will put these findings into context with the research goals stated in Chapter 2, and with the state of the art. The results will be critically compared to other published results, and it will be discussed why the research goal for waveguide attenuation was missed.

In the outlook, recommendations for further research and some application concepts will be given in order to advise other engineers and researchers who are working on optical networks.

8.1 EVALUATION OF RESULTS IN LIGHT OF THE RESEARCH GOALS

8.1.1 *Ink-jet printed optical waveguides on flexible foils*

In this thesis, it was demonstrated how optical waveguides can be fabricated on polymer foil substrates by ink-jet printing. Two different ink types, a solvent-based, and one with a reactive diluent, were investigated. Although the measured bulk attenuation was quite high, the latter one was selected for further experiments to gain understanding of the process of ink-jet printing of optical waveguides because of better process compatibility. After finding suitable process parameters, the expected benefits of ink-jet printing as a simple and reliable, yet flexible fabrication technique, could be demonstrated.

Because of the high bulk attenuation of the selected material, the attenuation of the waveguide was 1.4 dB/cm. As the stated research goal for the waveguide attenuation was to achieve a value below 1 dB/cm, the target was exceeded by about 50 %.

Yet, at the time of publication, the work presented in this thesis was the first to demonstrate that ink-jet printed optical waveguides on polymer foils are indeed possible. In the meantime, significant results were published[71, 72], which shows that very promising attenuation values can be achieved by ink-jet printing. Figure 8.1 shows the current result in comparison to other results.

Because the major part of the research effort was put into the process control of the available inks, it was not possible to find a solvent-free material with lower bulk attenuation. Only after understanding the behaviour of ink on the substrate, waveguides could be fabricated and characterised. At this point, no time was available to investigate a better base material with lower bulk attenuation. P. Theiler et al. [72] also report the use of an acrylic polymer, similar to the material class used in this project, but here, much lower attenuation values are
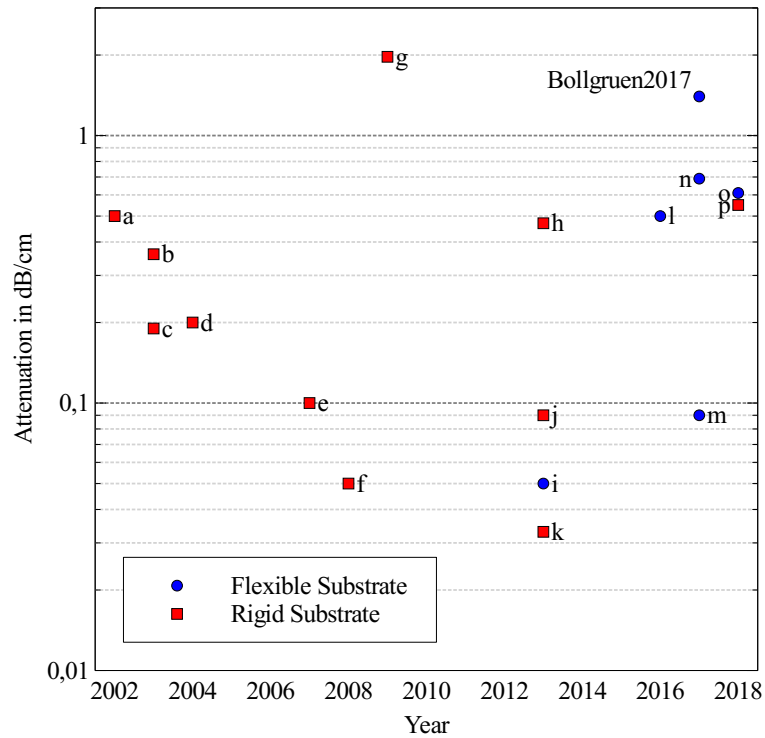
Figure 8.1: Overview of the attenuation of different polymer optical waveguides as shown in Chapter 2, with the result presented in this thesis added.

Table 8.1: Recent results of ink-jet printed optical waveguides.

	Year	Method	Attenuation (dB/cm)	Substrate	Reference
h	2010	Ink-jet printing	0.47 (850 nm)	rigid	Selviah et al. [69]
	2017	Ink-jet printing	1.4 (785 nm)	flexible	Bollgruen et al. [15]
o	2018	Ink-jet printing	0.61 (650 nm)	flexible	Theiler et al. [72]
p	2018	Ink-jet printing	0.55 (633 nm)	rigid	Alamán et al. [71]

reported. D. Selviah et al., on the other hand, used a polysiloxane, Alaman et al. [71] a more sophisticated ink that forms an organic-inorganic hybrid polymeric network. These results show that better attenuation values can be expected in the future with of the availability of more suitable base materials.

A second possible source for the high attenuation of the waveguide was the under-etching phenomenon. Microscope images showed a significant interaction between the substrate and the printed wave-

guide, which could be a cause for scattering. However, further research would be necessary to isolate the influence of this phenomenon.

The PMMA foil which was selected as substrate dissolves quite quickly. To reduce the under-etching, a chemically more stable substrate material should be considered. A promising alternative to polymer foils are ultra-thin glasses (D263 T eco, Schott, Mainz, Germany), which combine the flexibility of foils with the chemical resilience and superb optical properties of glass. The fact that the optical waveguides printed on glass[69, 71] show a much lower attenuation support this hypothesis. Additionally, a glass substrate would allow solvent-based inks, as it would not impose such strong restrictions on thermal evaporation and aggressive polymers.

8.1.2 *Method to print elevated structures on polymer substrates*

The second research goal was the development of methods to control the shape of the printed structures on the substrate. Two methods were investigated: thermally induced pinning in combination with the resting time effect, and the *Lightplate*.

The concept for the *Lightplate* was carried from the original idea to a prototype. Although polymerisation could be performed with the device, the printed structures did not show a different morphology when polymerised with this method. Therefore, the device could not be applied successfully. However, the principle was demonstrated, and should be revisited with more powerful diodes.

The second method, thermally induced pinning, was applied successfully. By using the influence of time and heat on the resulting contact angle of a printed droplet, this effect allowed to increase the contact angle on heated substrates from 15°to 37°, hereby more than doubling the aspect ratio of the fabricated structures.

The fact that the resulting contact angle of several layers of printed polymer ink can be increased by this factor by waiting alone poses a scientific novelty and was published [15], as it is relevant for all situations where elevated structures are fabricated by ink-jet printing.

Yet, although the effect is very strong in the present experiments, it is likely that it is connected with the observation of a dissolving substrate, which is in turn a suspected cause for light scattering and waveguide attenuation. Therefore, the method presented here directly opposes the first research goal to reach a low attenuation. This phenomenon could be reduced by using different substrate materials, but it is likely that materials that are not dissolved as strongly also show a weaker pinning effect.

Additionally, time is a critical factor in industrial fabrication, and the exploitation of the resting time effect to the degree it was shown in this project is unfeasible for industry. Here, the method presented recently by P. Theiler [72] is much more elegant. They solved the prob-

lem of printing elevated structures by first printing and polymerising a track of spherical caps with high aspect ratio, then connecting these by a second row of printed drops, forming liquid bridges. This approach is much more feasible for an industrial application, as it does not rely on time. Yet, the effect of thermally induced pinning should be considered and investigated whenever several layers of ink are printed without intermediate polymerisation, even with short time intervals between the deposition of individual layers.

8.1.3 *Integration of light sources*

To integrate light sources into the printed waveguides, two concepts were investigated: Discrete SMD elements and printed fluorescent elements. While both methods could be experimentally demonstrated, the integration of an SMD element proved to be unfeasible within the scale of the project, because the electrical tracks required to operate the diode increase the complexity of the system. The fluorescent elements, on the other hand, proved to be a simple and robust solution for the given task, and could be demonstrated experimentally with a simple setup.

Yet, if electrical tracks are present on the substrate, SMD light sources should be considered, as they are powerful, and, if the manufacturing challenges can be solved, durable. If, on the other hand, an all-polymer system is sufficient or even required, and the low intensity can be tolerated, fluorescent elements are a very interesting option, especially because they can easily be created with additive techniques such as ink-jet printing, and were quite robust in practical application.

8.2 OUTLOOK FOR NETWORKS OF OPTICAL WAVEGUIDES

Although optical waveguide networks promise to show several advantages in comparison to conventional electronics, it is still unusual to find this technology in research or a commercial application. To promote the technology, it is necessary to devise a technological application of optical waveguide networks that shows significant benefits over electronics, or even enables a device that would be impossible with electric components. Such an application would create market pull, instead of concept push, and hereby drive further development of the technology. A powerful application could either come from an environment where electronics are unsuitable, of from the use of a sensor principle that relies on light. Without a powerful application, it is unreasonable to shoulder the technological challenges of optical waveguide networks and the drawbacks caused by changing from electronics to optics, then back to electronics.

A common mistake when dealing with optical waveguides is to understand their behaviour analoguely to electrical tracks, as both are used to transmit signals. However, while electrical tracks merely require a continuous line of an electrically conductive material, the signal in optical waveguides is a lot more complex. Because of this, curvatures in printed optical waveguides, and especially beam splitters, are often underestimated. From geometry it can be derived that a curved waveguide increases the incident angle of a ray travelling in the waveguide. As a result, light which would travel within a straight waveguide will refract to the cladding in a curve. One strategy to approach this problem is to metallise the curved elements[127].

In order to promote optical waveguide networks, one research focus should be on the application of a suitable detector structures, either with integrated read-out capabilities directly on the substrate, or, similarly as the fluorescent light source, as a point in the optical network where the light couples out and can be detected from a distance. This would result in a complete transmission path, and enable an actual application of the developed network elements. If sources and detectors could be created without much effort, they would additionally enable a much more effective waveguide characterisation directly on the substrate.

One possible device that employs the technology presented in this thesis are disposable microfluidic chips with integrated sensor structures, possibly in a medical application. Here, a droplet of a sample would be dispensed into the channels, and an integrated sensor structure would enable a measurement based on an optical principle. A read-out unit would create light to power a fluorescent element, and cross-contamination between samples would be avoided by using a disposable, single-use concept. Being fabricated entirely by printing polymers, the device would be relatively cheap. With the absence of any electrical elements, the device would even be compatible with the high field intensities inside an MR scanner. For example, optical elongation or vibration sensors could be used to control a patients breathing pattern or heartbeat.

BIBLIOGRAPHY

[1] Paul Eisler. *Manufacture of electric circuit components*. US Patent 2,441,960, 1948.

[2] Paul Eisler. *My life with the printed circuit*. Bethlehem, PA: Lehigh University Press, 1989.

[3] David AB Miller. "Physical reasons for optical interconnection." In: *Intel J. Optoelectronics* 11 (1997), pp. 155–168.

[4] Simon Ramo, John R Whinnery, and Theodore Van Duzer. *Fields and waves in communication electronics*. New York: John Wiley & Sons, 2008.

[5] Hans Zappe. *Fundamentals of Micro-optics*. Cambridge: Cambridge University Press, 2010.

[6] Daniel Colladon. "On the reflections of a ray of light inside a parabolic liquid stream." In: *Comptes Rendus* 15 (1842), pp. 800–802.

[7] Jeff Hecht. *City of light: the story of fiber optics*. Oxford: Oxford University Press, 2004.

[8] Daniel Colladon. "La fontaine colladon." In: *La Nature* 12 (1884), pp. 325–326.

[9] Jeff Hecht and Larry Long. *Understanding fiber optics*. Vol. 3. Upper Saddle River: Prentice Hall, 1993.

[10] Richard Pitwon, Kai Wang, Akira Yamauchi, Takaaki Ishigure, Henning Schröder, Marcel Neitz, and Mayank Singh. "Competitive Evaluation of Planar Embedded Glass and Polymer Waveguides in Data Center Environments." In: *Applied Sciences* 7.9 (2017), p. 940.

[11] Ludger Overmeyer, Tim Wolfer, Alexander Schwenke, Yixiao Wang, Laszlo Sajti, Bernhard Roth, and Sebastian Dikty. "Polymer based planar optronic systems." In: *The 6th International Congress of Laser Advanced Materials Processing (LAMP2013). Niigata, Japan: Japan Laser Processing Society*. 2013.

[12] Stanislav Sherman and Hans Zappe. "Printable Bragg gratings for polymer-based temperature sensors." In: *Procedia Technology* 15 (2014), pp. 702–709.

[13] Meike Hofmann, Yanfen Xiao, Stanislav Sherman, Uwe Gleissner, Thomas Schmidt, and Hans Zappe. "Asymmetric Mach–Zehnder interferometers without an interaction window in polymer foils for refractive index sensing." In: *Applied optics* 55.5 (2016), pp. 1124–1131.

[14] Christian Kelb, Eduard Reithmeier, and Bernhard Roth. "Planar integrated polymer-based optical strain sensor." In: *MOEMS and Miniaturized Systems XIII*. Vol. 8977. International Society for Optics and Photonics. 2014, 89770Y.

[15] Patrick Bollgruen, Tim Wolfer, Uwe Gleissner, Dario Mager, Christof Megnin, Ludger Overmeyer, Thoams Hanemann, and Jan G Korvink. "Ink-jet printed optical waveguides." In: *Flexible and Printed Electronics* 2.4 (2017), p. 045003.

[16] Patrick Bollgruen, Uwe Gleissner, Tim Wolfer, Christof Megnin, Dario Mager, Ludger Overmeyer, Jan G Korvink, and Thomas Hanemann. "Ink-jet printed fluorescent materials as light sources for planar optical waveguides on polymer foils." In: *Optical Engineering* 55.10 (2016), pp. 107107–107107.

[17] Robert R Krchnavek, Gail R Lalk, and Davis H Hartman. "Laser direct writing of channel waveguides using spin-on polymers." In: *Journal of Applied Physics* 66.11 (1989), pp. 5156–5160.

[18] Marc J Madou. *Fundamentals of microfabrication: the science of miniaturization*. Boca Raton: CRC press, 2002.

[19] Albert Borreman, Sami Musa, Mart BJ Diemeer, and Alfred Driessen. "Fabrication of polymeric multimode waveguides and devices in SU-8 photoresist using selective polymerization." In: *Proc. Symp. IEEE/LEOS Benelux Chapter*. Citeseer. 2002, pp. 83–86.

[20] Joon-Sung Kim, Jae-Wook Kang, and Jang-Joo Kim. "Simple and low cost fabrication of thermally stable polymeric multimode waveguides using a UV-curable epoxy." In: *Japanese journal of applied physics* 42.3R (2003), p. 1277.

[21] Roger Dangel, Christoph Berger, RenÉ Beyeler, Laurent Dellmann, Max Gmur, Regis Hamelin, Folkert Horst, Tobias Lamprecht, Thomas Morf, Stefano Oggioni, et al. "Polymer waveguide based board level optical interconnect technology for datacom applications." In: *IEEE Transactions on Advanced Packaging* 31.4 (2008), pp. 759–767.

[22] Roger Dangel, Jens Hofrichter, Folkert Horst, Daniel Jubin, Antonio La Porta, Norbert Meier, Ibrahim Murat Soganci, Jonas Weiss, and Bert Jan Offrein. "Polymer waveguides for electro-optical integration in data centers and high-performance computers." In: *Optics express* 23.4 (2015), pp. 4736–4750.

[23] Maik Rahlves. "Fabrication of polymer based integrated photonic devices by maskless lithography." In: *Proceedings of SPIE-The International Society for Optical Engineering 9745 (2016)* 9745 (2016), p. 97450D.

[24] SJ Frisken. "Light-induced optical waveguide uptapers." In: *Optics letters* 18.13 (1993), pp. 1035–1037.

[25] Axel Günther, Ann Britt Petermann, Uwe Gleissner, Thomas Hanemann, Eduard Reithmeier, Maik Rahlves, Merve Meinhardt-Wollweber, Uwe Morgner, and Bernhard Roth. "Cladded self-written multimode step-index waveguides using a one-polymer approach." In: *Optics letters* 40.8 (2015), pp. 1830–1833.

[26] Axel Günther, Sergej Schneider, Maher Rezem, Yixiao Wang, Uwe Gleissner, Thomas Hanemann, Ludger Overmeyer, Eduard Reithmeier, Maik Rahlves, and Bernhard Roth. "Automated Misalignment Compensating Interconnects Based on Self-Written Waveguides." In: *Journal of Lightwave Technology* 35.13 (2017), pp. 2678–2684.

[27] Hidetaka Terasawa, Freddy Tan, Okihiro Sugihara, Daisuke Inoue, Akari Kawasaki, Tatsuya Yamashita, Manabu Kagami, Olivier Maury, Yann Bretonnière, and Chantal Andraud. "Light-induced self-written waveguide fabrication using 1550 nm laser light." In: *Optics Letters* 42.11 (2017), pp. 2236–2238.

[28] A Kolew, M Heilig, M Schneider, D Münch, R Ezzat, N Schneider, and M Worgull. "Hot embossing of transparent high aspect ratio micro parts." In: *Microsystem technologies* 20.10-11 (2014), pp. 1967–1973.

[29] Maher Rezem, Axel Günther, Bernhard Roth, Eduard Reithmeier, and Maik Rahlves. "Low-cost fabrication of all-polymer components for integrated photonics." In: *Journal of Lightwave Technology* 35.2 (2017), pp. 299–308.

[30] Xue Chuan Shan, Ryutaro Maeda, and Yoichi Murakoshi. "Micro hot embossing for replication of microstructures." In: *Japanese journal of applied physics* 42.6S (2003), p. 3859.

[31] Thomas Velten, Frank Bauerfeld, Sabine Scherbaum, Herbert Schuck, Christof Landesberger, and Karlheinz Bock. "Roll-to-roll hot embossing of microstructures." In: *Microsystem technologies* 17.4 (2011), pp. 619–627.

[32] Hirotaka Mizuno, Okihiro Sugihara, Toshikuni Kaino, Naomichi Okamoto, and Masahito Hosino. "Low-loss polymeric optical waveguides with large cores fabricated by hot embossing." In: *Optics letters* 28.23 (2003), pp. 2378–2380.

[33] Keun Byoung Yoon, Choon-Gi Choi, and Sang-Pil Han. "Fabrication of multimode polymeric waveguides by hot embossing lithography." In: *Japanese journal of applied physics* 43.6R (2004), p. 3450.

[34] Tze Yang Hin. "Materials and processes to enable polymeric waveguide integration on flexible substrates." PhD thesis. Loughborough University, 2009.

[35] Tim Wolfer, Patrick Bollgruen, Dario Mager, Ludger Overmeyer, and Jan G Korvink. "Printing and preparation of integrated optical waveguides for optronic sensor networks." In: *Mechatronics* 34 (2016), pp. 119–127.

[36] Gerd-Albert Hoffmann, Thomas Reitberger, Joerg Franke, and Ludger Overmeyer. "Conditioning of Surface Energy and Spray Application of Optical Waveguides for Integrated Intelligent Systems." In: *Procedia Technology* 26 (2016), pp. 169–176.

[37] Gerd-Albert Hoffmann, T Reitberger, L Lorenz, KJ Wolter, J Franke, and L Overmeyer. "Combination of Flexographic and Aerosol Jet Printing for Integrated Polymer Op-tical Step Index Waveguides." In: *Proceedings of 117th Annual Meeting of the DGaO*. 2016.

[38] Gerd-Albert Hoffmann, Tim Wolfera, Jochen Zeitlerc, Oliver Suttmannb, Jörg Frankec, and Ludger Overmeyera. "Manufacturing of polymer optical waveguides using self-assembly effect on pre-conditioned 3D-thermoformed flexible substrates." In: *Proc. of SPIE Vol*. Vol. 10115. 2017, pp. 1011503–1.

[39] Florian Loosen, Carsten Backhaus, Jochen Zeitler, Gerd-Albert Hoffmann, Thomas Reitberger, Lukas Lorenz, Norbert Lindlein, Jörg Franke, Ludger Overmeyer, Oliver Suttmann, et al. "Approach for the production chain of printed polymer optical waveguides–an overview." In: *Appl. Opt.* 56.31 (2017), pp. 8607–8617.

[40] Yongzhang Leng, Victor Yun, Lisa Lucas, Warren N Herman, and Julius Goldhar. "Dispensed polymer waveguides and laser-fabricated couplers for optical interconnects on printed circuit boards." In: *Applied optics* 46.4 (2007), pp. 602–610.

[41] Joseph C Dingeldein, Karl A Walczak, Brandon W Swatowski, Craig R Friedrich, Christopher T Middlebrook, and Michael C Roggemann. "Process characterization for direct dispense fabrication of polymer optical multi-mode waveguides." In: *Journal of Micromechanics and Microengineering* 23.7 (2013), p. 075015.

[42] Joseph C Dingeldein. *Direct write fabrication of waveguides and interconnects for optical printed wiring boards*. Dissertation: Michigan Technological University, 2012.

[43] Shin Morikawa and Takaaki Ishigure. "Fabrication of GI-core polymer optical waveguide using a dispenser and its application to optical printed circuit boards." In: *Photonics Society, 2010 23rd Annual Meeting of the IEEE*. IEEE. 2010, pp. 108–109.

[44] Kazutomo Soma and Takaaki Ishigure. "Fabrication of a graded-index circular-core polymer parallel optical waveguide using a microdispenser for a high-density optical printed circuit board."

In: *IEEE Journal of Selected Topics in Quantum Electronics* 19.2 (2013), pp. 3600310–3600310.

[45] Asami Takahashi and Takaaki Ishigure. "Fabrication for low-loss polymer optical waveguides with 90° bending using the Mosquito method." In: *CPMT Symposium Japan (ICSJ), 2014 IEEE*. IEEE. 2014, pp. 162–165.

[46] Daisuke Suganuma and Takaaki Ishigure. "Fan-in/out polymer optical waveguide for a multicore fiber fabricated using the Mosquito method." In: *Optics express* 23.2 (2015), pp. 1585–1593.

[47] Yuki Saito, Koji Fukagata, and Takaaki Ishigure. "Low-loss polymer optical waveguides with graded-index perfect circular cores for on-board interconnection." In: *Proc. of SPIE Vol.* Vol. 9750. 2016, pp. 975005–1.

[48] Dazhi Wang, Xiaojun Zhao, Yigao Lin, Tongqun Ren, Junsheng Liang, Chong Liu, and Liding Wang. "Fabrication of micro / nano-structures by electrohydrodynamic jet technique." In: *Frontiers of Mechanical Engineering* (2017), pp. 1–13.

[49] Erick Sutanto, Yafang Tan, M Serdar Onses, Brian T Cunningham, and Andrew Alleyne. "Electrohydrodynamic jet printing of micro-optical devices." In: *Manufacturing Letters* 2.1 (2014), pp. 4–7.

[50] Vishv Bhatia. "Fabrication of polymer multimode waveguides using Near Field Electrospinning." MA thesis. University of Freiburg, 2016.

[51] Oliver Brand, Gary K Fedder, Christofer Hierold, Osamu Tabata, Jan G Korvink, Patrick J Smith, and Dong-Youn Shin. *Inkjet-based micromanufacturing*. Vol. 9. Weinheim: Wiley-VCH, 2012.

[52] Stephen D Hoath. *Fundamentals of Inkjet Printing: The Science of Inkjet and Droplets*. Weinheim: Wiley-VCH, 2016.

[53] Dario Mager, Andreas Peter, Laura Del Tin, Elmar Fischer, Patrick J Smith, Jürgen Hennig, and Jan G Korvink. "An MRI receiver coil produced by inkjet printing directly on to a flexible substrate." In: *IEEE transactions on medical imaging* 29.2 (2010), pp. 482–487.

[54] Berend-Jan de Gans, Paul C Duineveld, and Ulrich S Schubert. "Inkjet printing of polymers: state of the art and future developments." In: *Advanced materials* 16.3 (2004), pp. 203–213.

[55] Jorge Alamán, Raquel Alicante, Jose Ignacio Peña, and Carlos Sánchez-Somolinos. "Inkjet Printing of Functional Materials for Optical and Photonic Applications." In: *Materials* 9.11 (2016), p. 910.

[56] Sumio Utsunomiya, Tomoyuki Kamakura, Masashi Kasuga, Mutsumi Kimura, Wakao Miyazawa, Satoshi Inoue, and Tatsuya Shimoda. "21.3: Flexible Color AM-OLED Display Fabricated Using Surface Free Technology by Laser Ablation/Annealing (SUFTLA®) and Ink-jet Printing Technology." In: *SID Symposium Digest of Technical Papers*. Vol. 34. 1. Wiley Online Library. 2003, pp. 864–867.

[57] Tom Aernouts, Tsvetan Aleksandrov, Claudio Girotto, Jan Genoe, and Jozef Poortmans. "Polymer based organic solar cells using ink-jet printed active layers." In: *Applied Physics Letters* 92.3 (2008), p. 22.

[58] Loïc Jacot-Descombes, MR Gullo, VJ Cadarso, and Jürgen Brugger. "Fabrication of epoxy spherical microstructures by controlled drop-on-demand inkjet printing." In: *Journal of Micromechanics and Microengineering* 22.7 (2012), p. 074012.

[59] Victor J Cadarso, Julia Perera-Núñez, Loïc Jacot-Descombes, K Pfeiffer, U Ostrzinski, A Voigt, A Llobera, G Grützer, and Jürgen Brugger. "Microlenses with defined contour shapes." In: *Optics express* 19.19 (2011), pp. 18665–18670.

[60] Xiaohui Lin, Amir Hosseini, Xinyuan Dou, Harish Subbaraman, and Ray T Chen. "Low-cost board-to-board optical interconnects using molded polymer waveguide with 45 degree mirrors and inkjet-printed micro-lenses as proximity vertical coupler." In: *Optics express* 21.1 (2013), pp. 60–69.

[61] Weldon Royall Cox, Donald J Hayes, Tin Chen, Daryl W Ussery, Duncan L MacFarlane, and E Wilson. "Fabrication of micro-optics by microjet printing." In: *SPIE Proceedings*. Vol. 2383. 1995, pp. 110–115.

[62] Royall W Cox, Ting Chen, and Donald J Hayes. "Micro-optics fabrication by ink-jet printers." In: *Optics and Photonics News* 12.6 (2001), pp. 32–35.

[63] Nicholas A Vacirca and Timothy P Kurzweg. "Inkjet printing techniques for the fabrication of polymer optical waveguides." In: *Proceedings of SPIE*. Vol. 7591. 2010, 75910A.

[64] David R Selviah, David A Hutt, Andy C Walker, Kai Wang, F Anibal Fernandez, Paul P Conway, Dave Milward, Ioannis Papakonstantinou, Hadi Baghsiahi, John Chappell, et al. "Innovative optical and electronic interconnect printed circuit board manufacturing research." In: *Electronics System-Integration Technology Conference, 2008. ESTC 2008. 2nd*. IEEE. 2008, pp. 867–872.

[65] Brandon W Swatowski, Chad M Amb, Sarah K Breed, David J Deshazer, W Ken Weidner, Roger F Dangel, Norbert Meier, and Bert J Offrein. "Flexible, stable, and easily processable optical silicones for low loss polymer waveguides." In: *Proc. SPIE*. Vol. 8622. 2013, p. 862205.

[66] Roger Dangel, Folkert Horst, Daniel Jubin, Norbert Meier, Jonas Weiss, Bert J Offrein, Brandon W Swatowski, Chad M Amb, David J DeShazer, and W Ken Weidner. "Development of versatile polymer waveguide flex technology for use in optical interconnects." In: *Journal of lightwave technology* 31.24 (2013), pp. 3915–3926.

[67] Jeroen Missinne, Sandeep Kalathimekkad, Bram Van Hoe, Erwin Bosman, Jan Vanfleteren, and Geert Van Steenberge. "Stretchable optical waveguides." In: *Optics Express* 22.4 (2014), pp. 4168–4179.

[68] John Chappell, David A Hutt, and Paul P Conway. "Variation in the line stability of an inkjet printed optical waveguide-applicable material." In: *Electronics System-Integration Technology Conference, 2008. ESTC 2008. 2nd*. IEEE. 2008, pp. 1267–1272.

[69] David R Selviah, Andy C Walker, David A Hutt, Kai Wang, Aongus McCarthy, F Anibal Fernández, Ioannis Papakonstantinou, Hadi Baghsiahi, Himanshu Suyal, Mohammad Taghizadeh, et al. "Integrated optical and electronic interconnect PCB manufacturing research." In: *Circuit World* 36.2 (2010), pp. 5–19.

[70] Aleksandra Samusjew, Markus Kratzer, Andreas Moser, Christian Teichert, Krzysztof K Krawczyk, and Thomas Griesser. "Inkjet Printing of Soft, Stretchable Optical Waveguides through the Photopolymerization of High-Profile Linear Patterns." In: *ACS applied materials & interfaces* 9.5 (2017), pp. 4941–4947.

[71] Jorge Alaman, Maria Lopez-Valdeolivas, Raquel Alicante, Francisco J Medel, Jorge Silva-Treviño, Jose Ignacio Peña, and Carlos Sanchez-Somolinos. "Photoacid catalyzed organic–inorganic hybrid inks for the manufacturing of inkjet-printed photonic devices." In: *Journal of Materials Chemistry C* 6.15 (2018), pp. 3882–3894.

[72] Pius M Theiler, Fabian Lütolf, and Rolando Ferrini. "Noncontact printing of optical waveguides using capillary bridges." In: *Optics express* 26.9 (2018), pp. 11934–11939.

[73] John Venn. "I. On the diagrammatic and mechanical representation of propositions and reasonings." In: *The London, Edinburgh, and Dublin Philosophical Magazine and Journal of Science* 10.59 (1880), pp. 1–18.

[74]   John Hagel, John Brown, Duleesha Kulasooriya, Craig Giffi, and Mengmeng Chen. "The future of manufacturing." In: *Deloitte University Press* (2017).

[75]   Jürgen Jahns. *Photonik: Grundlagen, Komponenten und Systeme.* München: Oldenbourg, 2009.

[76]   Stefan Bäumer. *Handbook of plastic optics.* Weinheim: Wiley-VCH, 2011.

[77]   Christian-Alexander Bunge, Roman Kruglov, and Hans Poisel. "Rayleigh and Mie scattering in polymer optical fibers." In: *Journal of lightwave technology* 24.8 (2006), p. 3137.

[78]   Gotzon Aldabaldetreku, Iñaki Bikandi, María Asunción Illarramendi, Gaizka Durana, and Joseba Zubia. "A comprehensive analysis of scattering in polymer optical fibers." In: *Optics express* 18.24 (2010), pp. 24536–24555.

[79]   Richard Phillips Feynman, Robert B Leighton, and Matthew Sands. *Feynman lectures on physics. vol. 1: Mainly mechanics, radiation and heat.* Boston: Addison-Wesley, 1963.

[80]   Alexander Rohrbach and Wolfgang Singer. "Scattering of a scalar field at dielectric surfaces by Born series expansion." In: *JOSA A* 15.10 (1998), pp. 2651–2659.

[81]   Alexander Rohrbach. *Lecture notes in Modern Optics I.* Freiburg, 2010.

[82]   Wolfgang Kaiser. *Kunststoffchemie für Ingenieure: von der Synthese bis zur Anwendung.* Munich: Carl Hanser Verlag GmbH Co KG, 2015.

[83]   Shlomo Magdassi et al. *The chemistry of inkjet inks.* Singapore: World scientific, 2010.

[84]   Bryan Ellis et al. *Chemistry and technology of epoxy resins.* Dordrecht: Springer Netherlands, 1993.

[85]   Andrew Hancock and Long Lin. "Challenges of UV curable ink-jet printing inks–a formulator's perspective." In: *Pigment & resin technology* 33.5 (2004), pp. 280–286.

[86]   Kurt Dietliker et al. "Advancements in photoinitiators—Opening up new applications for radiation curing." In: *Progress in organic coatings* 58.2 (2007), pp. 146–157.

[87]   Henrik Bruus. *Theoretical microfluidics.* Oxford: Oxford university press, 2007.

[88]   Thomas Young. "An essay on the cohesion of fluids." In: *Philosophical Transactions of the Royal Society of London* 95 (1805), pp. 65–87.

[89]   D. H. Bangham and R. I. Razouk. "Adsorption and the wettability of solid surfaces." In: *Transactions of the Faraday Society* 33 (1937), pp. 1459–1463.

[90]   Robert J Good. "Contact angle, wetting, and adhesion: a critical review." In: *Journal of adhesion science and technology* 6.12 (1992), pp. 1269–1302.

[91]   Rafael Tadmor. "Line energy and the relation between advancing, receding, and young contact angles." In: *Langmuir* 20.18 (2004), pp. 7659–7664.

[92]   Rafael Tadmor and Preeti S Yadav. "As-placed contact angles for sessile drops." In: *Journal of Colloid and Interface Science* 317.1 (2008), pp. 241–246.

[93]   Rafael Tadmor. "Approaches in wetting phenomena." In: *Soft Matter* 7.5 (2011), pp. 1577–1580.

[94]   Rafael Tadmor, Kumud Chaurasia, Preeti S Yadav, Aisha Leh, Prashant Bahadur, Lan Dang, and Wesley R. Hoffer. "Drop retention force as a function of resting time." In: *Langmuir* 24.17 (2008), pp. 9370–9374.

[95]   John W Harris and Horst Stöcker. *Handbook of mathematics and computational science*. New-York: Springer-Verlag, 1998.

[96]   Stephen H Davis. "Moving contact lines and rivulet instabilities. Part 1. The static rivulet." In: *Journal of Fluid Mechanics* 98.2 (1980), pp. 225–242.

[97]   Stefano Schiaffino and Ain A Sonin. "Formation and stability of liquid and molten beads on a solid surface." In: *Journal of fluid mechanics* 343 (1997), pp. 95–110.

[98]   Paul C Duineveld. "The stability of ink-jet printed lines of liquid with zero receding contact angle on a homogeneous substrate." In: *Journal of Fluid Mechanics* 477 (2003), pp. 175–200.

[99]   Pierre-Simon Laplace. "Theory of capillary attraction." In: *Supplements to the 10th book of Celestial Mechanics* (1807).

[100] Evonik. *Technical Information Plexiglas Film 99524*. 2015.

[101] Anja Voigt, Ute Ostrzinski, Karl Pfeiffer, Joo Yeon Kim, Vahid Fakhfouri, Jürgen Brugger, and Gabi Gruetzner. "New inks for the direct drop-on-demand fabrication of polymer lenses." In: *Microelectronic Engineering* 88.8 (2011), pp. 2174–2179.

[102] Ralf Buestrich, Frank Kahlenberg, Michael Popall, Roland Müller-Fiedler, Peter Dannberg, and Oliver Rösch. "ORMOCERs for optical interconnection technology." In: *Journal of Sol-Gel Science and Technology* 20.2 (2001), pp. 181–186.

[103] micro resist technology GmbH. *Processing guidelines InkEpo / InkOrmo*. 2013.

[104] micro resist technology GmbH. *Core and Cladding systems for waveguiding*. 2015.

[105]   Uwe Gleißner and Thomas Hanemann. "Tailoring the optical and rheological properties of an epoxy acrylate based host-guest system." In: *Optical Engineering* 53.8 (2014), pp. 087106–087106.

[106]   *SYNTHOLUX 291 EA*. Datasheet, Synthopol Chemie Dr. rer. pol. Koch. GmbH & Co. KG. Mar. 2014.

[107]   *Ethylene Glycol Dimethacrylate (EGDMA)*. TI/CP 0004 e. Datasheet, BASF SE. Sept. 2015.

[108]   Uwe Gleißner, Thomas Hanemann, Christof Megnin, and Felicia Wieland. "The influence of photo initiators on refractive index and glass transition temperature of optically and rheologically adjusted acrylate based polymers." In: *Polymers for Advanced Technologies* 27.10 (2016), pp. 1294–1300.

[109]   Zemax LLC. *Zemax Manual provided by the Simulation suite*. 2017.

[110]   Georg Hass and John E Waylonis. "Optical constants and reflectance and transmittance of evaporated aluminum in the visible and ultraviolet." In: *JOSA* 51.7 (1961), pp. 719–722.

[111]   Oliver Graydon, Amber Jenkins, Rachel Pei Chin Won, and David Gevaux. "Haitz's law." In: *Nature Photonics* 1.1 (2007).

[112]   Robert R Schaller. "Moore's law: past, present and future." In: *IEEE spectrum* 34.6 (1997), pp. 52–59.

[113]   Joshua N Winn, Yoel Fink, Shanhui Fan, and John D Joannopoulos. "Omnidirectional reflection from a one-dimensional photonic crystal." In: *Optics letters* 23.20 (1998), pp. 1573–1575.

[114]   Samuel Clark Ligon, Branislav Husar, Harald Wutzel, Richard Holman, and Robert Liska. "Strategies to reduce oxygen inhibition in photoinduced polymerization." In: *Chemical reviews* 114.1 (2013), pp. 557–589.

[115]   Je Hoon Oh and Si Yeon Lim. "Precise size control of inkjet-printed droplets on a flexible polymer substrate using plasma surface treatment." In: *Journal of Micromechanics and Microengineering* 20.1 (2009), p. 015030.

[116]   Vassili Karanassios. "Microplasmas for chemical analysis: analytical tools or research toys?" In: *Spectrochimica Acta Part B: Atomic Spectroscopy* 59.7 (2004), pp. 909–928.

[117]   Scott Weagant, Andrea T Smith, and Vassili Karanassios. "Mobile micro-and nano-instruments: Small, Cheap and under Wireless Control." In: *ECS Transactions* 28.14 (2010), pp. 1–6.

[118]   Giovanni Nisato, Donald Lupo, and Simone Ganz. *Organic and Printed Electronics: Fundamentals and Applications*. Boca Raton: CRC Press, 2016.

[119] Tim Wolfer, Patrick Bollgruen, Dario Mager, Ludger Overmeyer, and Jan G Korvink. "Flexographic and inkjet printing of polymer optical waveguides for fully integrated sensor systems." In: *Procedia Technology* 15 (2014), pp. 521–529.

[120] Patrick Bollgruen, Tim Wolfer, Uwe Gleissner, Dario Mager, Christof Megnin, Thomas Hanemann, Ludger Overmeyer, and Jan Korvink. "Optical waveguides fabricated by combination of ink-jet and flexographic printing." In: *NIP & Digital Fabrication Conference*. Vol. 2016. 1. Society for Imaging Science and Technology. 2016, pp. 294–297.

[121] Christian Kelb, Maik Rahlves, Eduard Reithmeier, and Bernhard Roth. "Realization and performance of an all-polymer optical planar deformation sensor." In: *IEEE Sensors Journal* 15.12 (2015), pp. 7029–7035.

[122] Bechir Hachicha and Ludger Overmeyer. "Functionalization of UV-curing adhesives for surface-integrated micro-polymer optical fibers." In: *Integrated Optics: Devices, Materials, and Technologies XX*. Vol. 9750. International Society for Optics and Photonics. 2016, 97500J.

[123] Christian Goßler, Colin Bierbrauer, Rüdiger Moser, Michael Kunzer, Katarzyna Holc, Wilfried Pletschen, Joachim Wagner, Klaus Köhler, Michael Schwaerzle, and Patrick Ruther. "GaN-based micro-LED arrays on flexible substrates for optical cochlear implants." In: *Journal of Physics D: Applied Physics* 47.20 (2014), p. 205401.

[124] Henning Meier, Ute Löffelmann, Dario Mager, Patrick J Smith, and Jan G Korvink. "Inkjet printed, conductive, 25 μm wide silver tracks on unstructured polyimide." In: *physica status solidi (a)* 206.7 (2009), pp. 1626–1630.

[125] David A Roberson, RB Wicker, and E MacDonald. "Ohmic curing of printed silver conductive traces." In: *Journal of electronic materials* (2012), pp. 1–14.

[126] Emine Tekin, Elisabeth Holder, Veronica Marin, Berend-Jan de Gans, and Ulrich S Schubert. "Ink-Jet Printing of Luminescent Ruthenium-and Iridium-Containing Polymers for Applications in Light-Emitting Devices." In: *Macromolecular rapid communications* 26.4 (2005), pp. 293–297.

[127] Mustafa A Sefunc, Willemijn Van De Meent, AR Coenen, Antonio Pace, Mindert Dijkstra, and Sonia Maria García-Blanco. "Low-loss sharp bends in low contrast polymer hybrid metallic waveguides." In: *Integrated Optics: Devices, Materials, and Technologies XIX*. Vol. 9365. International Society for Optics and Photonics. 2015, p. 93650V.

LIST OF OWN PUBLICATIONS

During the research project that led to this thesis, the following articles were published:

JOURNAL PUBLICATIONS

[J1] Patrick Bollgruen, Tim Wolfer, Uwe Gleissner, Dario Mager, Christof Megnin, Ludger Overmeyer, Thomas Hanemann, and Jan G Korvink. "Ink-jet printed optical waveguides." In: *Flexible and Printed Electronics* 2.4 (2017), p. 045003.

[J2] Patrick Bollgruen, Uwe Gleissner, Tim Wolfer, Christof Megnin, Dario Mager, Ludger Overmeyer, Jan G Korvink, and Thomas Hanemann. "Ink-jet printed fluorescent materials as light sources for planar optical waveguides on polymer foils." In: *Optical Engineering* 55.10 (2016), p. 107107.

[J3] Tim Wolfer, Patrick Bollgruen, Dario Mager, Ludger Overmeyer, and Jan G Korvink. "Printing and preparation of integrated optical waveguides for optronic sensor networks." In: *Mechatronics* 34 (2016), pp. 119–127.

CONFERENCE PUBLICATIONS

[C1] Patrick Bollgruen, Tim Wolfer, Uwe Gleissner, Dario Mager, Christof Megnin, Thomas Hanemann, Ludger Overmeyer, and Jan Korvink. "Optical waveguides fabricated by combination of ink-jet and flexographic printing." In: *NIP & Digital Fabrication Conference.* Vol.2016. 1. Society for Imaging Science and Technology. 2016, pp.294–297.

[C2] Patrick Bollgruen, Tim Wolfer, Dario Mager, Ludger Overmeyer, and Jan G Korvink. "Ink-jet printed Optical Taper Structures for Planar Optronic Systems." In: *Proceedings of 117th Annual Meeting of the DGaO.* 2016.

[C3] Patrick Bollgruen, Uwe Gleissner, Christof Megnin, Dario Mager, Jan G Korvink, and Thomas Hanemann. "Ink-jet printing of host-guest systems based on acrylates with fluorescent dopants." In: *Micro-Optics 2016*. Vol. 9888. International Society for Optics and Photonics. 2016, 98880G.

[C4] Meike Hofmann, Yanfen Xiao, Stanislav Sherman, Patrick Bollgruen, Thomas Schmidt, Uwe Gleissner, and Hans Zappe. "Inkjet

printed single-mode waveguides on hot-embossed foils." In: *Optical Systems Design 2015: Optical Fabrication, Testing, Metrology V*. Vol. 9628. International Society for Optics and Photonics. 2015, 96281R.

[c5] Tim Wolfer, Patrick Bollgruen, Dario Mager, Ludger Overmeyer, and Jan G Korvink. "Flexographic and inkjet printing of polymer optical waveguides for fully integrated sensor systems." In: *Procedia Technology 15* (2014), pp. 521–529.

SUPERVISED MASTER'S THESES

[m1] Vishv Bhatia. "Fabrication of polymer multimode waveguides using Near Field Electrospinning." MA thesis. University of Freiburg, 2016.

ACKNOWLEDGEMENTS

This thesis has been with me for the better half of a decade, and I would like to thank a number of people for making it happen.

First of all, I owe gratitude to Prof. Dr. Jan Korvink, who signed my first contract as a student assistant back in 2010, and who has influenced my career as a researcher significantly by entrusting me with a fascinating research project of my own. I always appreciated his good balance between giving direction to stay on track and allowing freedom to follow own ideas.

I can consider myself lucky that Prof. Dr.-Ing. Thomas Hanemann agreed to host me in Freiburg, so that I wouldn't have to do research in a cellar. I was able to spend two years in his lab, and I am thankful for having been a part of his research group. It was very valuable for me and my research.

Dario would always direct my ambition to pragmatic action and navigate me through the academic jungle of publications, meetings, conferences, and project proposals. Having run out of time at the institute, I probably wouldn't have finished my PhD-thesis without his continued support. When Dario left for Karlsruhe, Christoph was there to take over and make sure I stayed in shape. We were the envy of IMTEK for sure.

I was lucky to be part of a big research cluster, and I owe gratitude to the DFG for funding my work under the project SFB-TRR 123. I would especially like to thank the colleagues in Hanover, especially Tim Wolfer, whom I always considered to be the organised counterpart to my creative style. This connection was invaluable to get the project off the ground.

Being at IMTEK for 10 years, I probably won't be able to list all people who were always there to help me. Nan, Uwe, Robert, Jens, Roland, Agazi, Stanislav, Markus, Mikel, Dennis, Bilal, Jan, Falk (Special thanks for some decent photo-editing), and all the other PhD Students at IMTEK whom I could always rely on. It was a good time to work there, have discussions, share coffee in the afternoon, and rum in the evening. I also owe gratitude to the people working at IMTEK, especially Andreas, Gaby, Tania, and Bernd. I was also lucky enough to have the chance to guide a master student from job application to his defense. Working with Vishv was never easy, but always fun.

When my time at IMTEK ended, it still took me a few years to finish my thesis. I wouldn't have been able to get there without the support of all my friends, roommates, and fellow musicians, and, most importantly, my family, who would always encourage and motivate me to move forward. Thank you for that!